Removal of sulphur-dioxide by non-regenerative and regenerative solid sorbents

A thesis submitted

in partial fulfillment of the requirements

for the degree of

Master of Technology

by

Arun Kumar Gupta

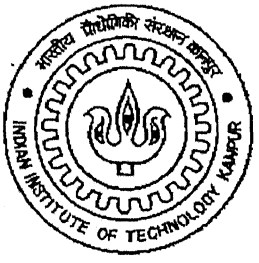

to the

Department of Chemical Engineering

INDIAN INSTITUTE OF TECHNOLOGY

KANPUR

February, 2002

CERTIFICATE

It is certified that the work contained in the thesis entitled ***Removal of sulphur-dioxide by non-regenerative and regenerative solid sorbents*** by **Arun Kumar Gupta**, has been carried out under my supervision and that this work has not been submitted elsewhere for a degree.

February, 2002

Dr. Nishith Verma
Assistant Professor
Department of Chemical Engineering
Indian Institute of Technology
Kanpur

ABSTRACT

In recent times, air pollution has considerably received increased attention all over the world. Sulphur dioxide (SO_2) is one of the major atmospheric pollutants resulting from the combustion of fossil fuels. The adverse effects of acid rain due to emission of SO_2 on human, vegetation and buildings are well known. With stringent environmental regulations, the removal of SO_2 by dry scrubbing methods has come into prominence because of its superior performance over the traditional wet scrubbing methods, especially in concentration levels of parts per million (ppm) and sub-ppm.

In the present work, a combined experimental and theoretical study has been carried out on the removal of SO_2 using solid sorbents. Both types of sorbents have been tested for their sorption behavior: non regenerative such as $Ca(OH)_2$, $CaCO_3$ and $Ca(CH_3COOH)_2$, and regenerative such as zeolites. Reactions have been carried out in a packed bed of sorbent materials under varying operating conditions such as temperature, flowrate, and concentration, etc.

CaO obtained on calcination of calcium acetate was found to be superior amongst all sorbents/adsorbents used in this work, with relatively longer breakthrough time and higher sulphate conversion (70%). Although 5A zeolites exhibited much shorter breakthrough time relative to calcium based sorbents under identical operating conditions, the former may still be preferred to non-regenerative types of sorbents due to their inherent regenerative characteristics. Use of a two-bed system, similar to PSA (pressure swing adsorption), may also be advantageous in the case of zeolite adsorbents.

Mathematical model has been developed to understand the mechanism of sorption by sorbent materials having bi-disperse pores (as in zeolites). The theoretical analysis incorporates the effects of gas diffusion in the adsorbent bed, in the macro-pore and within the crystal. A simplified approach based on linear driving approximation and average radial concentrations within the macro and micro-pores is used. The model predictions are observed to be in good agreement with the experimental data.

ACKNOWLEDGEMENT

It was highly eventful at the Department of Chemical Engineering working with a dedicated teaching community which I will cherish throughout my life. It is my great pleasure to express my sincere gratitude to my thesis supervisor Dr. Nishith Verma for introducing me to an interesting and intriguing topic. I am especially indebted to him for his interest, patience and understanding while guiding me. It was my privilege to have worked under him.

I extend my sincere thanks to Dr. (Mrs) Padma Vankar in the FEAT laboratory for helping me in my analysis. I am grateful to my Lab mates Kushal, Maymol, Masroor, Amit, Rohit, Satish, Vivek, Jyoti, and Debasish for the useful discussions, I had with them regarding my thesis work. Whenever I had some trouble, either personal or academic, they were always there to resolve it. I am really thankful to them for making the life enjoyable, apart from academics.

I will not forget the days spent with A-Wing friends who shared my joys and sorrow equally and stood by me during days of happiness and difficulties. They were always there to give me moral support in every situation in my life here.

I wish to pay my heartfelt regards to my parents, brother, sister and bhabhi for their endless love, encouragement and endurance during my stay at IIT Kanpur. Without them nothing would have been possible.

Finally, I am grateful to the Almighty for what I am today.

Arun Kumar Gupta

Contents

List of Figures

List of Tables

NOMENCLATURE

$a^{\oplus}$	External surface area per unit volume of the particle, m^2/m^3
C	Concentration of reactant gas, moles/m^3
$\bar{C}$	Average concentration of reactant gas, moles/m^3
D	Diffusion co-efficient of reactant gas, m^2/s
K	Equilibrium constant/partitioning coffecient (dimensionless)
K_m	Average mass transfer co-efficient, m/s
L	Length of the packed bed, m
Q	Flow rate, slpm
q	Concentration flux inside the crystal
$\overline{q}$	Volume-averaged Concentration flux over the crystal
$\overline{\overline{q}}$	Volume-averaged Concentration over the entire pellet
r	Radius co-ordinate in the crystal, m
R	Radial co-ordinate in the particles, m
T	Time, s
V	Superficial velocity, m/s
W	Amount of sorbent, gm
z	Axial position in the packed bed, m

Dimensionless Numbers

Pe	Peclet Number
Re	Reynolds number
Sc	Schmidt number
Sh	Sherwood number

Subscript

b	bed

c	crystal
e	effective diffusivity in the pores
g	grain
k	Knudsen
m	molecular
p	pores
z	axial position in the bed

Superscript

*	Dimensionless variables

Greek Symbols

$\in_b$	Bed porosity, dimensionless
α	Intra-particle porosity, dimensionless
ρ_B	Density of zeolite, kg/m^3
ρ	Density of gas, kg/m^3

CHAPTER 1
INTRODUCTION

Atmospheric emission of sulphur dioxide (SO_2) is primarily due to the combustion of fossil fuels such as coal and oil, which contain appreciable quantities of sulphur. Electric power plants are the major industrial users of these fossil fuels [Liu and Liptak, 1980]. On a worldwide perspective, SO_2 emissions are the dominant precursors of acid rain formation. Figure1.1 schematically summarizes typical fate of a SO_2 species in atmosphere, beginning with the emission (anthropogenic and natural sources), transport to atmosphere and chemical and physical transformation leading to acid rain and the formation of aerosols in atmosphere.

There are at present two major widely accepted technologies to control SO_2 emission: wet scrubbing using suitable solvent and dry scrubbing using solid sorbents. Wet methods are generally advantageous over dry methods in terms of capital and operation cost and for the requirement of secondary treatment of wastes produced during the wet method. These processes however suffer from the disadvantages that they are not efficient if SO_2 concentrations are in low levels i.e. parts per million (ppm) and sub ppm. If operating parameters are optimized to improve the removal efficiency for low levels of SO_2 concentrations in the vent gas, the process often becomes non-economical. Further, these processes are generally not energy efficient. As a matter of fact many industries employing wet scrubbing techniques had to be shut down as they failed to keep the emissions within environmental regulations [Flood, 1971].

Dry scrubbing methods using suitable sorbents have been in practice for some time for controlling emission of acid gases such as SO_2. Most of the earlier works done in this area, however, focussed on the aspect of corrosion on the interior sidewalls of the boiler, which recovered waste heat from gases emitted from the coal-based power plants. Among these works Boll and Patel (1961) analyzed the problem of corrosion and gas–side fouling in turbines and boilers by determining the composition of the flue gases. On the same line, Cutler et al. (1980) have analyzed the problem of corrosive gases environment created in fire–side boiler caused by combustion gases and ash particles. With increasing stringent

environmental regulations some studied were carried out only in recent years to develop suitable technology to control SO_2 emissions in low levels.

According to the present environmental regulations the atmospheric concentration of SO_2 emitted by the industries is not allowed to exceed 0.3 ppm on an annual mean concentration basis [Seinfeld and Pandis, 1998]. Dry scrubbing usually employs a packed bed reactor of solid sorbents for the reduction of these emissions. Both non-regenerative as well as regenerative types of materials may be used. Common examples of regenerative type of sorbents are calcium-based sorbents such as calcium carbonate, calcium hydroxide, and calcium acetate. The sorption process is usually carried out at high temperatures. The sorbents, however, suffer from rapid loss of reactivity and incomplete utilization. In the present study sulfation of these commercially available materials following calcination at high temperatures has been carried out. Precipitated $CaCO_3$ is prepared by calcining $CaCO_3$ followed by making Calcium hydroxide solution in water and passing CO_2 gas in the solution. The effect of $CaCl_2$ as an additive in precipitate CaO on SO_2 capturing efficiency is also studied. The effects of various operating variables such as types of sorbents, reaction temperature, SO_2 inlet gas concentrations, sorbent particle size on SO_2 capturing efficiency are ascertained.

In recent times, zeolites have drawn considerable interest in air pollution applications. The studies have shown that a number of air pollutants such as SO_2, NOx and volatile organic compounds (VOCs) may be removed using zeolites [Kopac et al. (1997), Srinivasan et al. (1999), Coker et al. (1999)]. The major advantage of using such type of materials is their ability for regeneration. The reaction temperature is also low. In the present study, SO_2 sorption by 5A commercial zeolites has been carried out. The experimental variables are reaction temperature, SO_2 inlet gas concentrations and particle size. Mathematical models are developed primarily to predict breakthrough characteristics of the sorbent materials. The theoretical analysis takes into account intra-particle diffusion within the mono-pores of CaO based sorbents and bi-pores of zeolites materials. The removal process is mainly due to irreversible reaction in the case of CaO sorbents and reversible adsorption in the case of zeolites adsorbents.

1.1 Objectives:

The main objectives of the present study are as follows:

1) design, fabrication and set-up of an experimental test bench to carry out the experimental study.
2) determining optimal calcination temperature for Ca-based sorbents.
3) determining breakthrough characteristic of the materials under varying operating conditions such as particle diameter, flue gas concentration, amount of sorbent and flow rate of the gas, on the removal of SO_2.
4) preparing the modified $CaCO_3$ by commercial $CaCO_3$ and study the breakthrough characteristic as same defined in steps 2 and 3.
5) study the effect of $CaCl_2$ on modified $CaCO_3$ on the sorption of SO_2 removal process
6) determining the optimal adsorption temperature for Zeolite .
7) determinig the breakthrough characteristic of Zeolite on the adsorption of SO_2 by study the same operating condition as defined in steps 2 and 3 .
8) development of a theoretical analysis and mathematical model for both types of adsorbent.
9) model verification with experimental results for both types of sorbents
10) a detailed breakthrough as well as oxide to sulphate conversion analysis of all the experiments .
11) surface analysis (SEM and BET area measurements).

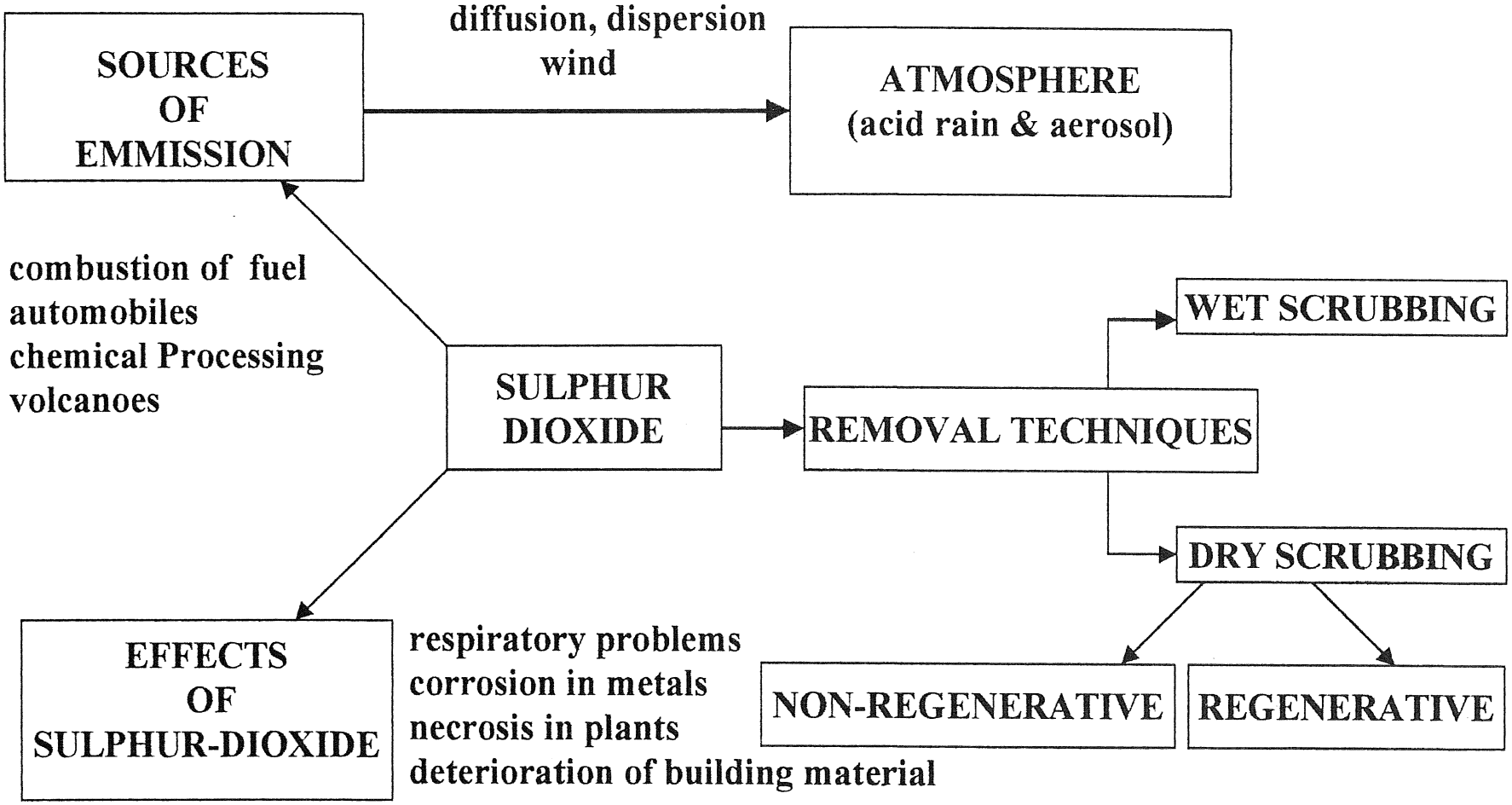

Figure1.1: SO_2: Sources , effects and control techniques

CHAPTER 2
LITERATURE SURVEY

In this chapter, a review of the experimental studies on SO_2 removal by non-regenerative (i.e. CaO) and regenerative (i.e. zeolites and activated carbon) types of sorbents has been presented. A review of various theoretical analysis carried out to understand the mechanism of sorption (in case of CaO) and adsorption (in case of zeolites) of SO_2 has also been presented. The studies done so far range from experimental investigations on change in surface morphology (pores structure) of the sorbents during reaction to ascertaining relative reactivity of various types of sorbents with SO_2 to preparation of sorbents of relatively larger surface area. Various mechanisms have also been proposed in these studies to explain the gas-solid reactions. An attempt has been made in the present work to identify areas, which require further study.

Dogu et al. (1980) have studied the pore structure variation during the gas-solid reaction. He reported that the initial pore structure of the solid reactant has significant effects on the kinetics of reactions. The initial pore size distribution of solid reactant (CaO) was found to influence both the diffusion resistance of the gaseous reactant (SO_2) through the pores and the active surface area of the solid. The pore size distribution of the calcined CaO sample was also found to be affected considerably by the calcination temperature. The authors experimentally determined that the sample calcined at 950 °C had the lowest diffusion resistance and the highest activity for SO_2 removal.

Dogu et al. (1982) studied the breakthrough of SO_2 during reaction with calcined limestone. In the experiment, a sigmoidal type of output SO_2 concentration vs. time profiles was observed. It was also observed that reaction temperature shifted the sigmoidal breakthrough curves to the left. The longest breakthrough time reported was at 720° C and the corresponding maximum sulfate conversion was 35 %.

Jorgensen et al. (1987) studied the reaction between sulfur dioxide and alkaline sorbents carried out in a fixed bed reactor at low temperature. Three major groups of sorbents were tested: clacitic and dolomitic hydrated lime, sodium bicarbonate, and lime stone (calcite and aragonite) mixed with salt additives such as calcium chloride ($CaCl_2$), sodium chloride (NaCl), and nitrates of calcium and sodium. Three major variables were found to influence the SO_2 removal: SO_2 concentration in the flue gas, the dry bulb

temperature of the gas and relative humidity. The most notable result was a significant increase in SO_2 removal using $CaCl_2$ as an additive in an optimum proportion (0.1g/1g). It was believed that the $CaCl_2$ having a high water affinity (hygroscopic) increased the amount of water absorbed by the particle, thereby reducing the SO_2 ash blinding effect. Relative humidity was found to be critical in the removal of SO_2. Lowering of the relative humidity from 70%to 50% stopped virtually all reactions of SO_2 with $CaCO_3$.

Bruce et al. (1989) experimentally compared the SO_2 reactivity of CaO obtained from $CaCO_3$ as well as $Ca(OH)_2$. The variations of porosity and conversion during the course of the reaction were determined and conclusions were drawn that CaO obtained from $Ca(OH)_2$ gave a superior performance than that from limestone.

Yiannis et al. (1993) have studied the effectiveness of commercially available calcium magnesium acetate from cryogenic technology (Aldrich) (CMA) as sulphur capturing agent and explored the possibility of using CMA as a " dry scrubbing" medium in boiler injection. In addition to versatility of the water–soluble CMA for being relatively easily sprayed during dry injection and therefore, eliminating grinding costs, there was additional useful property associated with CMA. CMA exhibited ability to form highly cenospheric, "popcorn"-like oxide particles on heating at high temperature (750-1150°C). These cenospheres posses thin porous walls with blowholes that enable penetration of SO_2 in the interior of the particle and promotes complete utilization of the sorbent particles. The utilization of CMA depended on the cenospher wall thickness rather than the particle size and thus, outperformed other sorbents regardless of the size of resulting oxide particles.

Mahuli et al. (1997) developed a new method to prepare $CaCO_3$, which on calcination produced CaO of relatively larger surface area resulting in the surfate conversion of 70-75% compared to 30-35% for commercial sorbents under identical conditions. The sulfation characteristics were investigated at high temperatures: 900, 1000, and 1080°C and short contact times (20-600 ms) using small particle sizes (< 5μm) in entrained flow reactor. The modified carbonate was prepared by carbonation-precipitation in a slurry bubble column reactor using different surfactants in small concentration of about 2% by weight. The carbonate used in this study was prepared by bubbling CO_2 at a flowrate of 2.25 slpm for 20 min through a $Ca(OH)_2$ suspension (2.25wt.% solid concentration). The post-reaction slurry was filtered and dried in a vacuum oven at 75°C for 24 hr. The calcination and sulfation studies were performed at a fixed reaction temperature. Calcination was carried out under

inert N_2 environment. The gas composition for the sulfation runs was maintained at 5.45% O_2, 3900 ppmv SO_2 and balance N_2. The sulfation characteristic of this modified carbonate (MC) was compared with the commercial Linwood carbonate (LC) and a modified hydroxide (MH). It was observed that in spite of the pore properties of MH and MC being similar, the modified carbonate reactivity was much higher than that of MH. This was attributed to the evolution of pore structure. It was observed that, under conditions of interest an optimum pore-size range existed between 50-200 ^{0}A, which provided sufficient surface area for the sulfation reaction without causing rapid pore filling and pore-mouth plugging. The development of ppt-CaO having larger surface area has also been reported elsewhere [Ghosh-Ddostidar et al., 1996].

In a recent work, Dasgupta et al. (2001) has carried out a combined experimental and theoretical study to understand the kinetics and mechanism of SO_2 removal by CaO sorbents. The breakthrough characteristics and sulphate conversion analysis were carried out for the sorption process. Mathematical models were developed for non-porous as well as porous materials. It was found that the model assuming a porous structure of CaO explained the breakthrough characteristics, even if the sorbent materials had small surface area (~1-10 m^2/g). It was observed that sorption process was best suited for low concentration levels of SO_2 i.e. in ppm and sub ppm. The favorable operating temperature for SO_2-CaO reactions was determined to be 950°C. Shorter breakthrough time and lower sulphate conversion at above 1000°C were attributed to breaking of the pore structure of the sorbent. No appreciable reaction was observed below 750°C. It was also observed that the particle of smaller diameter resulted in longer breakthrough and higher conversion. However, the pressure drop and particle agglomeration in the packed bed increased with decrease in the particle size.

A literature survey shows that not much work has been done on the application of zeolites in control of SO_2. Only in the past few years, some of the works have beginning to emerge in this area, as environmental laws become stringent.

Kopac et al. (1997) have studied adsorption behavior of SO_2 on commercially available molecular sieves (5A, 4A and AW300 Zeolites). The experiments were carried out in the temperature range of 523-718 K. The adsorption equilibrium parameters were obtained from non-isobaric pulse chromatographic experiments and using a method of "moment-analysis". It was found that the equilibrium or partition constant decreased

considerably with increase in the temperature. Fro example, in the case of SO_2 adsorption on 5A molecular sieve, an increase of temperature from 523K to 673K resulted in decrease of the equilibrium constant from approximately 150 to 12. It was also found that the adsorption of SO_2 by various adsorbents used were found to decrease in the order of AW300 > 4A >5A. The heats of adsorption of SO_2 on these zeolites determined experimentally were found to be in the order of 10.0 kcal/mol.

In another study, Kopac et al. (1998) studied the adsorption behavior of SO_2 on 13X molecular sieve and activated carbon in a temperature range of 353-453K and 523-673K, respectively. The exothermic heats of adsorption of SO_2 on activated carbon and 13X molecular sieve 13X were determined as 8.99 and 12.4 kcal mol^{-1}, respectively.

Tsibranska et al. (2000) developed a mathematical model for adsorption of SO_2 on natural clinoptilolite. These materials are bi-porous in nature having macro and micro pores, similar to zeolites molecular sieves. The model accounted for macro-pore diffusion, micro-particles size distribution, concentration dependent micro-pores diffusivity and nonlinear adsorption equilibrium on the micro-particle surface. The external mass transfer in the film around the particles and axial dispersion in the bed were also taken into account. The kinetic and equilibrium parameters of the model were extracted from the experimental data on breakthrough. The nature of micro particle size distribution was independently experimentally determined from SEM analysis. A good agreement between the experimental data and model results was obtained for larger pellets where macro-pore diffusion control was of greater importance. On the other hand, in micro-particles where micro-pore diffusion is rate limiting, the model prediction was observed to be less satisfactory.

In this work, experimental studies on non-regenerative sorbents carried out by Dasgupta (2001) have been extended to include other types of Ca-based sorbents. The especially prepared precipitated calcium carbonate sorbents have also been tested for their sorption performance. The focus of the present work is on the application of regenerative type of sorbents like zeolites in control of SO_2, which have shown potential in adsorbing several air pollutant gases, such as SO_2, NOx, and volatile organic compounds (VOCs). Extensive theoretical and experimental studies have been carried out in this work to determine the breakthrough characteristic of 5A zeolite molecular-sieve materials during the adsorption of SO_2.

CHAPTER 3
THEORETICAL ANALYSIS

3.1 Non-regenerative sorbent (CaO):

In non-regenerative types of the sorbents (CaO), the removal of SO_2 takes place through two reaction steps, a) calcination of the sorbent materials ($CaCO_3$) to produce CaO of higher surface area and porosity, b) reaction with SO_2 (sulfation) in the presence of O_2 to form the higher molar volume solid product, $CaSO_4$. These steps are represented by the following chemical reactions:

a. $Ca(OH)_2 \longrightarrow CaO + H_2O$

$CaCO_3 \longrightarrow CaO + CO_2$

b. $CaO + SO_2 + 1/2\ O_2 \longrightarrow CaSO_4$

The commercially available limestone is generally non-porous and possesses a very low surface area. However, on calcinations it yields a porous CaO, which is responsible for SO_2 capture. CaO reacts with SO_2 in the presence of oxygen to form a solid product, $CaSO_4$. The overall rate of reaction of this process is mainly dependent on $CaSO_4$ formation on CaO. The molar volume of $CaSO_4$ is sufficiently large enough so as to usually plug the pores prior to complete utilization of the sorbent. Pore plugging and thus the loss of porosity of the particle are the dominant cause of premature termination and incomplete utilization of the sorbent.

The mathematical models for SO_2 removal by the sorbent materials assuming non-porous and porous structure have been described in details by Dasgupta (2001). Figures 3.1 and 3.2 are the schematic representations of the overall sorption process in a non-porous and porous particle, respectively. In the porous-model, a particle or grain of CaO is assumed to consist of spherical sub-grains of uniform size separated by pores through which the reacting gases diffuse. As the reaction proceeds, a shell of the reaction products is gradually formed on the surface of the sub-grains, which inturn offers resistance to the diffusion of SO_2 within the pores.

The details of the mathematical formulation can be obtained from the aforementioned work [Dasgupta, 2001]. In brief, the theoretical analysis for the model assuming non-porous structures consisted of a species balance in the packed bed of CaO,

in the product sold layers of $CaSO_4$ and on the surface of the un-reacted CaO. The variation in the radius of the reaction front of CaO was also incorporated in the analysis. It was assumed that an isothermal plug flow existed in the bed. The pressure drop was assumed to be negligible and there was no variation in the fluid velocity along the length of the bed.

The theoretical analysis assuming a porous structure incorporates a species balance within the pores or sub-grains of CaO (diffusion of gases within the pores), in addition to that in the packed bed and on the surface of the material. As pointed out earlier in the text (Chapter 2), the model assuming a porous structure could explain the breakthrough characteristics of CaO over the entire experimental conditions used in the work.

3.2 Regenerative sorbent (zeolite):

Zeolites are crystalline aluminosilicates of alkali or alkali earth elements such as sodium, potassium, and calcium, represented by the stoichiometry:

$$M_{x/n}\,[(AlO_2)\ x\ (SiO_2)\ y]\ z\ H_2O$$

where, x is the integer with y/x equal to or greater than 1, n is the valence of cation M, and z is the number of water molecules in each unit cell called sodalite cage [Yang et al.1997]. More than 150 types of zeolite have been synthesized to-date. These are designated by a letter or groups of letters: type A, X, Y, ZSM, and so on, depending upon the structure of the crystals. When the units are linked through four member rings zeolite of type A is formed. In the present work, SO_2 breakthrough analysis has been carried out on 5A zeolite. Type A Zeolite contains 24 tetrahedral, 12 AlO_4 and 12 SiO_4. When fully hydrated, 27 water molecules are contained in the central cage or cavity of the unit cell, and in eight smaller sodalite cages.

Zeolite solids are available in the pellets form, and these pellets are made by compressing zeolite crystals together, usually with a small percentage of binder to join the crystals together [Do et al.1998]. This results in a porous structures having macro and micro pores. Figure 3.3 is the schematic representation of such a biporous particle. The crystals are of the order of 0.1 to 1 micron, and the zeolite pellets are of that of 1 mm. The void between the microparticle contributes to the micro-pores of the particle. These pores act as conduit to transport molecules from the surrounding in to the interior of the particle. Once inside the particle, molecules adsorb at the pore mouth of the micropores and thence

the adsorbed species diffuse into the interior of the crystal. Micro pores within the crystal provide the adsorption space to accommodate adsorbate molecules. The diffusion process in the macropore and the micropore follows the combination of the molecular and Knudsen mechanisms while the diffusion process inside the crystal follows an intra crystalline diffusion mechanism.

The mathematical model developed to explain the breakthrough of SO_2 in the packed bed consisting of zeolite pellets is based on the following assumptions:

1) The temperature is uniform throughout the bed, pellet and crystals
2) Negligible pressure drop along the length of the bed
3) There is constant fluid velocity through out the bed
4) Linear adsorption isotherm

3.2.a. ***Mass Balance in the packed bed reactor:***

Since the SO_2 concentration level is in sub-ppm level, therefore SO_2 exothermic heat of absorption is negligible and isothermal condition can be assumed [Yang et al, 1997]. Consider an isothermal plug flow system in a packed bed of spherical pellets. By making a SO_2 mass balance in the packed bed of porosity ε_b, the following equation is obtained:

$$\frac{\partial C_b}{\partial t} + \frac{V_z}{\epsilon_b}\frac{\partial C_b}{\partial z} = \frac{D_z}{\epsilon_b}\frac{\partial^2 C_b}{\partial z^2} - \frac{1}{\epsilon_b}a^* f(z) \qquad (3.2.1)$$

A B C D

Here, A = Transient term, B = Dispersion term, C = Convective term, D = Diffusion flux term at the outer surface of the pellet and represents diffusion of the gas from the bulk into the macropores of the zeolite pellets.

In equation (3.2.1), $f(z) = K_m(C_b - C_p\big|_{R=R_p})$ (3.2.2)

C_b = concentration of reactant gas at an arbitrary location z in the bed.

D_z = axial dispersion co-efficient in the packed bed.

V_z = superficial velocity

a^* = external surface area per unit volume of the pellet $= \frac{3(1-\epsilon_b)}{R_p}$

K_m = average mass transfer co-efficient

C_p = concentration of the reactant gas in the macropores of the pellet

Rp = radius of the pellet

z = axial distance along the bed

The boundary conditions for the above equation are

at $t = 0$, $C_b = 0$ (3.2.3)

at $t > 0$, $z = 0$ $C_b = C_{b0}$ (3.2.4)

$z = L$ $\frac{\partial C_b}{\partial z} = 0$ (3.2.5)

3.2.b. ***Mass balance at any location R within the macro-pore volume of the pellet located at a distance of z in the bed:***

Considering radial diffusion within the pore volume and adsorption at the pore mouth of the crystals, the following equation is obtained:

$$\alpha \frac{\partial C_p}{\partial t} - \frac{1}{R^2}\frac{\partial (R^2 N_R)}{\partial R} + 3(1-\alpha)\frac{\partial \bar{q}}{\partial t} = 0 \qquad (3.2.6)$$

E F G

E = Transient term, F = Diffusion flux in the radial direction of the pellet, G = Rate of adsorption at the pore-mouth (or opening) of the crystals.

Here, α = void fraction of the macro-pores

Cp= gas concentration in the macropores of pellet

N_R = molar diffusion flux in the radial direction of the pellet

q = concentration of the adsorbate inside the crystal

$\bar{q}$ = average amount adsorbed at a radial location R within the pellet

3.2.c. ***Mass balance at any location r within the micro-pore of the crystal located at a distance of R in the pellet:***

Mass balance in the crystal is given by the following solid diffusion equation:

$$\frac{\partial q}{\partial t} = \frac{D_c}{r^2}\frac{\partial (r^2 \partial q / \partial r)}{\partial r} \qquad (3.2.7)$$

where D_c = diffusivity of the adsorbate within the crystal

The governing equations (3.2.1), (3.2.6) and (3.2.7) form the basis of the model developed in this study for predicting the adsorbents performance, especially breakthrough, in the

bed. As these equations are coupled partial differential equations (independent variables being time, axial and radial directions, both in r and R), an approach is adopted in the present work to simplify numerical computations and significantly reduce the CPU time. Essentially, in this approach radial (r and R) concentration profiles within the solid pores (both macro and micro) are averaged and then, the average gas phase concentrations within the pores of the pellets and the average adsorbate phase concentrations within the crystals are determined [Yang et al.1997, Gupta, 2002]. The salient advantage of this mathematical approximation is the reduction of 2nd order PDEs to 1st order PDE with variation only in z direction. Moreover, the number of the equations is reduced to two. The detailed computational steps are as follows:

First, the particle volume averaged quantities are calculated as follows:

$$\overline{C}_p = \frac{3}{R_p^3}\int C_p R^2 dR \tag{3.2.8}$$

$$\overline{q} = \frac{3}{R_c^3}\int q r^2 dr \tag{3.2.9}$$

where, the terms on the left hand side of the expressions are the volume average surface concentration in the pores and within the crystals (radius R_c) , respectively.

Second, by integrating equation (3.2.6) with respect to R and using the volume averaged quantities the following equation is obtained:

$$\alpha\frac{\partial \overline{C}_p}{\partial t} + \frac{3}{R_P} N_{R|R=R_P} + 3(1-\alpha)\frac{\partial \overline{\overline{q}}}{\partial t} = 0 \tag{3.2.10}$$

where, $\overline{C}_p$=Average concentration of reactant gas in the macropores of the pellet

$\overline{\overline{q}}$ = Averaged concentration of the adsorbate over the entire pellet and defined as volume average concentration:

$$\overline{\overline{q}} = \frac{3}{R_p^3}\int \overline{q} R^2 dR \tag{3.2.11}$$

The required initial and boundary conditions for Eq. (3.2.10) are as follows:

$$\text{At } t = 0, \quad \overline{C}_p = 0 \text{ and } \overline{\overline{q}} = 0 \tag{3.2.12}$$

and t >0, at R = 0 $$\frac{\partial \overline{C_p}}{\partial R} = 0 \qquad (3.2.13)$$

In the integration of Eq. (3.2.6), the following boundary conditions were used: $N_R = 0$ at R = 0, due to symmetricity. At the surface ($R = R_p$), the diffusion flux into or out of the pores, $N_R\big|_{R=R_p}$ is given by the boundary condition in pellet:

$$N_{R|R=R_p} = K_m(C_b - C_{P|R=R_p}) \qquad (3.2.14)$$

Substituting equation (3.2.14) in equation (3.2.10) we obtain

$$\frac{\partial \overline{C_p}}{\partial t} - \frac{3}{R_p}\frac{K_m}{\alpha}(C_b - C_{P|R=R_p}) + \frac{3(1-\alpha)}{\alpha}\frac{\partial \overline{\overline{q}}}{\partial t} = 0 \qquad (3.2.15)$$

Third, parabolic concentration profiles for Cp and q were assumed within a pellet as follows:

$$C_p = C + DR^2 \qquad (3.2.16)$$

$$q = A + Br^2 \qquad (3.2.17)$$

Fourth, this has been mathematically shown that a parabolic concentration profile q(r) combined with the solid diffusion equation (3.2.7) leads to the following linear driving force (LDF) approximated equation [Yang et al.1997]:

$$\frac{\partial \bar{q}}{\partial t} = \frac{15D_c}{R_c^2}(q_{|r=R_c} - \bar{q}) \qquad (3.2.18)$$

Taking the volume–average of Eq. (3.2.18) over the entire pellet we obtain

$$\frac{\partial \overline{\bar{q}}}{\partial t} = \frac{15D_c}{R_c^2}(\bar{q}_{|r=R_c} - \overline{\bar{q}}) \qquad (3.2.19)$$

where, $q_{|r\ Rc}$ is in equilibrium with C_p at location R in the pellet.

Therefore, assuming a linear isotherm for the gas adsorbed at the pore mouth, the following relationship between the adsorbate within the crystal and the gas phase in macro-pore is assumed:

$$q_{|r=R_c} = KC_p \qquad (3.2.20)$$

or, $$\bar{q}_{|r\ R_c} = K\overline{C_p} \qquad (3.2.21)$$

Here, K is the adsorption equilibrium constant/partitioning coefficient between macro-pores and crystal surface.

The volume-averaged concentration $(\overline{q})$ over the crystal is obtained by averaging equation (3.2.17) and using equation (3.2.9) as follows:

$$\overline{q} = A + \frac{3}{5} B R_c^2 \tag{3.2.22}$$

Similarly, the volume-averaged concentration over the pellet is obtained by averaging equation (3.2.16) and using Eq. (3.2.8):

$$\overline{C}_p = C + \frac{3}{5} D R_p^2 \tag{3.2.23}$$

From equation (3.2.16) the concentration at $R = R_p$ is evaluated as:

$$C_{p|R=R_p} = C + D R_p^2 \tag{3.2.24}$$

Combining equations (3.2.23) and (3.2.24) C and D are calculated as:

$$D = \frac{5}{2 R_p^2} [C_{p|R=R_p} - \overline{C}_p] \tag{3.2.25}$$

and

$$C = (\frac{5}{2} \overline{C}_p - \frac{3}{2} C_{p|R=R_p}) \tag{3.2.26}$$

Substituting the values of C and D in equation (3.2.16) we obtain

$$C_p = (\frac{5}{2} \overline{C}_p - \frac{3}{2} C_{p|R=R_p}) + \frac{5}{2 R_p^2} [C_{p|R=R_p} - \overline{C}_p] R^2 \tag{3.2.27}$$

Differentiation of (3.2.27) with respect to R we obtain

$$(D_p \frac{\partial C_p}{\partial R})_{|R=R_p} = \frac{5}{R_p} [C_{p|R=R_p} - \overline{C}_p] \tag{3.2.28}$$

The boundary condition at the pellet surface Eq. (3.2.14) can be written as:

$$(D_p \frac{\partial C_p}{\partial R})_{|R=R_p} = K_m (C_b - C_{p|R=R_p}) \tag{3.2.29}$$

Combining equations (3.2.28) and (3.2.29) we obtain

$$K_m (C_b - C_{p|R=R_p}) = \frac{5}{R_p} [C_{p|R=R_p} - \overline{C}_p] \tag{3.2.30}$$

Rearranging equation (3.2.30) we obtain

$$C_{p|R=R_p} = \frac{(K_m C_b + \frac{5 D_p}{R_p} \overline{C_p})}{(K_m + \frac{5 D_p}{R_p})} \quad (3.2.31)$$

Substituting equations (3.2.16) and (3.2.17) in equation (3.2.20) to obtain

$$(A + Br^2)_{|r=R_c} = K(C + DR^2) \quad (3.2.32)$$

Comparing term by term in equation (3.2.32), we obtain

$$A = KC \quad (3.2.33)$$

$$BR_c^2 = KDR^2 \quad (3.2.34)$$

Substituting the values of C and D from equations (3.2.26) and (3.2. 25) in equations (3.2.33) and (3.2.34), A and B are calculated as follows:

$$A = K(\frac{5}{2}\overline{C_p} - \frac{3}{2}C_{p|R=R_p}) \quad (3.2.35)$$

$$B = \frac{K \frac{5}{2R_p^2}[C_{p|R=R_p} - \overline{C_p}]R^2}{R_c^2} \quad (3.2.36)$$

On integration of equation (3.2.11) we obtain an expression for $\overline{\overline{q}}$ as follows:

$$\overline{\overline{q}} = K[C + \frac{9}{25}DR_p^2] \quad (3.2.37)$$

Substituting the values of C and D from equations (3.2.25) and (3.2.26) we obtain an expression for q:

$$\overline{\overline{q}} = \frac{K}{5}[8\overline{C_p} - 3C_{p|R=R_p}] \quad (3.2.38)$$

Finally, substituting equation (3.2.38) and equation (3.2.21) in equation (3.2.19), an expression for the mass balance of the average adsorbate phase is obtained as follows:

$$\frac{\partial \overline{\overline{q}}}{\partial t} = \frac{15 D_e}{R_c^2}[K\overline{C_p} - \frac{K}{5}(8\overline{C_p} - 3C_{p|R=R_p}) \quad (3.2.39)$$

The equation is further rearranged by substituting the value of $Cp_{|R=Rp}$ from equation (3.2.31) in equation (3.2.39) to obtain

$$\frac{\partial \overline{q}}{\partial t} = \frac{9 D_c K K_m}{R_c^2 (K_m + \frac{5 D_p}{R_p})} (C_b - \overline{C_p}) \tag{3.2.40}$$

The above equation is substituted in equation (3.2.15) to obtain a governing equation for the average pore concentration:

$$\frac{\partial \overline{C}_p}{\partial t} + \frac{(C_b - \overline{C}_p) K_m}{(K_m + \frac{5 D_p}{R_p})\alpha} [\frac{27 D_C K (1-\alpha)}{R_C^2} - \frac{15 D_p}{R_p^2}] = 0 \tag{3.2.41}$$

Similarly, on substitution equation (3.2.2) and equation (3.2.31) in equation (3.2.1), the equivalent simplified governing equation for the bed is obtained as follows:

$$\frac{\partial C_b}{\partial t} + \frac{V_z}{\epsilon_b} \frac{\partial C_b}{\partial z} = \frac{D_z}{\epsilon_b} \frac{\partial^2 C_b}{\partial z^2} - \frac{15(1-\epsilon_b) K_m D_p (C_b - \overline{C}_p)}{\epsilon_b R_p^2 (K_m + \frac{5 D_p}{R_p})} \tag{3.2.42}$$

The 2nd order PDE equations (3.2.41) and (3.2.42) are the governing equations to predict the breakthrough characteristics of the bi-porous adsorbents like zeolite in a fixed packed bed. Thus, by assuming the volume-averaged quantities and parabolic concentration profiles in the macro and micro pores, the number of partial differential equation reduced 3 to 2, which reduces the computational work/time to a large extent.

3.3 Non-dimensionalisation of governing equations and Initial and Boundary conditions:

The following dimensionless variables are used:

Bulk gas concentration: $C^*_b = \frac{C_b}{C_{b0}}$; Time: $t^* = \frac{t}{t_{residence}}, t_{residence} = \frac{l}{V_z}$, Distance in Axial Direction: $z^* = \frac{z}{l}$, Radius of the pellet, $R^* = \frac{R}{R_p}$

Introducing the dimensionless variables in governing equation (3.2.42), the following non-dimensionalised equation is obtained:

$$\frac{\partial C_b^*}{\partial t^*} = \gamma \frac{\partial C_b^*}{\partial z^*} + \frac{1}{Pe} \frac{\partial^2 C_b^*}{\partial z^{*2}} - \eta (C_b^* - \overline{C_p^*}) \tag{3.3.1}$$

where the constant terms are defined as

$$\gamma = -\frac{1}{\epsilon_b}, \qquad Pe = \frac{\epsilon_b V_z l}{D_z}, \qquad \eta = \frac{15(1-\epsilon_b)K_m D_p l}{\epsilon_b R_p^2 V_z (K_m + \frac{5D_p}{R_p})}$$

From the above expressions, it is easy to infer that *Pe* is nothing but the Peclet number, which compares convective flux to the flux by dispersion in the packed bed. Similarly η can be construed as the resistance to the overall mass transfer determined by film mass transfer coefficient and diffusivity in the macro-pore of the pellet.

The non-dimensionalized boundary conditions are:

at t*=0 $\quad C_b^* = 0$

at t>0 $\quad$ Z*=0 $\quad C_b^* = 1$

$$\text{Z*=1} \quad \frac{\partial C_b^*}{\partial z^*} = 0$$

To non-dimensionlize equation (3.2.41), the following variables are used:

Average gas concentration inside the pellet, $\overline{C}_p^* = \frac{\overline{C}_p}{C_{b0}}$; Dimensionless time constant:

$$t^* = \frac{t}{(R_p^2 / D_p)}.$$

The non-dimensionlized form obtained is as follows:

$$\frac{\partial \overline{C_p^*}}{\partial t^*} + \delta (C_b^* - \overline{C_p^*}) = 0 \qquad (3.3.2)$$

where the constant coefficient δ is defined as

$$\delta = \frac{K_m R_p^2}{(K_m + \frac{5D_p}{R_p})\alpha D_p} [\frac{27 D_c K (1-\alpha)}{R_C^2} - \frac{15 D_p}{R_p^2}]$$

A close inspection of the above coefficient δ reveals that it is a product of two terms. While the first term includes the effect of film mass transfer coefficient and diffusivity within the pellet, the second term contains the adsorption equilibrium constant. It is important to point out that for a zeolite to be a sink for the adsorbing gas, the second term

must be negative. Thus, for a zeoilte-SO_2 system, the above term puts a constraint on, or in other words, defines a upper limit for the value of equilibrium constant K as:

$$K < \frac{15 D_p R_c^2}{R_p^2 27 D_c (1-\alpha)} \qquad (3.3.3)$$

For a given zeolite pellet and the adsorbing gas, the terms on the right hand side are known. Assuming Rp = 0.16 mm, Rc = 2x10^{-6} mm, De = 2.54x10^{-6} m^2/s, Dc = 1x10^{-12} m^2/s, and α = 0.64, K is evaluated to be 613.

The non-dimensionlized initial and boundary conditions are as follows:

$t^* = 0$ $\qquad \overline{C}_p^* = 0$

t*>0 R*=0 $\qquad \frac{\partial \overline{C}_p^*}{\partial R^*} = 0$

Equations (3.3.1) and (3.3.2) are the non-dimensionlized forms of the governing equations that are numerically solved in the present work to predict breakthrough times in a packed fixed bed consisting of bi-porous zeolite adsorbents.

3.4 Numerical solution Technique:

For the gas solid sorption reaction taking place we have two partial differential equations 3.3.1 and 3.3.2 containing two dependent variables C_b^* and $\overline{C}_p^*$ as a function of time and axial location. These equations are solved simultaneously by finite difference formulation using the NAG Fortran library. The Fortran codes are produced in the appendix.

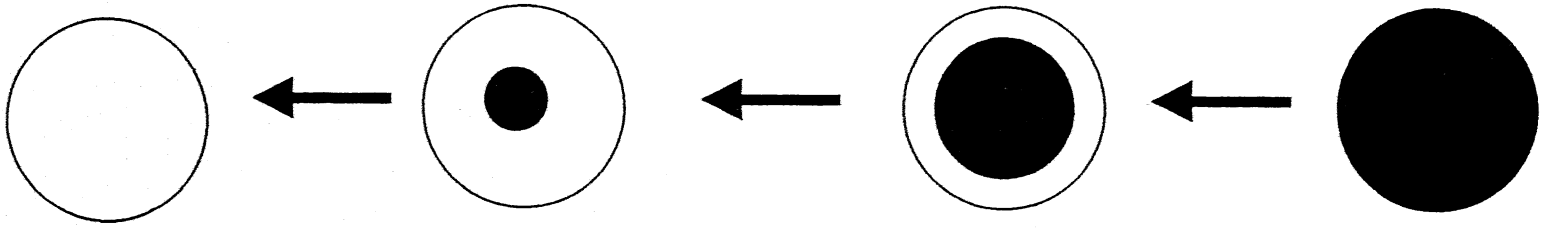

Periphery
(completed reacted grain)
($CaSO_4$ deposited)

Core of particle
(no reaction)
(CaO)

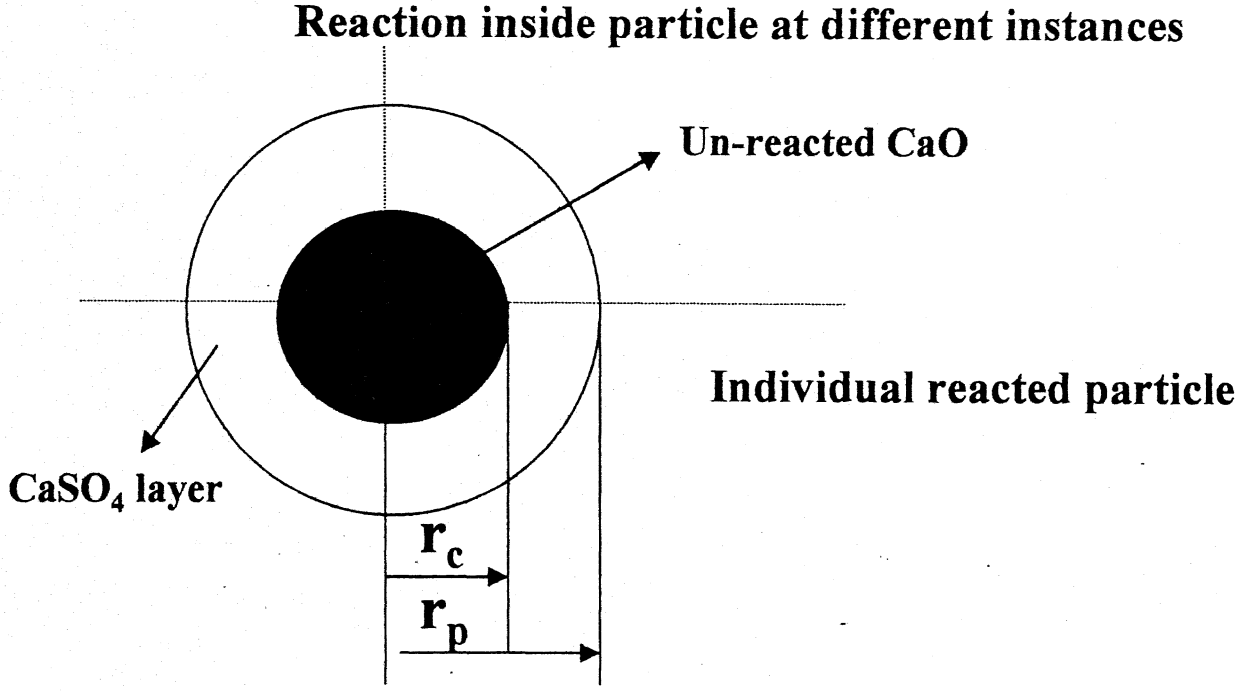

Figure 3.1 : Schematic diagram of sorption mechanism underlying non-porous model

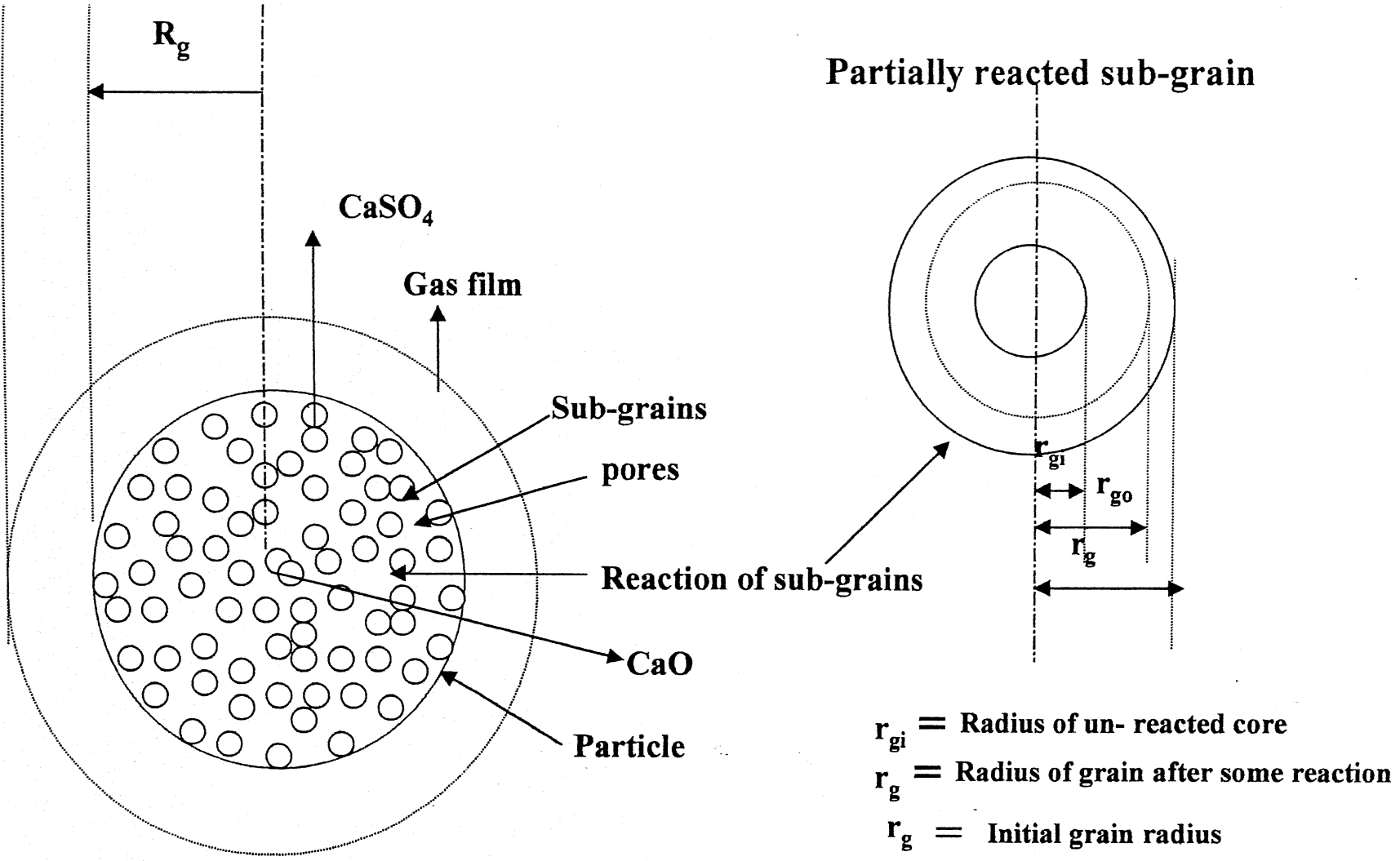

Figure 3.2: Schematic diagram of sorption mechanism underlying porous model

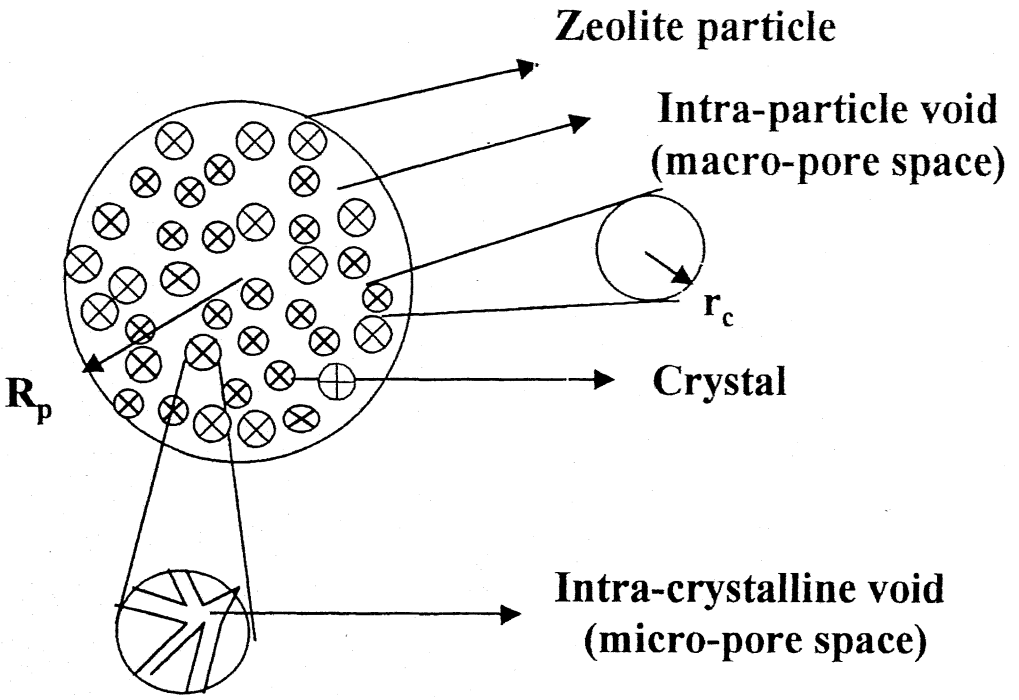

Figure 3.3 Schematic diagram of a bi-porous zeolite pellet

CHAPTER 4
EXPERIMENTAL STUDIES

Experiments were carried out under several operating conditions such as temperature, flow rate, particle diameter, amount of CaO and zeolite, and the inlet SO_2 concentration to study SO_2 sorption or adsorption. This chapter describes the experimental set-up and the experimental procedure.

The experimental set-up used is the same as that designed and developed by Dasgupta (2001), except for a few modifications. A separate set-up was designed and developed to prepare precipitated CaO.

4.1 Experimental Set up:

The experimental set-up used in the process consisted of three sections as shown in Figure 4.1: a) gas mixing section, b) test section, and c) analytical section. In the gas mixing section two electronic mass flow controllers (Model PSFIC-I, Bronkhorst, Netherlands) were used to control and regulate the flow of SO_2, O_2 or N_2. A mixture of gases (SO_2, O_2 or N_2) of the desired concentration was prepared by mixing the two individual streams in a gas-mixing chamber (135 mm long and 25 mm I.D.) made of stainless steel tube. The O_2 stream was purified using silica gel purifier to removal moisture in the gas. The gas-mixing chamber can be bypassed directly to the G.C for calibration as well as measurement of the inlet concentration of the gas mixture entering the reactor.

The test section consists of a reactor and a furnace with a proportional temperature controller. An inconel reactor having an internal diameter 14mm and length 150mm was used for the reaction of the sorbents with the inlet gas from the gas mixing section. The reactor was vertically mounted co-axially in a 200mm long tubular furnace. The top end of the reactor was connected to the gas line using 1/4 " swage lock fittings and specially mounted unions made of SS. Power to the furnace was supplied through a 15 A variac. The temperature of the furnace was controlled using a proportional temperature controller (Blue Bell, Kanpur). The temperature in the reactor was measured using a chromel-alumel thermocouple inserted in a S.S thermo well (O.D 3mm). The effluent gas stream from the reactor was passed to the analytical section. A manometer

was also connected to the two ends of the reactor to measure the pressure drop across the sorbent bed. The analytical section consisted of a gas chromatography (GC) connected to a data station. A computer was connected to the data station to store the chromatogram and the peak areas. Thermal conductivity detector (TCD) was used to detect and measure SO_2 concentration in the gas stream. The calcination of the sorbent materials was done in a vertical quartz tube (50mm ID) having a purge arrangement. The calcination tube was vertically mounted in a movable furnace having diameter 35 cm and length 54cm. The temperature of the furnace was controlled by a proportional temperature controller (Model 961 HLTC, ionelectricals, Mumbai). The furnace temperature was measured using chromel-alumel thermocouple (Century Pvt. Ltd., Kanpur) of 12mm diameter and 25 mm length. Power to the furnace was supplied through a 15 A variac.

Precipitation of $CaCO_3$ was done in a Pyrex reactor (35mm ID x 360 mm L). A PVC pipe with several small pore openings (~0.025 mm diameter) was used for bubbling CO_2 in the aqueous slurry of $Ca(OH)_2$. The flow of CO_2 was controlled by a needle valve and measured by a rotameter (0-5 slpm). Mixing of slurry was done with the help of a magnetic stirrer (Remi equipments, Kanpur) using Teflon needle. The precipitated solution was filtered using Whatman filter paper of 1 qualitative, 125mm-diameter circles. Filtered materials were dried in an oven (Mahendra Scientific Instrument Mfg., Kanpur).

Activation of zeolites was done in a vacuum oven. Vacuum (650mm) was created with the help of a vacuum pump (Vacnik Rotary Vacuum pump, Model V2M5, Lawrence & Mayo (India Pvt. Ltd., Delhi).

4.2 Experimental Procedure:

All calcium based sorbents such as calcium carbonate ($CaCO_3$), calcium hydroxide ($Ca(OH)_2$), calcium acetate(CaA), and calcium magnesium acetate (CMA) as well as molecular sieve zeolite (type 5A) were obtained from Merck Co, Germany.

To obtain CaO form $CaCO_3$, $Ca(OH)_2$ and $Ca(CH_3COOH)_2$ powders, calcination was carried out under inert N_2 environment with a flow rate of 1.6 slpm at 750, 850, 950, and 1050°C in a vertical, movable quartz furnace (refer Figure 4.2). The optimum calcination temperature for $CaCO_3$ and $Ca(OH)_2$ was determined to be 950°C, while for the calcinations of $Ca(CH_3COOH)_2$ a temperature of 1050°C was chosen. The

calcinations time in each case was 4 hours. The calcinations temperatures and time were determined after repeat of experiments (trial and error) so as to be consistent with stoichiomentric calculations for weight loss due to the evolution of CO_2.

The ppt-carbonate was prepared by carbonation-precipitation method in a slurry bubble column reactor (refer Figure 4.3). First, an aqueous slurry of calcium hydroxide was prepared by mixing a known quantity of CaO (2.5 gm) in approximately 130 cc of distilled water. The amount of water was used based on the reported solubility data for CaO in water [Guthrie et al.1901]. Calcium lignosulfonate was used as a surfactant medium in small quantity (2wt.% based on the weight of $Ca(OH)_2$)) to uniformly disperse suspended calcium hydroxide in the slurry at 25°C held constant with the aid of a thermostat. Thereafter, carbonation was carried out by bubbling CO_2 at a steady flow rate of 100 cc/min for 4 hr through the $Ca(OH)_2$ slurry. The post-reaction slurry was filtered by #1 filter paper and dried in the oven at 75°C for 24 hr. In the case of $CaCl_2$ used as an additive in the sorbents, $CaCl_2$ was added to the filtered sample already dried for 10hr in the oven. Thereafter, the solid mixture was further dried for 14 hr before used for the sulfonation reaction.

The zeolite materials obtained in the form of cylindrical pellets were crushed and sieved. The fractions investigated in this study comprised three size ranges: 1.115 mm, 0.16mm, and 0.385 mm. N_2 was used as a carrier gas. Rest of the operating parameters were kept the same as used in the case of CaO

The required quantity of the sorbents (either CaO or zeolite) was then fed to the reactor. The reactor was heated to the desired reaction temperature and further kept at that temperature for 2 hours so that the system was stabilized and a uniform temperature existed in the bed. The flow rate of the gas was adjusted using MFC.

Mesh and quartz wools were put at both ends of the reactor tube so as to prevent any carry over of the sorbent. The thermo well for holding thermocouple was then placed co-axially in the center of the reactor tube. The gas line was connected using swage lock fittings. First, O_2 was allowed to pass through the reactor at a desired flow rate controlled by MFC. The identical flow rate reading by the rotameter installed at the downstream end of the tube, as that by MFC implied that the set up was free from any gas leakage. The sorbent was then heated to the required temperature. The concentration of the inlet

gaseous mixture in the line bypassing the reactor was measured by GC, prior to the start of the sorption reaction. The total experimental time included 2 hrs to pre-heat the bed to the desired temperature and 2 hours to stabilize. The reaction time varied between 2 and 6 hrs depending upon the operating conditions including the type of sorbents, flow rates and the amount used. The concentration of exit gas from the reactor was measured by the GC.

4.3 Product Analysis:

The product gas was analyzed by gas chromatography using Porapak Q-column. The column (length 6-inch, I.D. 2.0mm) was used to separate O_2 and SO_2 using thermal conductivity detector (Model 5700.Nucon). Hydrogen at 22 ml/min was used as a carrier gas. The filament current was kept at 246 mA. The temperatures of the injector, detector and oven were maintained constant at 150°C, 160° C and 120° C, respectively. All the GC data were stored in a computer using a data station (Winchrom software) connected between the chromatograph and the computer. The areas obtained in the computer were in proportion to the concentrations as pre-defined in the software. After the run the product was analyzed for the amount of sulphate formed using UV spectrometer analysis. Limited SEM analysis and the BET area measurements were also carried out for the samples of commercial calcium carbonate, ppt-calcium carbonate with and without $CaCl_2$.

4.4 Experimental variables:

The experiments were performed in the packed bed reactor under different operating conditions such as bed temperature, inlet gas concentration, particle size, flow rate, and the amount and the type of the sorbents used. A comparative study was done by taking 2 g of the sorbent materials in powder form for each case. The gas concentration was kept constant at 10000 ppm, and flow rate at 600 slpm. To study the effect of reaction temperature on the removal of SO_2 the bed temperature was varied between 750° C and 950° C, and the remaining parameters were kept constant.

In case of zeolite, the reaction temperature was varied between 50°C and 100°C. The amount taken was 5 g. To study the effect of inlet gas concentration, particle size, and flow rate, one of the variables was changed and the remaining parameters were kept constant as shown in Table 4.1.

Experimental variables	Experimental conditions		
Gas flow rate (cc/min)	300	600	
Temperature (^{o}C)	50	75	100
Sorbent particle radius (mm)	0.164	1.115	0.385
Inlet SO_2 concentration (ppm)	5000	10000	25000

Table 4.1: Different experimental variables for SO_2 sorption

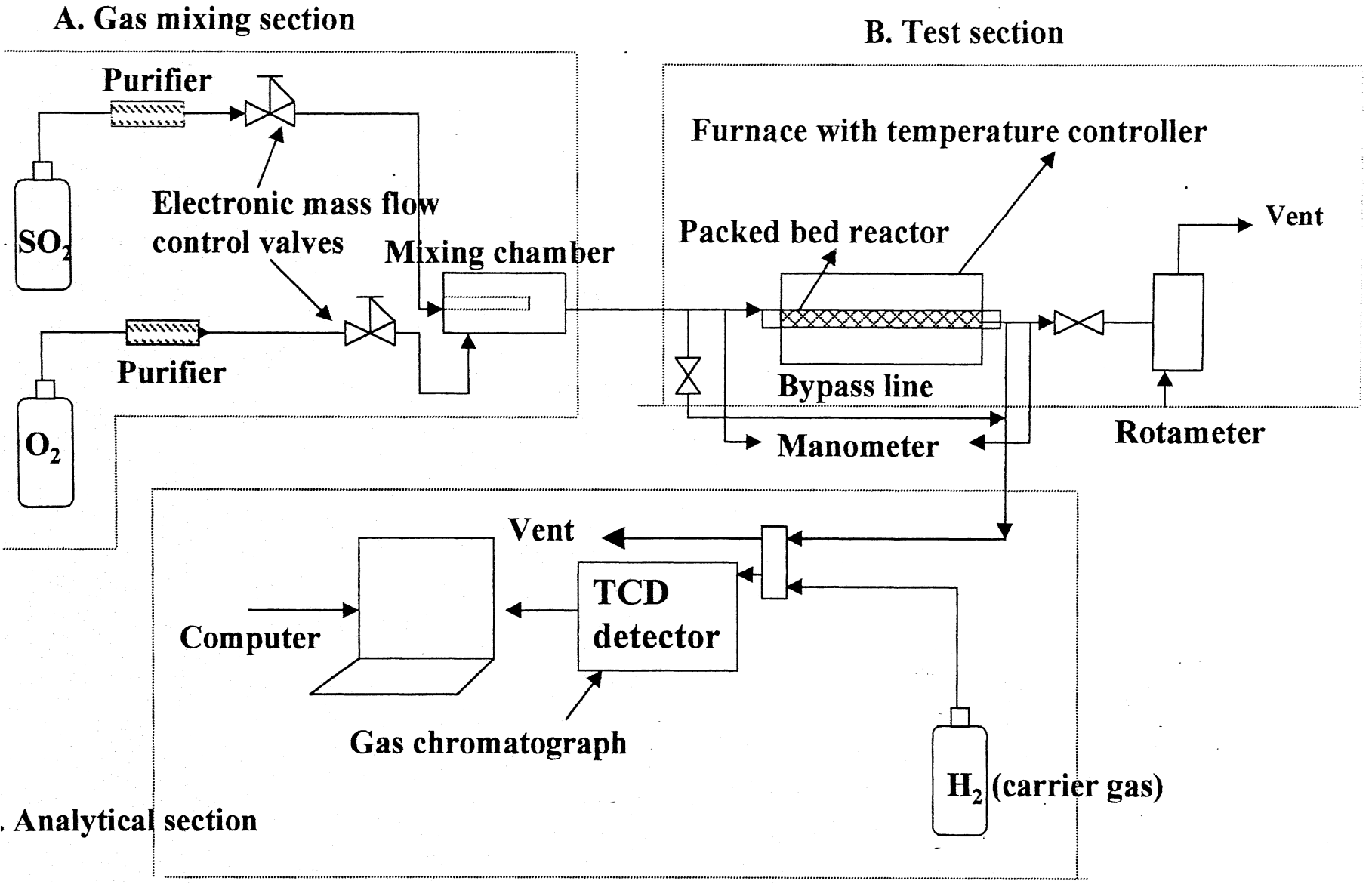

Figure 4.1: Schematic diagram of experimental set up

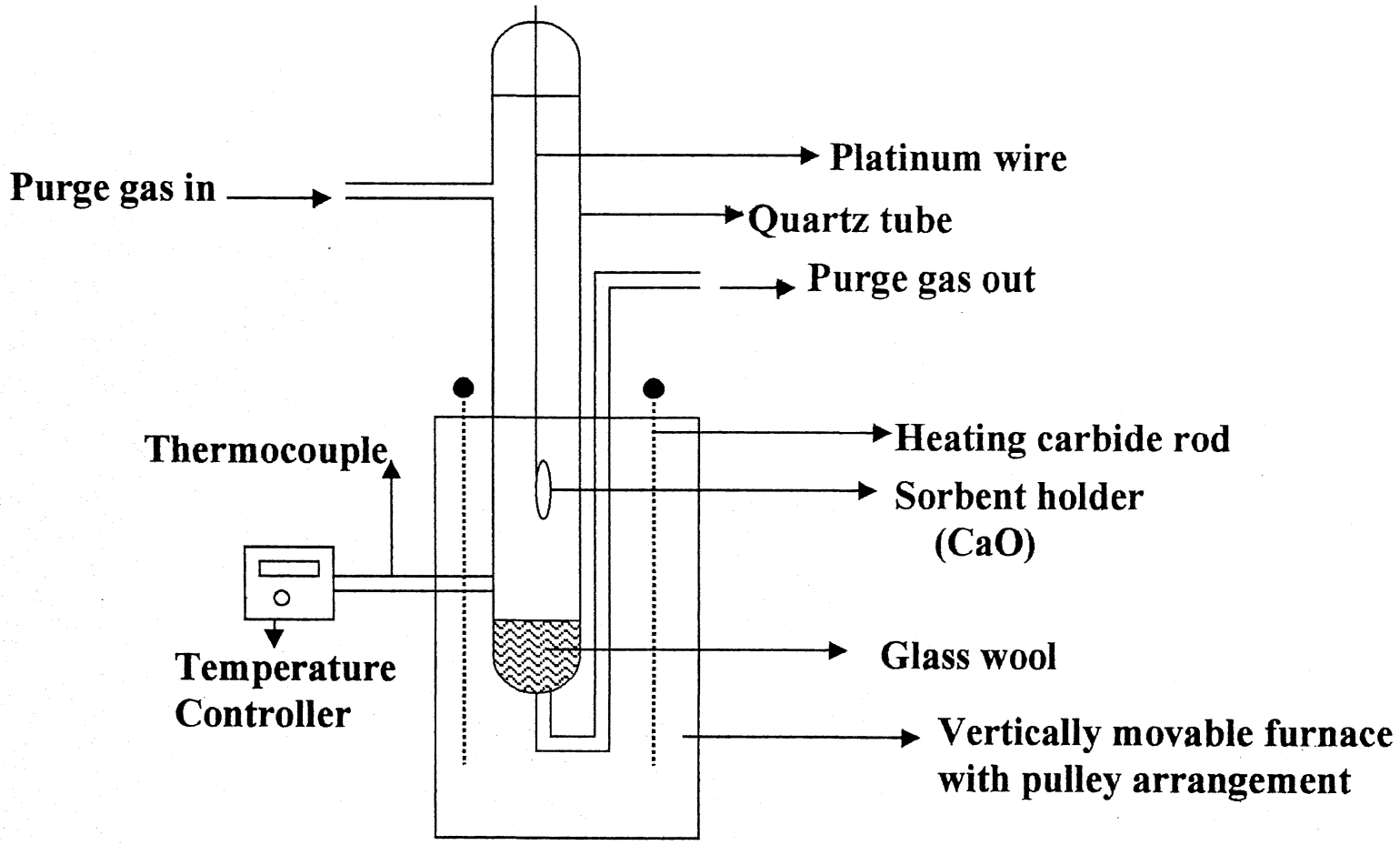

Figure 4.2: Arrangement for calcination at high temperature

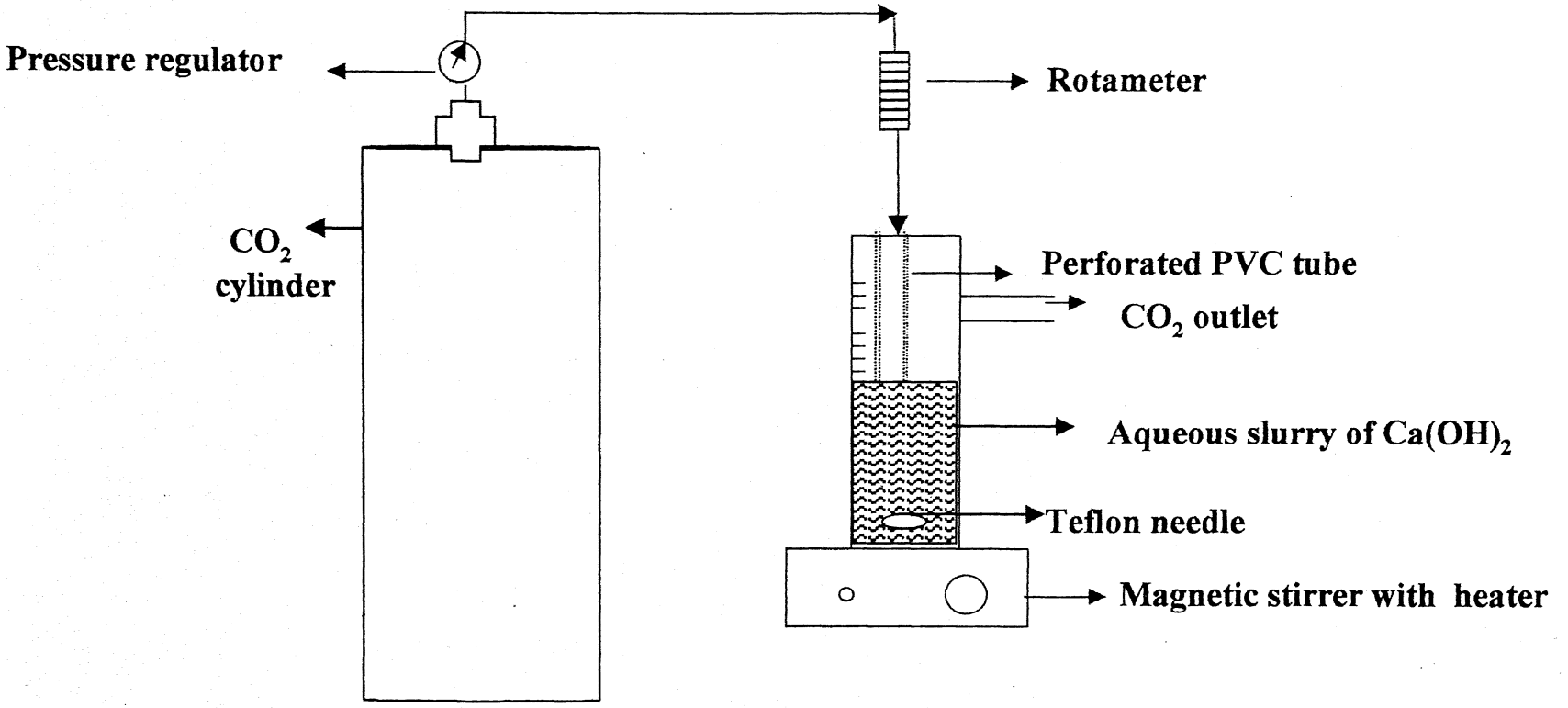

Figure 4.3: Arrangement for Preparation of precipitated- CaO

CHAPTER 5
RESULTS AND DISCUSSION

In this chapter, both experimental and modeling results have been presented on the study of the sorption/adsorption behavior of SO_2 on calcium oxide and zeolites sorbents. In the case of CaO sorbents, analysis has been done for breakthrough as well as total sulphate conversion.

5.1 Non-regenerative sorbent:

The term *breakthrough* refers to the response of an initially clean bed (i.e. free of adsorbate) to an influent containing an adsorbate or a mixture of adsorbates. In the typical experiments performed, the reactor bed initially consisting of pure CaO is heated to a particular reaction temperature and fed with a gas containing mixture at a constant flow rate. During the initial stage of sorption reaction, most of SO_2 entering the bed is removed by chemical reaction occurring at the surface of each sub-grain in the pores. During this stage, no or very low concentration of SO_2 is observed at the reactor outlet. However, a product layer of $CaSO_4$ is gradually formed which offers resistance to the diffusion of SO_2 within the pores and preventing it from reacting with the CaO sub-grains. This resistance progressively increases till the diffusion of SO_2 completely stops, implying that the overall sorption process is completed. Under this condition, the concentration of SO_2 at the reactor outlet becomes equal to that at the inlet. In the present work, the transient change in SO_2 concentration at the reactor outlet was determined using a gas chromatograph. Such transient behavior of concentration is called breakthrough and the corresponding concentration vs. time plot is called breakthrough curve. In the conversion analysis, the total amount of sulphate formed at the completion of the, calcium ion and any other metals present in the sorbent were determined by atomic absorption technique.

For the model analysis the following quantities were calculated based on the experimental conditions: superficial gas velocity, residence time, bed porosity, density of the gas, Reynolds number, Schmidt number, dispersion co-efficient, Peclet number and mass transfer co-efficient. The corresponding calculations have been presented in the appendix.

5.1.1 Effect of Temperature on sorbent:

To determine the effect of reaction temperature on the SO_2 removal process, the experiments were carried out at 750, 850, and 950°C. In all the runs, the flow rate was kept constant at 600 cc/min and 2 gm of the sorbents (powdered size) were used. The inlet SO_2 concentration was maintained constant at 10000 ppm. The breakthrough curves of CaO obtained from $CaCO_3$, under various temperatures are described in Figure 5.1. As observed from the figure, the breakthrough times are approximately 25 min for both temperatures: 750 and 950°C. However, the total or final reaction time (at the instance the reactor exit gas concentration asymptotically reaches the inlet gas concentration) is significantly greater at 950 (380 min) than at 750°C (150 min). The sulphate analysis of the reactant product was also carried out at the end of each run. As observed from Table 5.1, the sulphate conversion increases from 24.63 % to 52.98 % as the temperature is increased from 750 to 950°C. As also clearly observed from the tabulated results on breakthrough times and the total amount of sulfate formed, the sorption of SO_2 may be assumed to be insignificant at or below 750 °C. These results are consistent with those obtained by Dasgupta [2001]. In the present work, 950 °C was henceforth chosen as the reaction temperature for the sorption tests. As mentioned in Chapter 2, in an earlier study of Dasgupta [2001] sintering effects were observed to occur at high temperatures resulting in immediate breakthrough of the sorbents bed. In most of the experiments, the weight of the sample, gas flowrate and inlet concentrations were also henceforth kept the same (i.e. 2 gm, 600 cc/min, and 10000 ppm, respectively) for a comparative study of various types of the sorbents.

Figure 5.2 describes the breakthrough characteristics of CaO obtained from $Ca(OH)_2$ at various reaction temperatures: 750, 850, and 950°C. The corresponding breakthrough times at 750, 850, and 950°C were approximately 10, 60, and 90 min, respectively. A comparative analysis suggests that CaO obtained from hydroxide performed significantly better than that obtained from carbonate under identical conditions.

5.1.2 Sorbents obtained from acetate:

CaO sorbents were also prepared by calcination of commercially available $Ca(CH_3COOH)_2$. The corresponding breakthrough characteristics of SO_2 at reaction

temperatures of 750, 850, and 950°C are described in Figure 5.3. As observed from the figure, the breakthrough time increased from 60 to 100 min with increase in the reaction temperature from 750 to 850°C. With further increase in the reaction temperature to 950°C, the breakthrough time, however, decreased to 65 min. Referring to Table 5.1, the sulphate conversions at the reaction temperatures of 750, 850, and 950°C were determined to be 54.77%, 56.08% and 49.02%, respectively. The corresponding reaction times (for the reactor exit gas concentration equal to that at the inlet) were 235, 480, and 395 min, respectively. These results (breakthrough combined with sulphate analysis) clearly show that SO_2 sorption by calcium acetate based sorbents is most effective at 850°C, in comparison with 950 °C for carbonate and hydroxide based sorbents.

Figure 5.4 describes the sorption efficiency of MgO obtained on calcinations from magnesium acetate at 750, 850, and 950°C. The breakthrough results clearly indicate that the sorption of SO_2 by MgO is insignificant, as the breakthrough occurs instantaneously, and in less than 10 min the reactor exit gas concentration reaches more than 60% of the inlet gas concentration. Furthermore, the breakthrough characteristics were observed to be invariant with the reaction temperatures.

It is important to point out that Yiannis et al. (1993) carried out the sorption study on commercially obtained (from Cryogenic Technologies) calcium magnesium acetate (CMA), a mixture of calcium and magnesium acetates, and reported a significant superior performance of the sorbents in comparison with that of CaO obtained from the hydroxide or carbonate. In the present work, due to locally non-availability of this type of mixture or salt, a mixture of CaO and MgO obtained on calcination from their respective acetates was prepared in the laboratory by mixing in different proportions. Since the sorption capacity of pure MgO was observed to be insignificant, MgO was mostly used as an additive in the mixture of CaO and MgO.

Figure 5.5 compares the breakthrough characteristics of various mixtures of MgO and CaO prepared in different ratios: 1:20,1:8,1:4,1:2.6, and 8:1 those pure of MgO and CaO. A mixture containing higher amount of MgO than CaO was also tested for comparison purpose. Table 5.2 summarizes the breakthrough times and total sulphate conversions corresponding to total reaction times for different mixture ratios. A comparison of the sorption characteristic of these CaO-MgO mixtures with that from CaO

obtained from calcium acetate (ref. Table 5.1) suggests that the mixing of MgO with CaO did not result in improvement of the breakthrough time or the sulphate conversion, though the overall performance of the mixture was observed to be marginally superior to that of carbonate based sorbents and to some extent, comparable with that of hydoxide based sorbents. This is in contrary to the observations or conclusion made by Yiannis et al. (1993) with regard to the superior performance of CMA in comparison with that od hydroxide or carbonate based calcium sorbents.

A comparative performance of CaO sorbents obtained from different sources; namely: $CaCO_3$, $Ca(OH)_2$ and $Ca(CH_3COOH)_2$ is shown in Figure 5.6. The results are presented for the sorption carried out at the respective optimum reaction temperatures of these sorbents. As observed, acetate based sorbents exhibit longer breakthrough and reaction times than hydroxide based sorbents under identical operating condtions. On the other hand, the performance of carbonate based sorbents is inferior to hydroxide as well as acetate based sorbents.

5.1.3 Precipitated (ppt) CaO based sorbents with and without $CaCl_2$ (additives):

The CaO-sorbents obtained from the calcination of the laboratory made ppt-$CaCO_3$ were tested for their sorption efficiency at reaction temperatures of 750 and 950 °C. In some samples, additives $CaCl_2$ were added in small quantities to determine the effect of moisture on SO_2 sorption. $CaCl_2$ being hygroscopic in nature, it was expected that some amount of moisture will be absorbed in the solid mixture. Figure 5.7 and 5.8 compare the breakthrough characteristics of commercial and ppt-carbonate sorbents with and without $CaCl_2$ mixed in various proportions, at 750 and 950 °C, respectively. Tables 5.3 and 5.4 compare the breakthrough and reaction times, along with the corresponding sulphate conversion for ppt-$CaCO_3$ with those for commercially available carbonate at the reaction temperatures of 750 and 950 °C, respectively.

As observed from Table 5.3, the sulphate conversion at 750 °C for either sorbents (ppt and commercial) is barely 25%. However, addition of chloride increases the conversion to approximately 50% in 260 min. The corresponding breakthrough time increases from 35 min to 40 min.

Similar to the sorption process at higher temperature, the total sulphate conversion increased significantly at 950 °C. However, the performance of ppt-CaO was

observed to be marginally higher than that of commercially obtained CaO, in terms of both reaction and breakthrough times. On the other hand, it was also observed that a certain amount of $CaCl_2$ significantly improved the sorption capacity of ppt-CaO. As observed from Figure 5.8 and Table 5.4, the breakthrough time for the mixture of $CaCl_2$ and CaO (0.05:1) considerably increased to as high as 120 min. The total reaction time was 410 min and the corresponding sulphate conversion obtained was 62%. Any other ratio higher or lower than 0.05 : 1 for $CaCl_2$ and CaO yielded in shorter breakthrough time and lower conversion.

Therefore, we conclude that in the present work, amongst various types of non-regenerative sorbents tested for SO_2 control under identical conditions, including commercial CaO obtained from carbonate, hydroxide, and acetate, commercial MgO, the solid mixture of CaO and MgO, laboratory prepared ppt-CaO with and without $CaCl_2$, ppt-CaO mixed with $CaCl_2$ in 1:0.05 ratio had the longest breakthrough and reaction times and highest sulphate conversion. Table 5.5 summarizes these comparative findings.

5.1.4. Model results:

As shown in the study of Dasgupta [2001], the model predictions assuming a porous structure of calcium based sorbents explained reasonably well the breakthrough characteristic of SO_2. In the proposed mechanism, the overall SO_2 sorption by CaO in a fixed bed reactor under constant temperature conditions was determined by following rate-determining steps:

a) diffusion from the bulk gas to the particle surface through a gas film surrounding the particle (bulk diffusion).

b) diffusion of the gas within the pores (pore diffusion)

c) reaction of SO_2 at the surface of sub-grain or particle surface (chemical reaction)

The diffusion of the gas from the bulk to the particle is dependent on the mass transfer co-efficient, which inturn is determined by the particle radius and gas flow rate. The chemical reaction rate constant has Arrehenius temperature depednecne. The diffusion of the gas in the pores is primarily dependent on the pore size of the sorbents. In line with the observations made by other investigators (Dogu[1982], Bruce[1989]) the pore size is assumed to vary during the sorption reaction, as the reaction products (sulphate) begin to gradually fill the pore, eventually resulting in pore-plugging.

Therefore, the effective diffusivity in the pores also varies during the course of the reaction. The variation of the porosity as the reaction proceeds was assumed to be represented by an exponential function: $\alpha = \alpha_0 e^{(-\frac{t}{\delta})^n}$ where, α_0= initial intraparticle porosity and δ and n are constants. Therefore, the proposed model had two adjustable parameters (δ and n) to explain the experimental results on SO_2 breakthrough by the porous (mon-pore) sorbent particles. The rest of the parameters such as effective pore diffusivity taking into account Knudsen diffusivity, gas molecular diffusivity, gas film mass transfer coefficient and reaction rate constants were calculated based on the initial existing conditions.

The model predictions of SO_2 breakthrough on various types of the sorbents under varying operating conditions are shown in Figures 5.7 and 5.8. As observed, the predictions compare reasonably well with the experimental data. The breakthrough characteristics of various calcium based sorbents is further explained by analyzing model predicted variation in the porosity, diffusivity, and gas concentration within the pores of the CaO particles during the course of the sulfonation reaction. In the simulation, the molecular diffusivity of SO_2 was calculated be 6.39 $X10^{-5}$ and 8.36$X10^{-5}$ at 950°C and 750°C, respectively. The reaction rate constant was calculated to be 5 and 8.46 m/s at 750 and 950°C, respectively and the initial porosity of the CaO particle was assumed to be 0.52 [Dogu, 1980]. Based on the intitial porosity and pore size, initial Knudesn ($4.58x10^{-4}$ m^2/s) and effective diffusivity ($3.33x10^{-5}$ m^2/s) in CaO sorbents were also calculated. The results are shown in Appendix).

As the sulfation proceeds the porosity of the CaO particles gradually decreases at the reaction temperatures. Incomplete conversion occurs when the porosity within the grain asymptotically becomes zero. Figure 5.9 describes the variation in porosity at 750°C, as predicted by the model. As also observed, the porosity decreases at a slower rate for p-$CaCO_3$ mixed with $CaCl_2$ in a mixing ratio 0.1/1.0, compared with the sorbents of other mixing ratios. The decrease in the porosity is highest for c-CaO. Figure 5.10 describes the model predicted corresponding decrease in the effective diffusivity of the reacting gas in the pores of CaO particle at temperature 750°C. The porosity and hence diffusivity were gradual for 0.1/1 than other mixing ratios. Figure 5.11 describes the average concentration

profile in the pore of CaO particles, as predicted by the model. As observed from the figure, concentration profiles decrease slowly for mixing ratio, 0.1:1 that supports the higher sulphate conversion. Similar observations were observed at 950°C for the case of mixing ratio 0.05:1.0. The average concentration profiles in the pore are shown in Figure 5.13. Figures 5.14 and 15 depict the variations in the porosity and diffusivity, respectively. The behavior observed for the mixture ratio 0.05:1 at 950°C are identical to those for the mixture ratio of 0.1:1.0 at 750°C.

Since in this work, the BET area of the sorbent was measured to be low (2~10 m^2/g) the combined experimental and model results suggest that sorption mechanism of SO_2 on CaO based sorbents is mainly pore diffusion controlled.

5.2 Regenerative sorbents (zeolite)

5.2.1 Adsorption temperatures for zeolites:

Similar to the experiments carried out on calcium based sorbents to determine optimum temperature for maximum SO_2 sorption, the tests were also carried out on 5A zeolites at various temperatures to obtain the optimum temperature for maximum adsorption of SO_2. Figure 5.15 describes the breakthrough characteristics of SO_2 during dynamic adsorption by zeolite materials in a fixed packed bed at reaction temperatures of 100, 75, and 50°C. The gas flow rate was kept constant at 300 cc/min and the gas inlet SO_2 concentration was maintained at 10000 ppm. The zeolites materials commercially available in the form of pellets were crushed to prepare a 5 gm test sample having average particle size 1.115 mm. It was observed that at temperatures greater than 100°C and lower than 50°C, there was practically no significant adsorption, resulting in instantaneous (< 3 min) breakthrough of the bed. At temperature as high as 200°C, zeolite pellets were, in fact, burnt off.

As observed from Figure 5.15, the optimum temperature for SO_2 removal was obtained at 75°C. The breakthrough time at this temperature was approximately 50 min, while it took more than 90 min for the reactor exit gas concentration to approximately reach the inlet concentration (10000 ppm). On the other hand, at 100 °C, the breakthrough time decreased to 35 min. The corresponding adsorption time was 80 min. At 50 °C, the breakthrough of the bed occurred in less than 10 min. The adsorption temperature for all the experiments hence after was selected as 75 °C. The suitability of 5A zeolites within a

temperature range of 50 to 100°C for the maximum adsorption of SO_2 has also been reported elsewhere Tsibranska [1999].

Model predictions were done under identical experimental conditions. As described in the section on theoretical analysis, the mathematical model is based on two governing equations; one for the bulk gas phase and the other in the macro-pore. The concentration profiles within the zeolite crystal due to the radial diffusion in the intra (or micro)-pores of crystals was averaged and the partitioning between the interface of the crystal surface and marco-pores was assumed to be determined by a parameter, called equilibrium constant. This dimensionless equilibrium constant has been used as an adjustable parameter in the model, wherever necessary, to explain the experimental data. The remaining variables such as gas film mass transfer coefficient around the pellet, dispersion coefficient in the packed bed and macro-pore diffusivity incorporating Knudsen effects and intra-particle porosity were calculated. The temperature effects on variation in gas, pore or crystal diffusivities were incorporated, as necessary. The macro-pore size for 5A zeolites was assumed to be 0.3 μm based on reported value Do et al [1998]. The sample numerical calculations are reported in Appendix.

Under the experimental conditions chosen for the results on Figure 5.15, the gas film mass transfer coefficient and the effective pore diffusivity were calculated to be 0.05 m/s and 2.54×10^{-6} m^2/s, respectively. As observed, a reasonable good agreement is observed between the model predictions and the data within the experimental and computational errors. The values for partition coefficient K at 50, 75 and 100 °C were adjusted at 45, 13, and 4, respectively. The decrease in the values of K with increase in the temperature is also consistent with an independent work Kopac et al [1997]. It may be pointed out that in the aforementioned study, the equilibrium constant was defined between the bulk gas phase and crystal surface concentrations, as against between the macro-pore and the crystal surface concentrations in this work. Assuming Arrhenius type temperature dependence, the activation energy for adsorption/partitioning was calculated to be 46.4 KJ/mol. The model predicted values of the average concentration within the macro-pores of the pellets at these temperatures are described in Figure 5.16. The characteristics of these curves are consistent with the proposed mechanism. The macro-

pores get saturated with the adsorbate at the instance the tube exit concentration reaches the inlet gas concentration.

5.1.2 Effect of particle size:

The experiments were carried out for three different particle (pellet) sizes: 0.160 mm, 0.385 mm and 1.115 mm under varying gas flow rates and inlet SO_2 concentrations. The test samples having a particle size of 0.16 mm were in nearly powdered form, while those having higher size particles were in spherical pellet forms. The amount of zeolite materials was taken as 5 g in each case. In one test run, the inlet SO_2 gas concentration and flow rate were kept constant at 5000 ppm and 600 cc/min, respectively, and in the second run, these values were 10000 ppm and 300 cc/min, respectively. Figure 5.17 and 5.18 describe the effects of particle sizes on the breakthrough characteristics for these runs. As observed from the figures, decrease in particle size results in increase in breakthrough and also, total adsorption times. However, as the particle size is decreased (below 0.385 mm), the reductions in these times are observed to be minimal. From these experimental data it was concluded that lower the particle size, superior is the performance of zeolites, in terms of breakthrough time or adsorption capacity, the remaining operating conditions being identical. Thus, if pressure drop or agglomeration of the particles is not a limiting factor, the adsorbents in powdered form should be used in the packed bed.

Model predictions were done to explain the effect of particle size on the observed breakthrough times. It was found that as per the constraint imposed by eq. (3.3.3) on the upper limit of K for the term δ to be negative, the equilibrium constant value (model parameter) was adjusted to approximately 613 corresponding to the particle size of 0.16 mm. The gas film mass transfer co-efficient was calculated to be 0.05 m/s for 1.115 mm size (radius) particle, as compared to 0.23 m/s for 0.16 mm size particle.

The superior performance of relatively smaller size zeolite materials can be explained as follows. With the increase in mass transfer co-efficient due to smaller particle radius, the amount of gas or the flux of SO_2 (mol/m^2-s) diffusing into the adsorbents increases. This, in turn, results in higher adsorption rate. As the particle radius is decreased for the same amount of sorbent the interfacial area per unit volume (a^*) also increases. Hence, there is a combined effect of mass transfer rate as well as the interfacial area per unit volume on the total SO_2 flux entering the pores of the pellet. The increase in

mass transfer coefficient and the interfacial area due to reduction in particle size, however, could not explain the corresponding improved breakthrough characteristics.

Referring to the assumptions in the model analysis, the crystal radius of zeolite materials was assumed to be constant ($2x10^{-6}$m). Since there was no temperature variation between two conditions, the gas diffusivities (both bulk as well as Knudsen) were unchanged. Since intra-particle porosity (determined by bulk and solid densities) may be assumed to be constant for both particle sizes, the number of crystals is less in smaller size particle than in larger size particle, for the same quantity of zeolites. Therefore, for the same amount of the gas in the macro-pore as well as within crystal, the concentration (moles/cc) within the crystal volume, q, is more. The partioning coefficient/equilibrium constant between the gas concentration in the macro-pores and within the crystals was accordingly increased from 14 to 605 to explain the experimental observations, as the pellet size decreased from 1.115 to 0.16 mm. The model predicted values of the average concentration within the macro-pores of the pellets at these pellets size are described in Figure 5.20.

5.2.3 Effect of flow rate:

To observe the effect of flow rate the experiments were carried out at optimum selected temperature i.e. 75°C on 5 g of adsorbents having particle size 0.16mm. The inlet gas concentration was kept constant at 5000 ppm. Figure 5.21 describes the breakthrough characteristics at these operating conditions. As observed from Figure 5.21, the breakthrough time decreases from 98 to 28 min as the gas flowrate increases from 300 to 600 cc/min. This decrease is attributed to an early saturation of the bed due to relatively larger amount of SO_2 at higher flowrate. In this case, the data could be explained by the model with a marginal change in the model parameter K (from 605 to 601 i.e. less than 1%).

5.2.4 Effect of concentration:

To observe the effect of concentration the experiments were carried out for different gas inlet concentrations:10000 and 5000 ppm, the remaining operating variables were kept the same as for the conditions of the previous section. Figure 5.21 describes the breakthrough characteristics at these concentrations. As observed from the figure, the

breakthrough time increases from 12 min to 28 min with decrease in the inlet gas concentration from 10000 ppm to 5000 ppm.

This can be explained as follows. With decrease in the inlet gas concentration for identical flowrates, the total amount of SO_2 entering the maco-pores of the pellet is less. Therefore, saturation of the pores occurs in relatively longer time. In this case also, the data could be explained by the model with a marginal change in the model parameter K (from 605 to 598 i.e. less than 1%). The model predicted values of the average concentration within the macro-pores of the pellets at these concentrations are described in Figure 5.23.

5.2.5 Effect of adsorbent amounts:

To observe the effect of weight of the adsorbing materials (5A zeolite), the experiments were carried out on two different amounts: 2g and 5 g. The particle size in each case was 0.16 mm. The inlet gas concentration and flow rate were kept constant at 5000 ppm and 600 cc/min, respectively.

Figure 5.24 describes the SO_2 breakthrough charcteristics for these amounts. As observed, the breakthrough time increases from 8 min to 28 min, with increase in the weight of zeolites from 2 to 5 g. The increase in the breakthrough time is obviously due to approximately 45% increase in the total surface area for adsorption of SO_2. Once again, the data could be explained by the model with a marginal change the parameter K (from 605 to 610 i.e. less than 1%).

Table 5.8 summarizes the various input parameters used in the model, such as diffusivity, mass transfer coefficient, etc corresponding to the various experimental operating conditions used in this work, such as gas flowrate, temperature and concentrations, etc. The last column lists the adjusted values of the model parameter K for these conditions to explain the observed breakthrough characteristics of SO_2 on 5A zeolites.

5.3 Pressure drop across the packed bed:

Referring to Figure 4.1 describing the schematic of the experimental setup, a U-type manometer (CCl_4 as a medium) was used to measure the pressure drop across the adsorbent bed for various sorbent amounts, particle sizes, and the gas flow rates. The measurements are reported in Tables 5.9 and 5.10 for particle size 1.115 mm and 0.16

mm, respectively. As observed from Table 5.9, the measured pressure drop across the packed bed increases with increase in the flow rate. For the particle size 1.115 mm the pressure drop across the bed at flow rate 300 cc/min was approximately 7.04 N/m^2, which increases to 83.63 N/m^2 at the flow rate 600 cc/min. The effect of particles size on the pressure-drop can also be observed from the tables. The pressure drop across the bed increases from 7.04 N/m^2 to 83.63 N/m^2 with decrease in the particle size from 1.115 mm to 0.16 mm.

The tables also compare the experimentally measured pressure drop with those theoretically obtained using well known Ergun equation for the pressure drop in a packed fixed bed [McCabe et al, 1997]. The detailed calculations are described in Appendix. A significant difference between the experimental and calculated values may be due to large pressure drop across the mesh (wool) installed at the reactor inlet to support the adsorbents, and at the inlet to prevent any carryover of the powdered particles with the flowing gas.

For industrial purposes, adsorbents of larger pellet sizes may be desirable to minimize the pressure drop across the bed. The pressure drop calculation is also required to determine the gas blower capacity.

5.4 Comparative performance of calcium based sorbents and zeolites:

A comparative performance of calcium based sorbents and 5A zeolites for control of SO_2 is described in Figures 5.25 and 5.26. Comparison has been made between these materials (non-regenerative and regenerative types) at their respective optimum reaction temperatures (i.e. for zeolites, T = 75 °C and for CaO, T= 850 °C). However, the weight of the sorbents/adsorbents and the gas flowrates were kept the same for comparison. Figure 5.25 compares the breakthrough characteristics of 5A zeolites with those of CaO obtained from acetate for various gas flowrates. It may be recalled that acetate based sorbents were found to be superior in comparison with those obtained from carbonate or hydroxide. Figure 5.26 compares the breakthrough characteristics of these materials for varying inlet gas concentrations. As observed from each figure, calcium acetate may be considered far superior to zeolites, as the breakthrough and total reaction times for the former are at least 10 or in some cases, 100 times greater than those for the latter. However, due to their inherent regenerative characteristics, zeolites may still be preferred to non-regenerative

types of sorbents such as CaO. Use of a two-bed system, similar to PSA (pressure swing adsorption), may also be advantageous in the case of zeolite adsorbents.

5.5 Model simulation of control of a large-scale SO_2 emission:

Model simulations were carried out to determine the total amount of adsorbents in a fixed bed to control a large-scale SO_2 emission from an industry. With the help of the model, the SO_2 breakthrough and reactions times were also predicted. The simulations were done for various gas flow rates between 3000 and 10000 slpm. A vertical reactor (adsorbent bed) of 0.3 m I.D. and 3.15 m height containing 120 kg of zeolites (average particle size 1.115 mm) was assumed for the control of SO_2 emission. The emission level was assumed to be 10000 ppm. The bed was operated isothermally at 75° C. Figure 5.27 describes the simulated breakthrough curves for varying flow rates of the gaseous effluents. As observed from the figure, the breakthrough times were predicted to be approximately 220, 90 and 10 min corresponding to the gas flowrates of 3000, 5000 and 10000 slpm, respectively. Thus, with the help of the above-simulated results, changeover or regeneration time to put a bed of fresh adsorbent can be estimated. For example, if the gas flow rate is 3000 slpm, a changeover time of approximately 4 hours may be required. Hence, the simulated results are useful in designing an industrially sized adsorber.

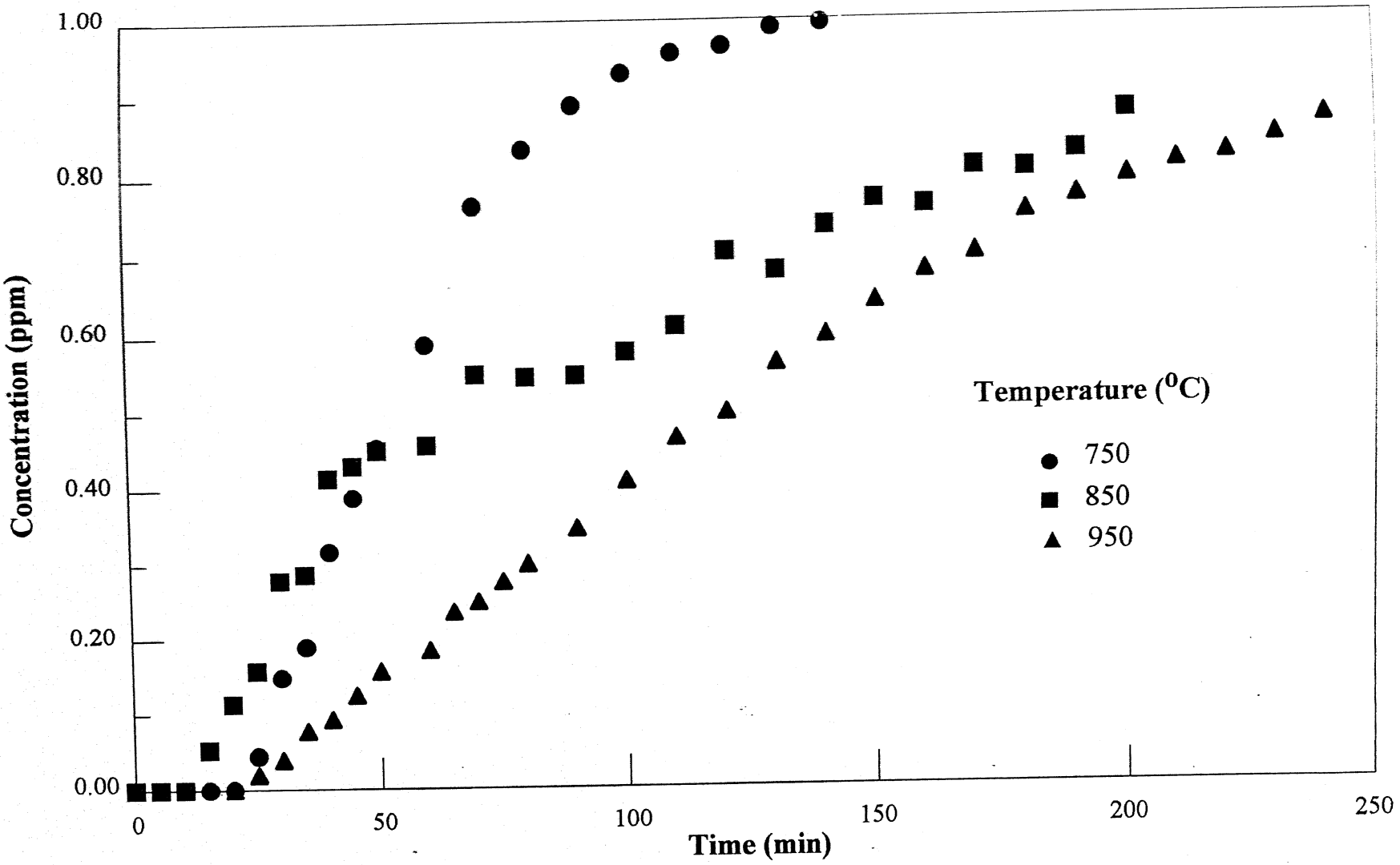

Figure 5.1: Effect of temperature on SO_2 sorption by CaO obtained from carbonate (Q_{SO_2} = 6 cc/min, Q_{O_2} = 600 cc/min, $Cg_{,\,inlet}$ = 10000 ppm, W = 2 g)

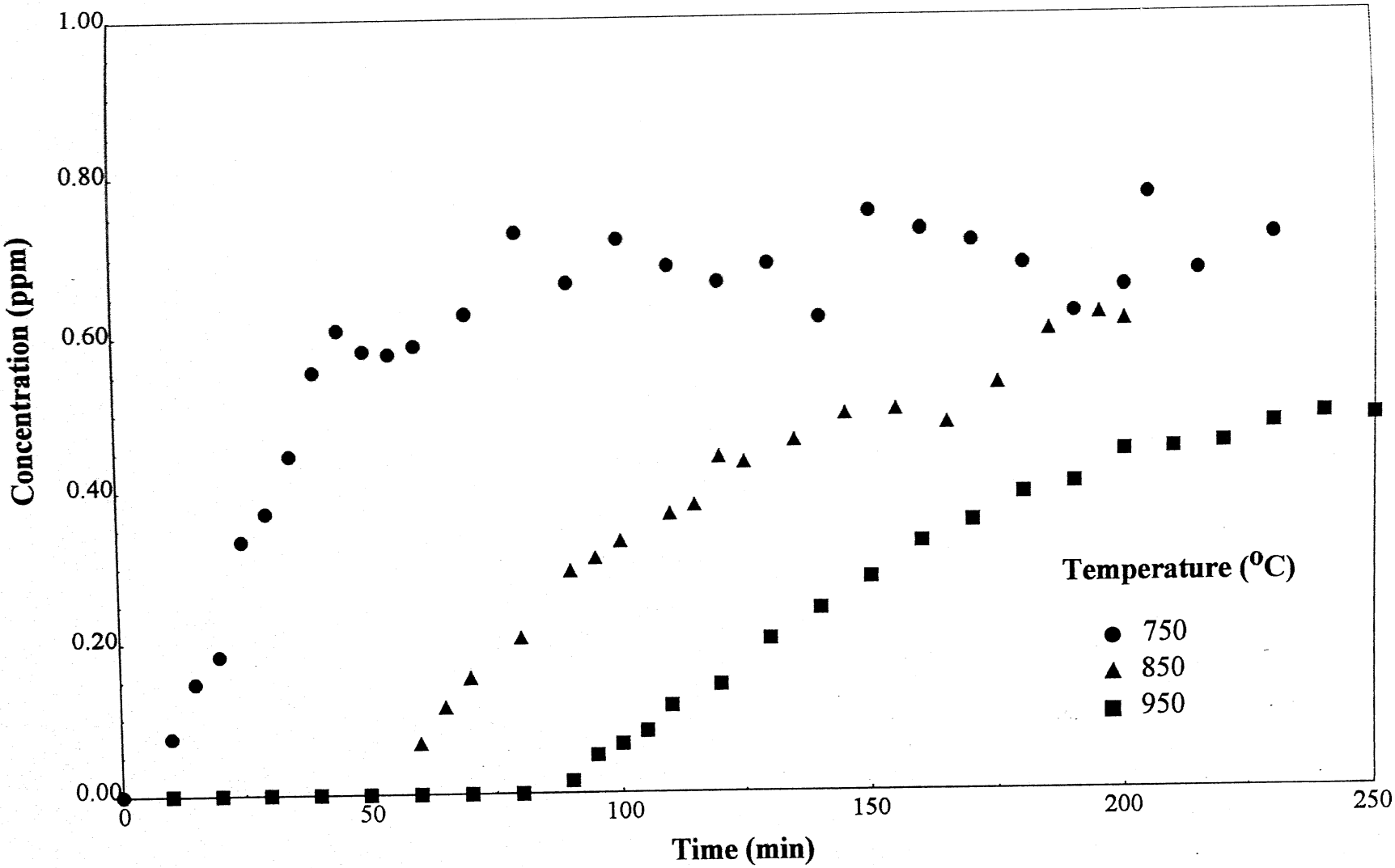

Figure 5.2: Effect of temperature on SO_2 sorption by CaO obtained from hydroxide

(Q_{SO_2} = 6 cc/min, Q_{O_2} = 600 cc/min, $Cg_{,\,inlet}$ = 10000 ppm, W = 2 g)

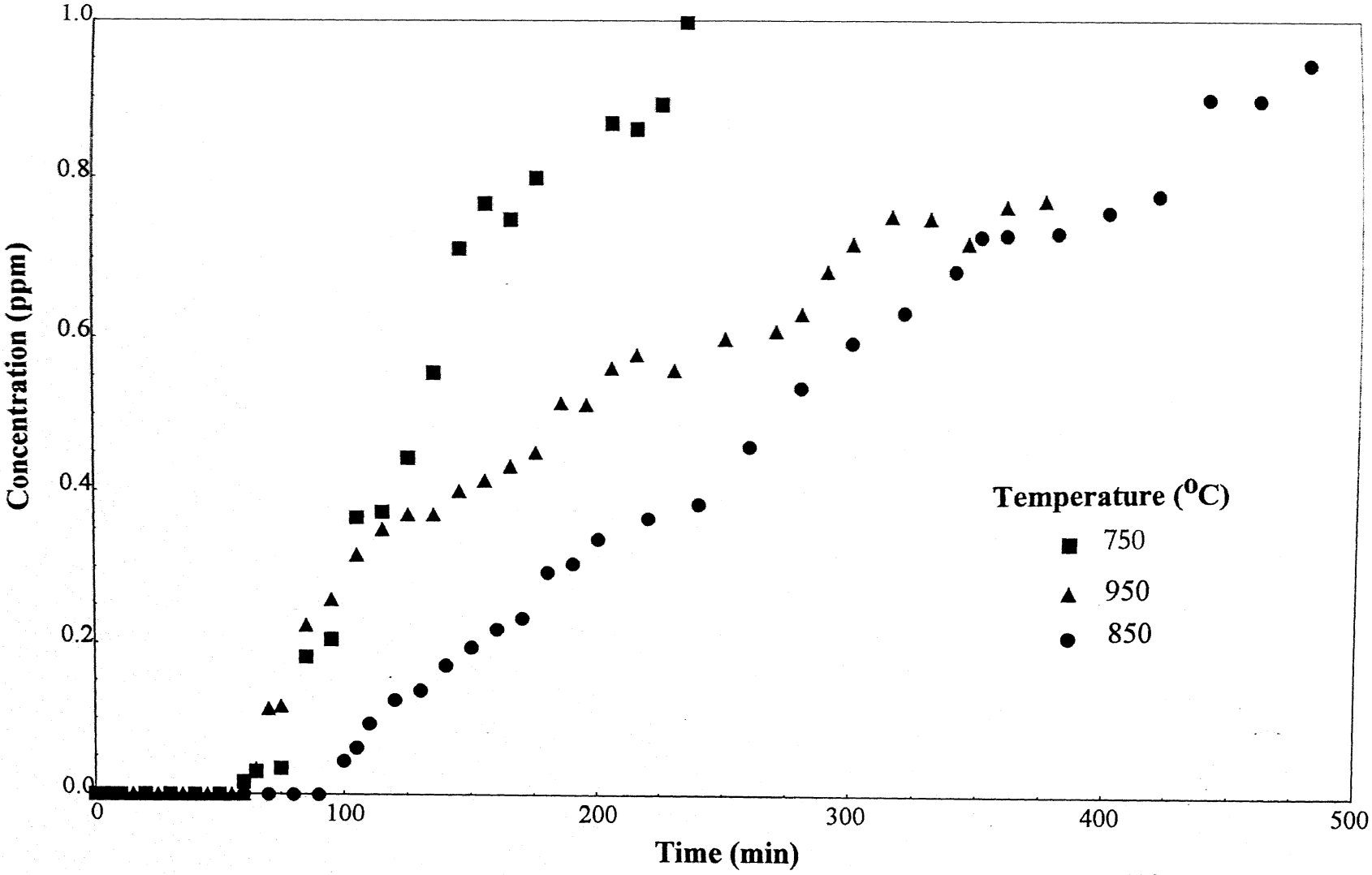

Figure 5.3: Effect of temperature on SO_2 sorption by CaO obtained from acetate (Q_{SO_2} = 6 cc/min, Q_{O_2} = 600 cc/min, $Cg_{,\,inlet}$ = 10000 ppm, W = 2 g)

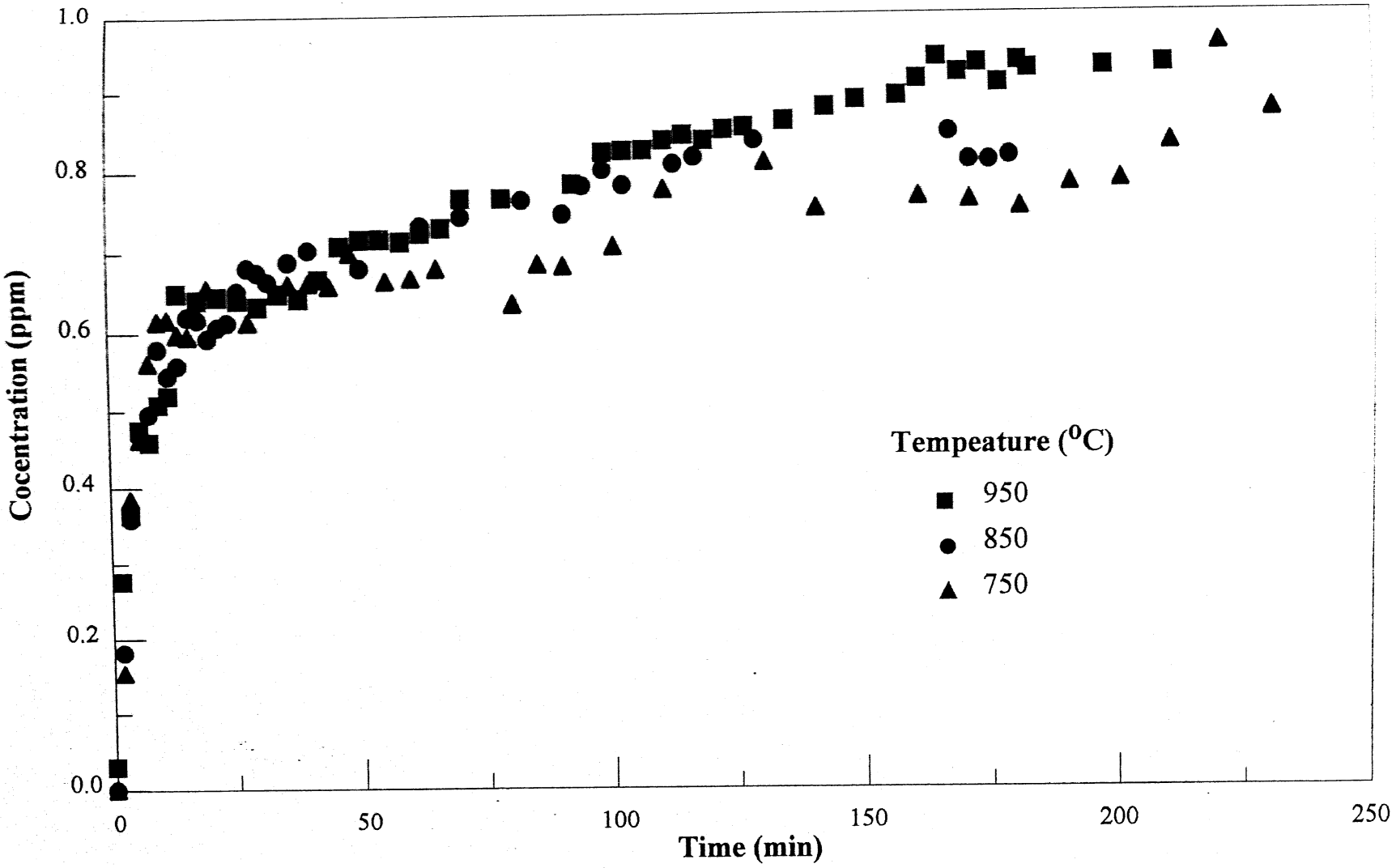

Figure 5.4: Effect of temperature on SO_2 sorption by MgO obtained from acetate

(Q_{SO_2} = 6 cc/min, Q_{O_2} = 600 cc/min, $Cg_{,\,inlet}$ = 10000 ppm, W = 2 g)

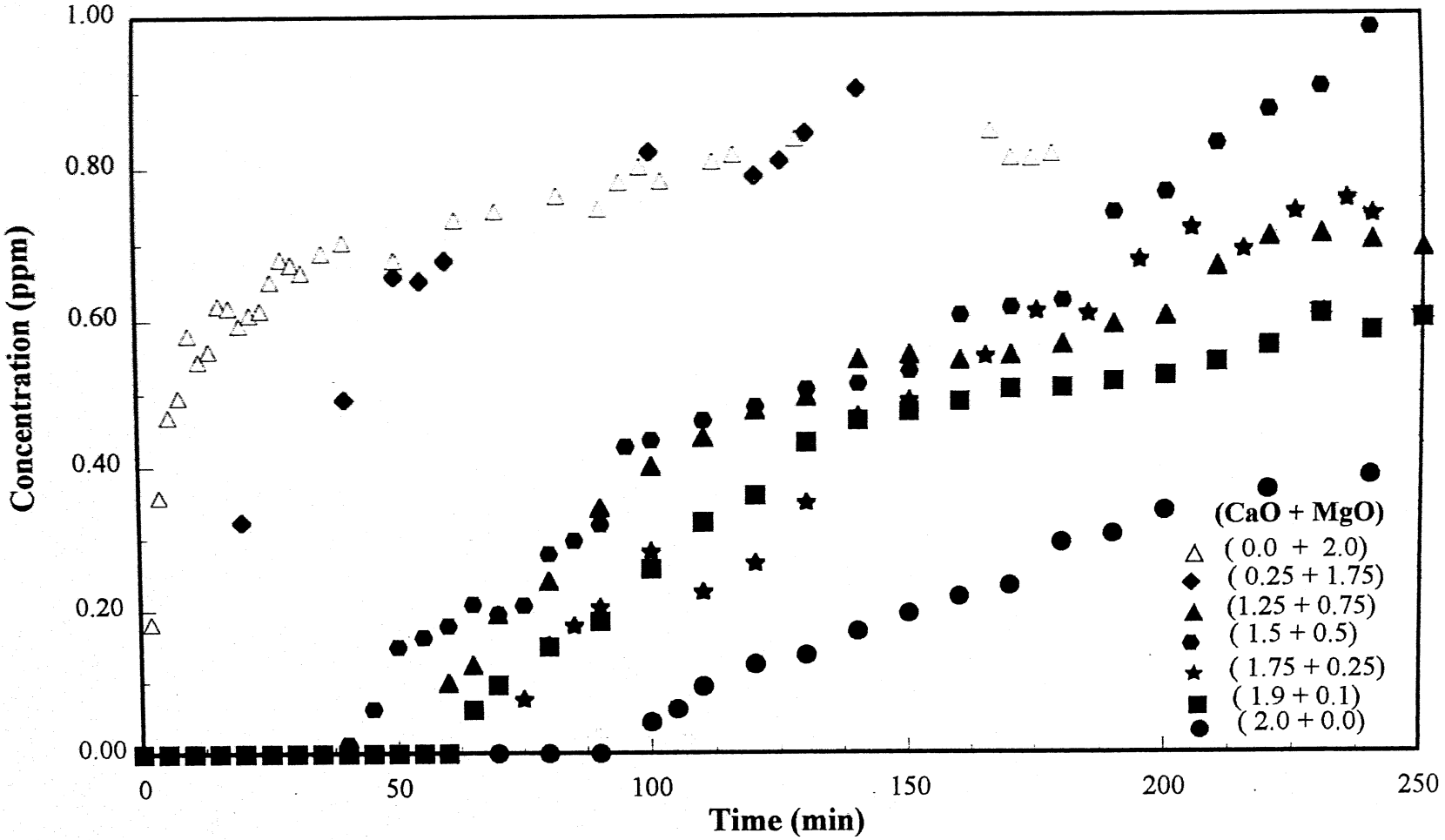

Figure 5.5: Data on the effect of mixture (CaO and MgO) composition on SO_2 sorption

(Q_{SO_2} = 6 cc/min, Q_{O_2} = 600 cc/min, T = 850°C, W = 2 g)

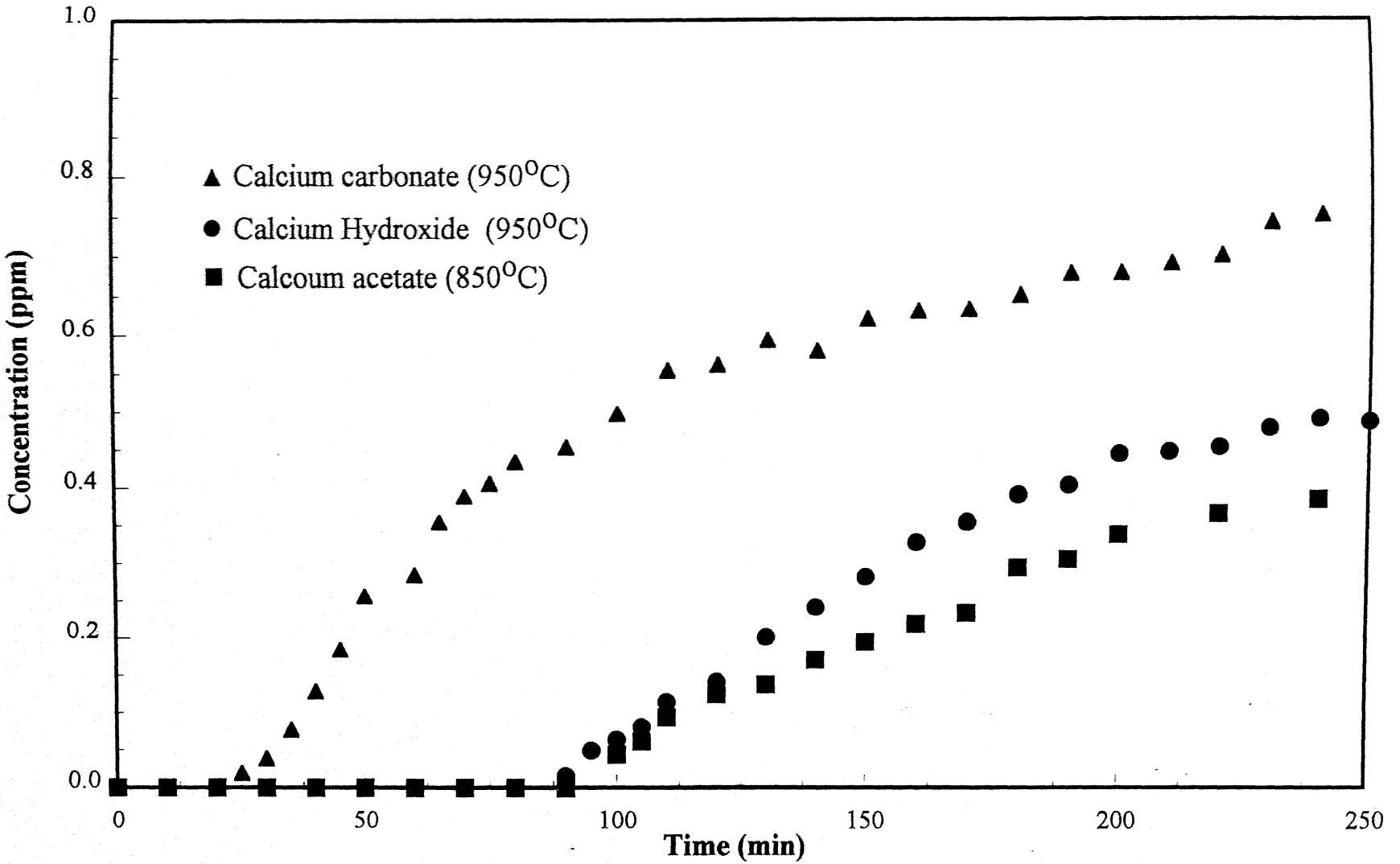

Figure 5.6: Comaprative breakthrough curves on SO_2 sorption by CaO obtained from different sources (Q_{SO_2} = 6 cc/min, Q_{O_2} = 600 cc/min, W = 2 g)

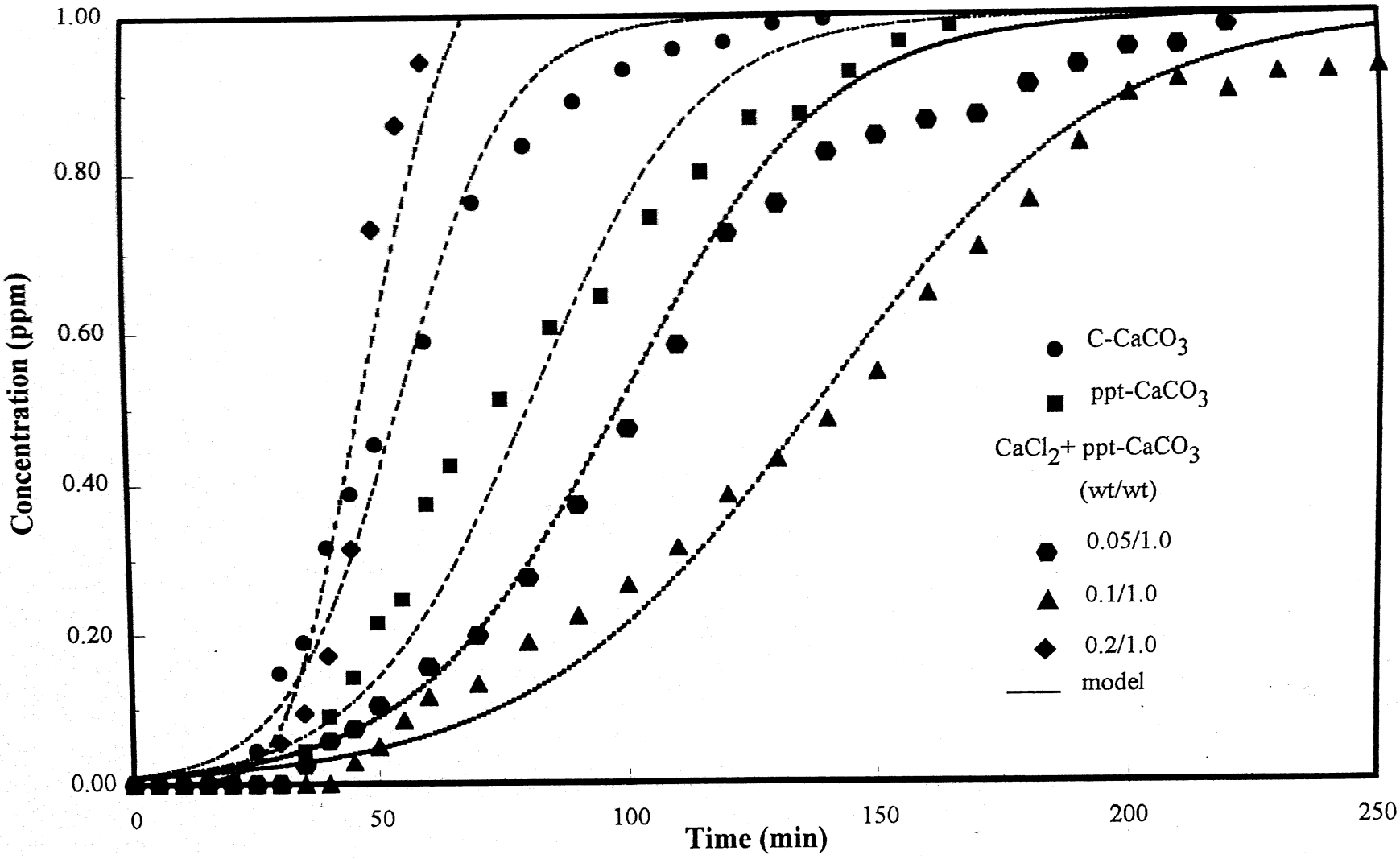

Figure 5.7: Effect of additive ($CaCl_2$) in ppt-CaO on SO_2 sorption

(Q_{SO_2} = 6 cc/min, Q_{O_2} = 600 cc/min, T = 750°C, W = 2 g)

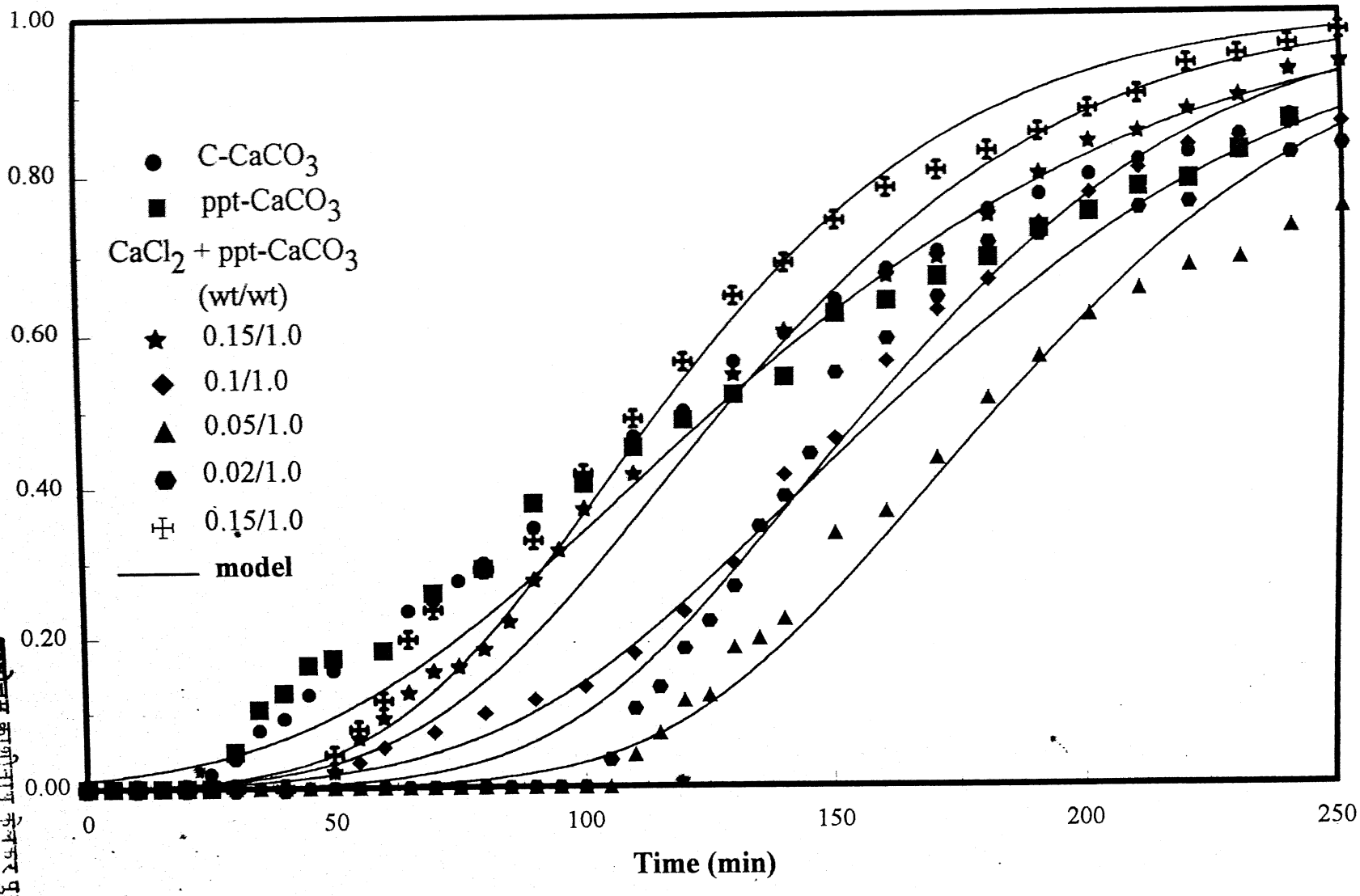

Figure 5.8: Effect of additive ($CaCl_2$) in ppt-CaO on SO_2 sorption

(Q_{SO_2} = 6 cc/min, Q_{O_2} = 600 cc/min, T = 950^{0}C, W = 2 g)

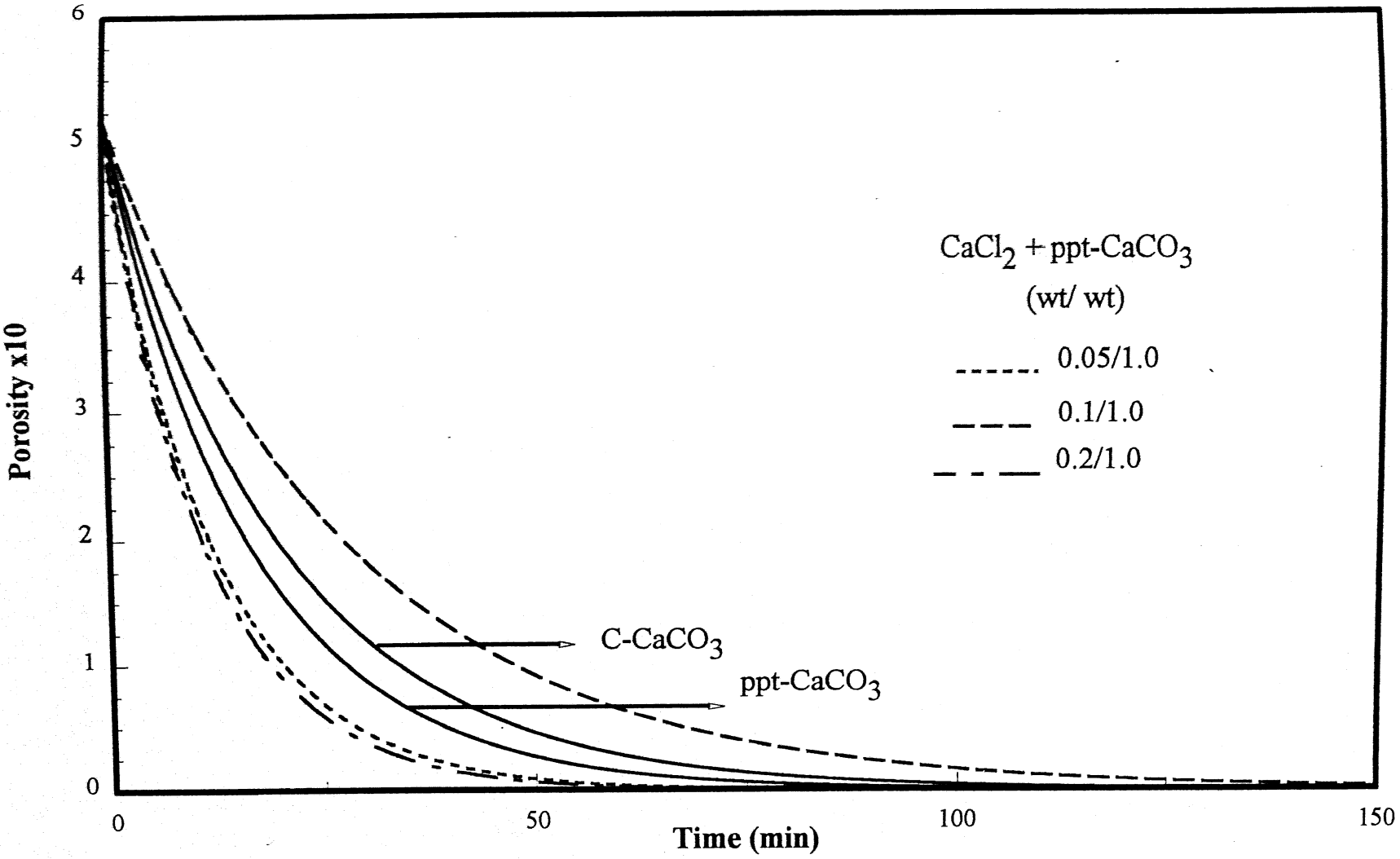

Figure 5.9: Model predictions of variation of porosity during SO_2 sorption

(Q_{SO_2}= 6 cc/min, Q_{O_2}= 600 cc/min, T = 750^{o}C, W = 2 g)

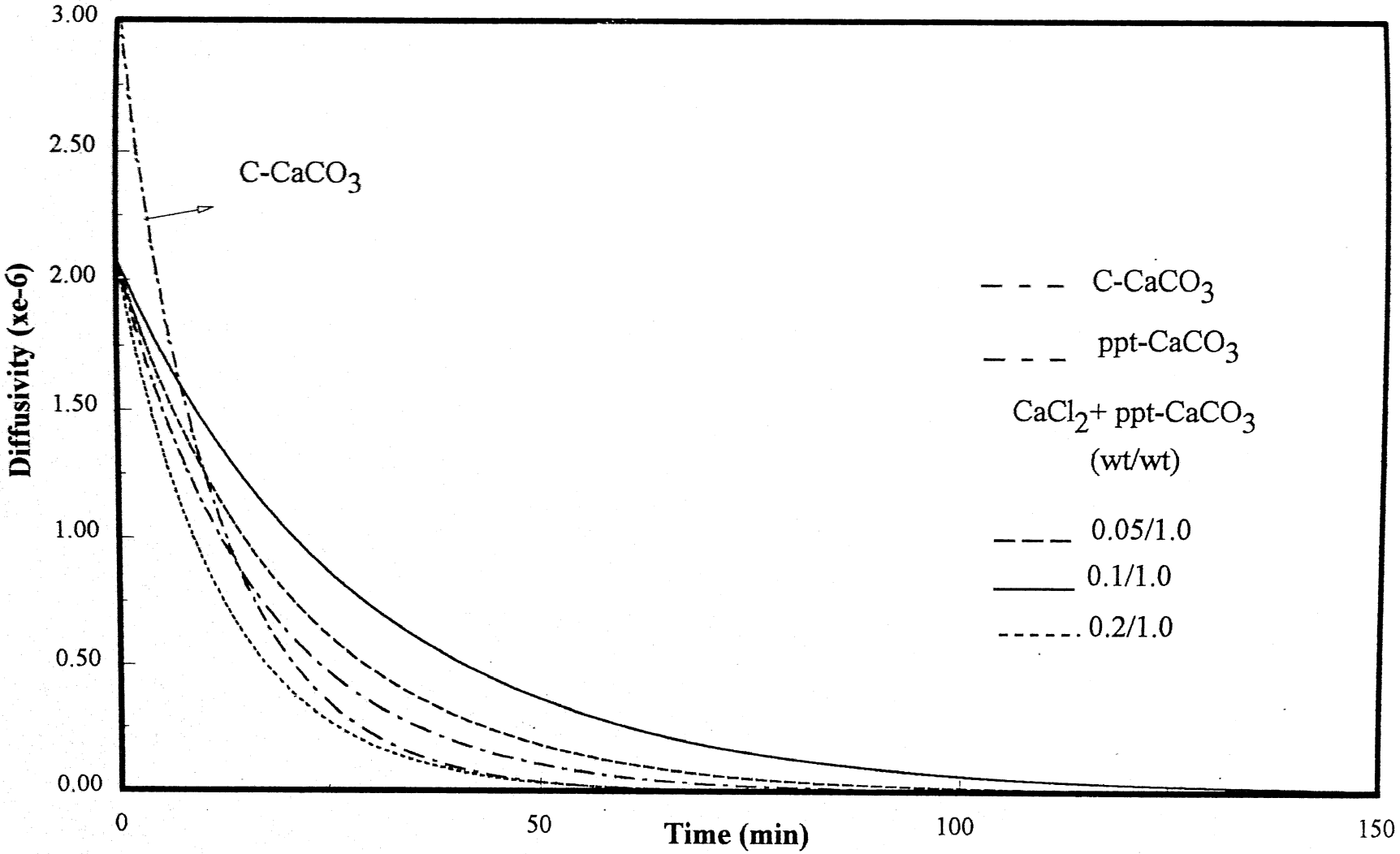

Figure 5.10: Model predictions of variation of diffusivity with time for additive ($CaCl_2$) in ppt-CaO

(Q_{SO_2}= 6 cc/min, Q_{O_2}= 600 cc/min, T = 750^{o}C, W = 2 g)

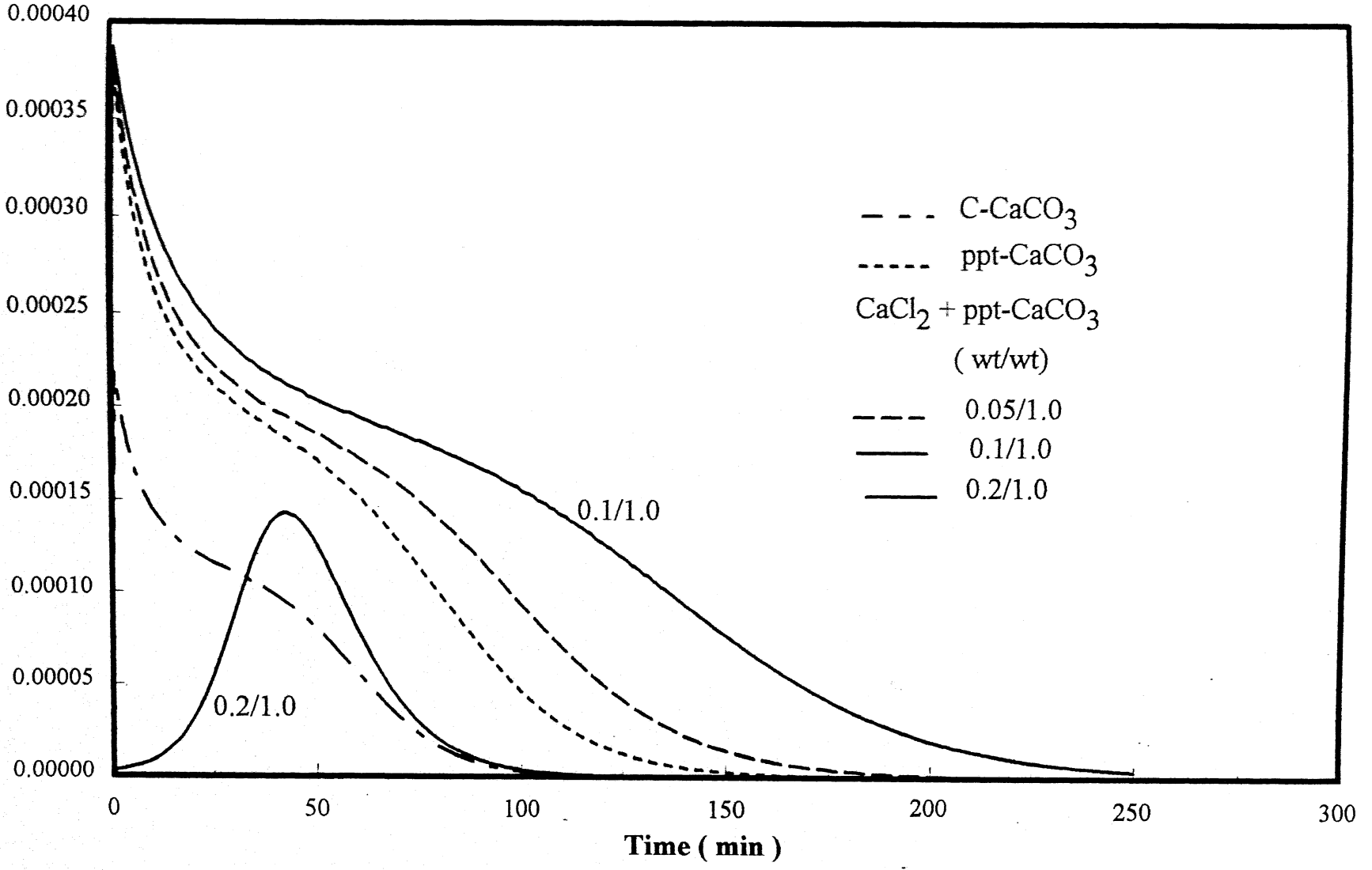

Figure 5.11: Model prediction for average concentration profiles in the pores on SO_2 sorption

(Q_{SO_2}= 6 cc/min, Q_{O_2}= 600 cc/min, T = 750^{0}C, W = 2 g)

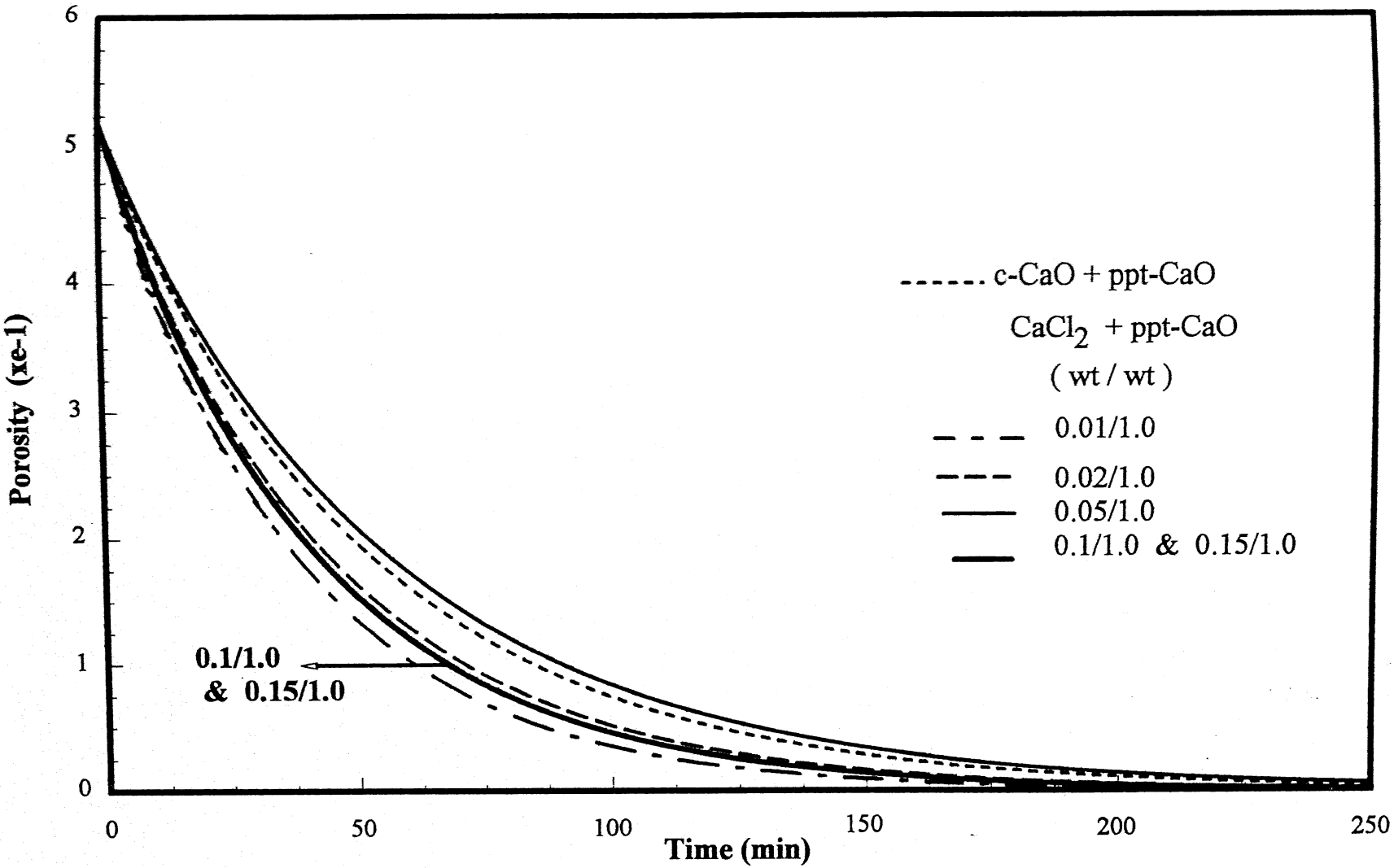

Figure 5.12: Model predictions of variation of porosity with time for additive ($CaCl_2$) on SO_2 sorption

(Q_{SO_2}= 6cc/min, Q_{O_2}= 600 cc/min, T= 950^{0}C, W = 2 g)

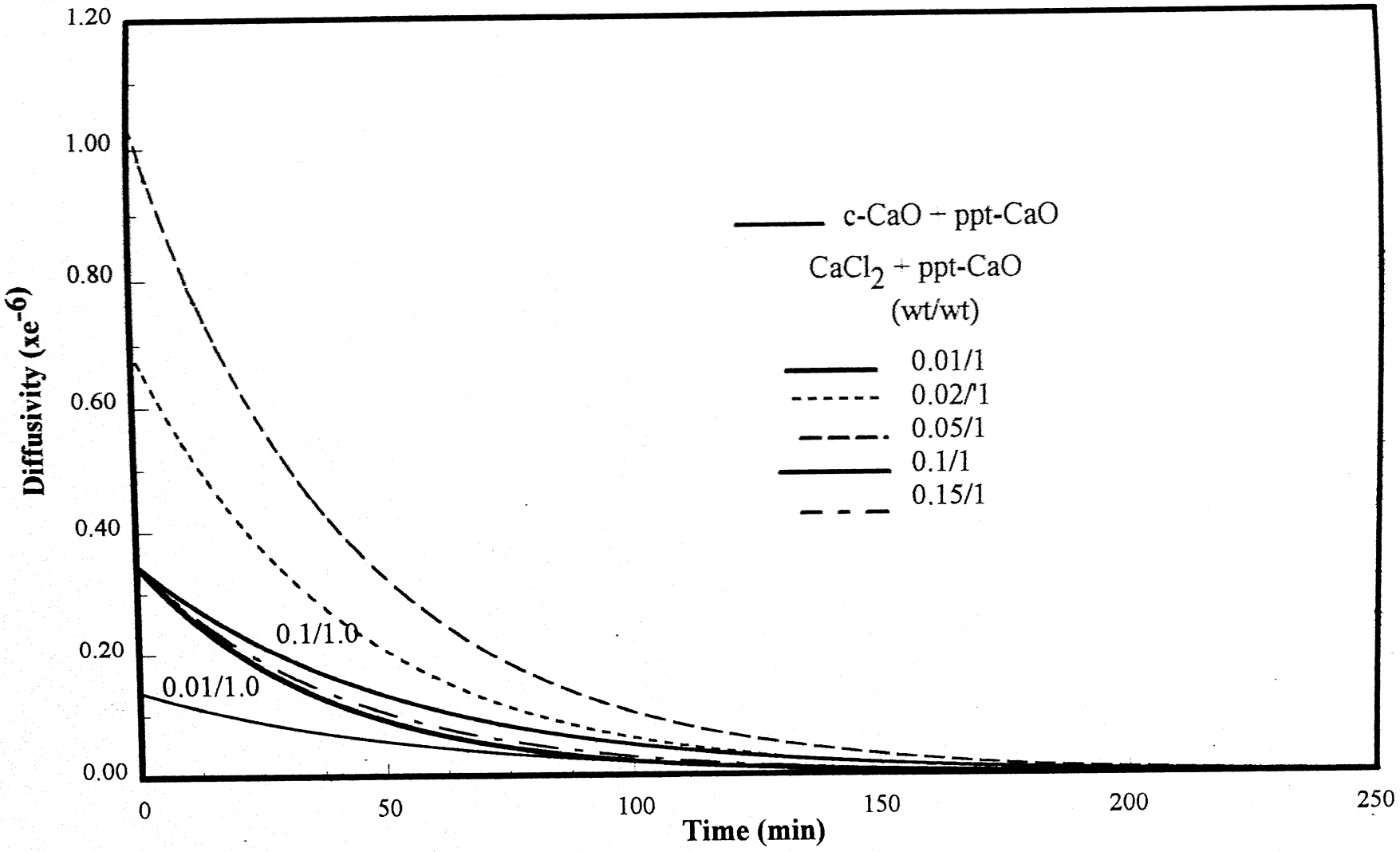

Figure 5.13: Model predictions of variation of diffusivity with time for additive ($CaCl_2$) in ppt-CaO

(Q_{SO_2} = 6 cc/min, Q_{O_2} = 600 cc/min, T = 950^{0}C, W = 2 g)

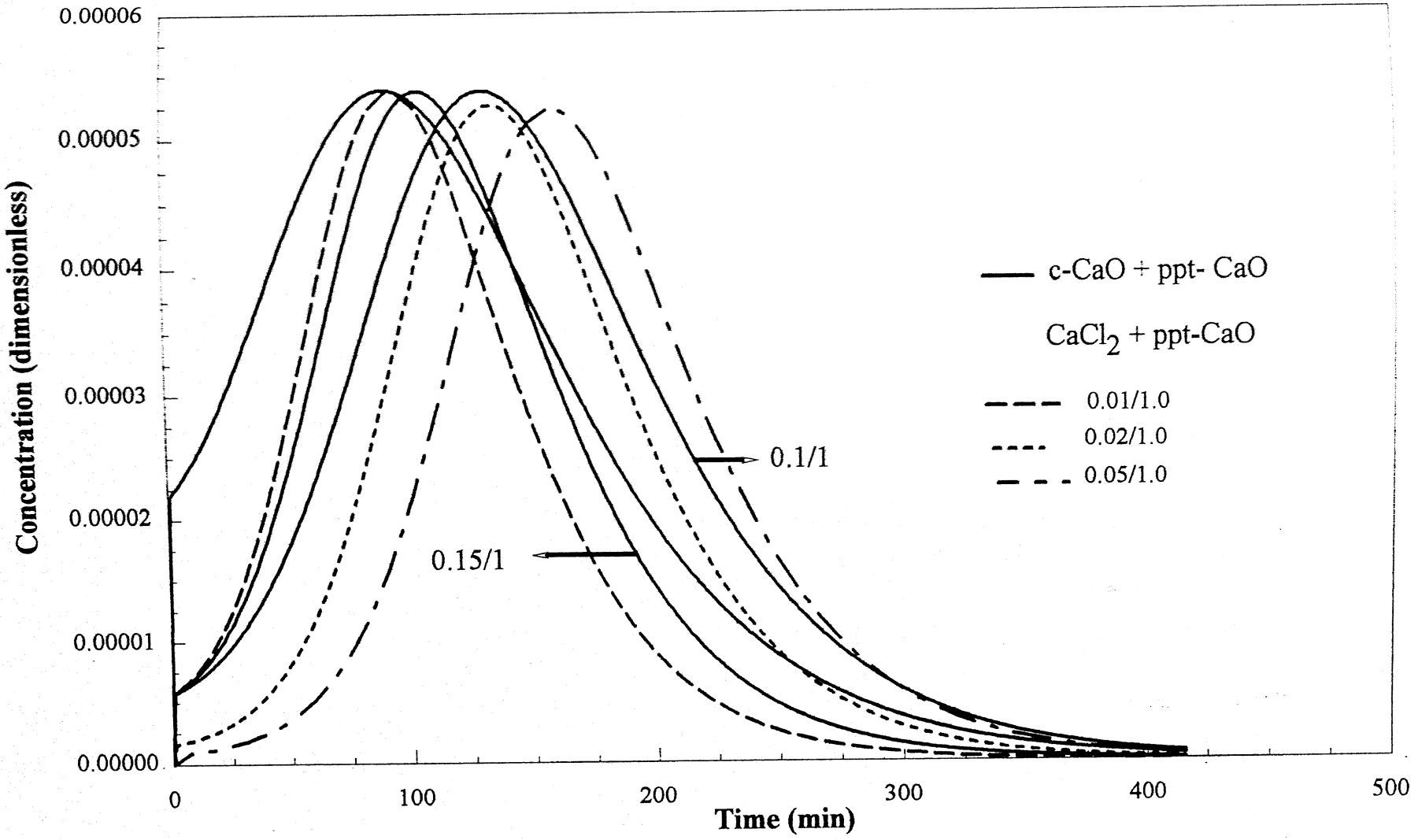

Figure 5.14: Model prediction for average concentration profiles in the pore on SO_2 sorption

(Q_{SO_2}= 6cc/min, Q_{O_2}= 600 cc/min, T = 950^{0}C, W = 2 g)

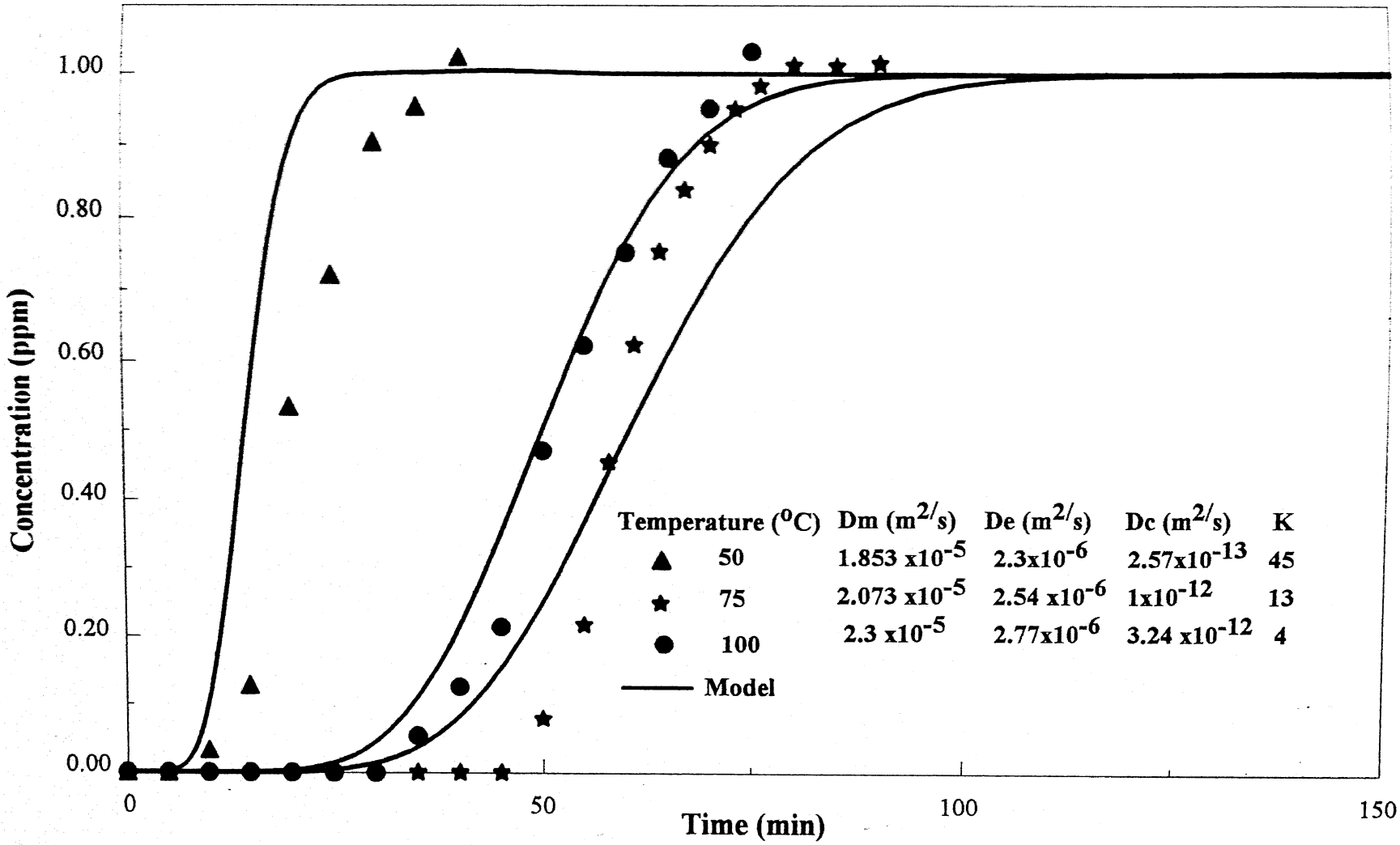

Figure 5.15: Effect of temperature on SO_2 adsorption by zeolite

(Rp = 1.115 mm, Q = 300 cc/min, Cg_{inlet} = 10000 ppm, W = 5 g)

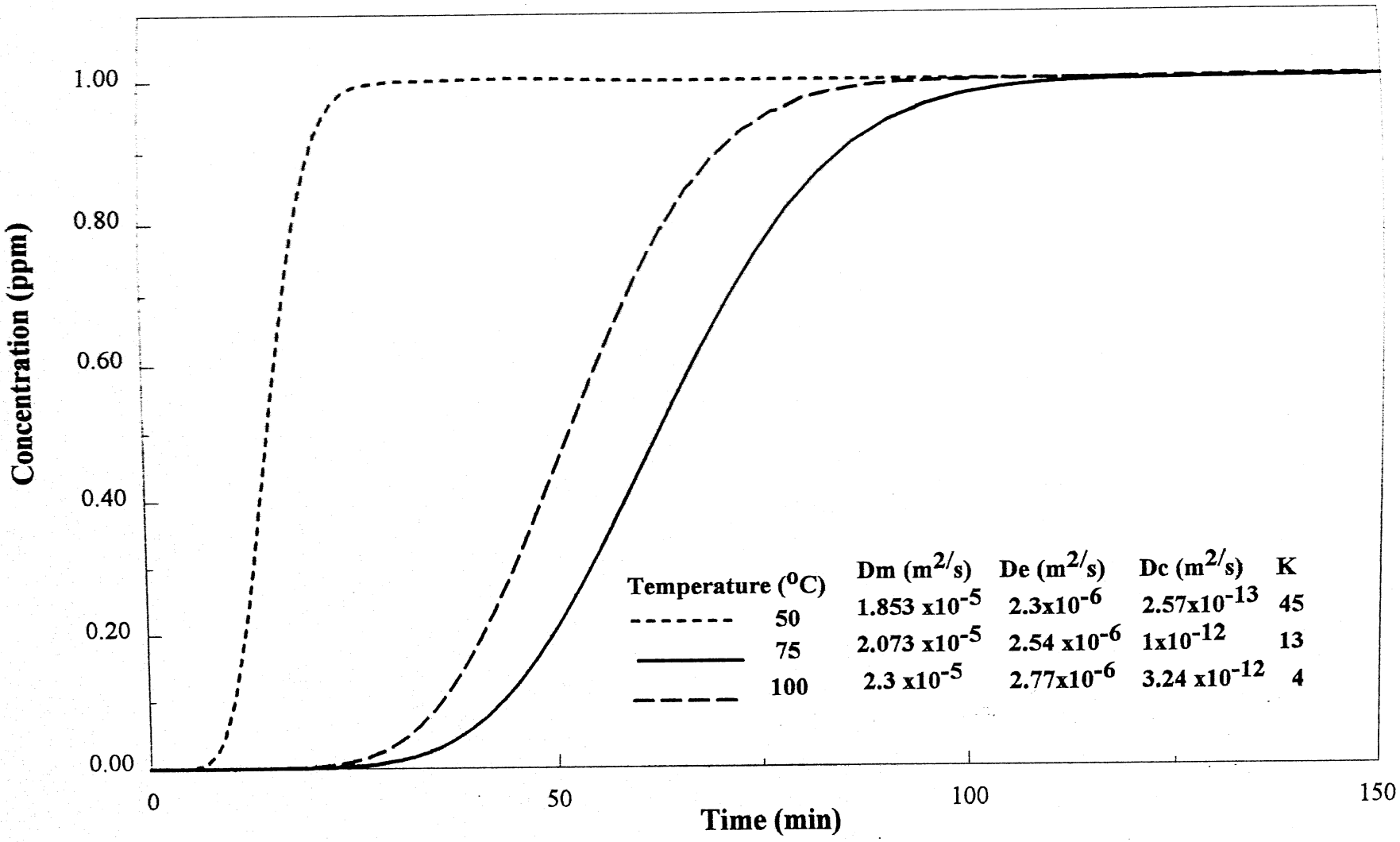

Figure 5.16: Average concentration in macro-pore during SO_2 adsorption by zeolite

(Rp = 1.115 mm, Q = 300 cc/min, Cg_{inlet} = 10000 ppm, W = 5 g)

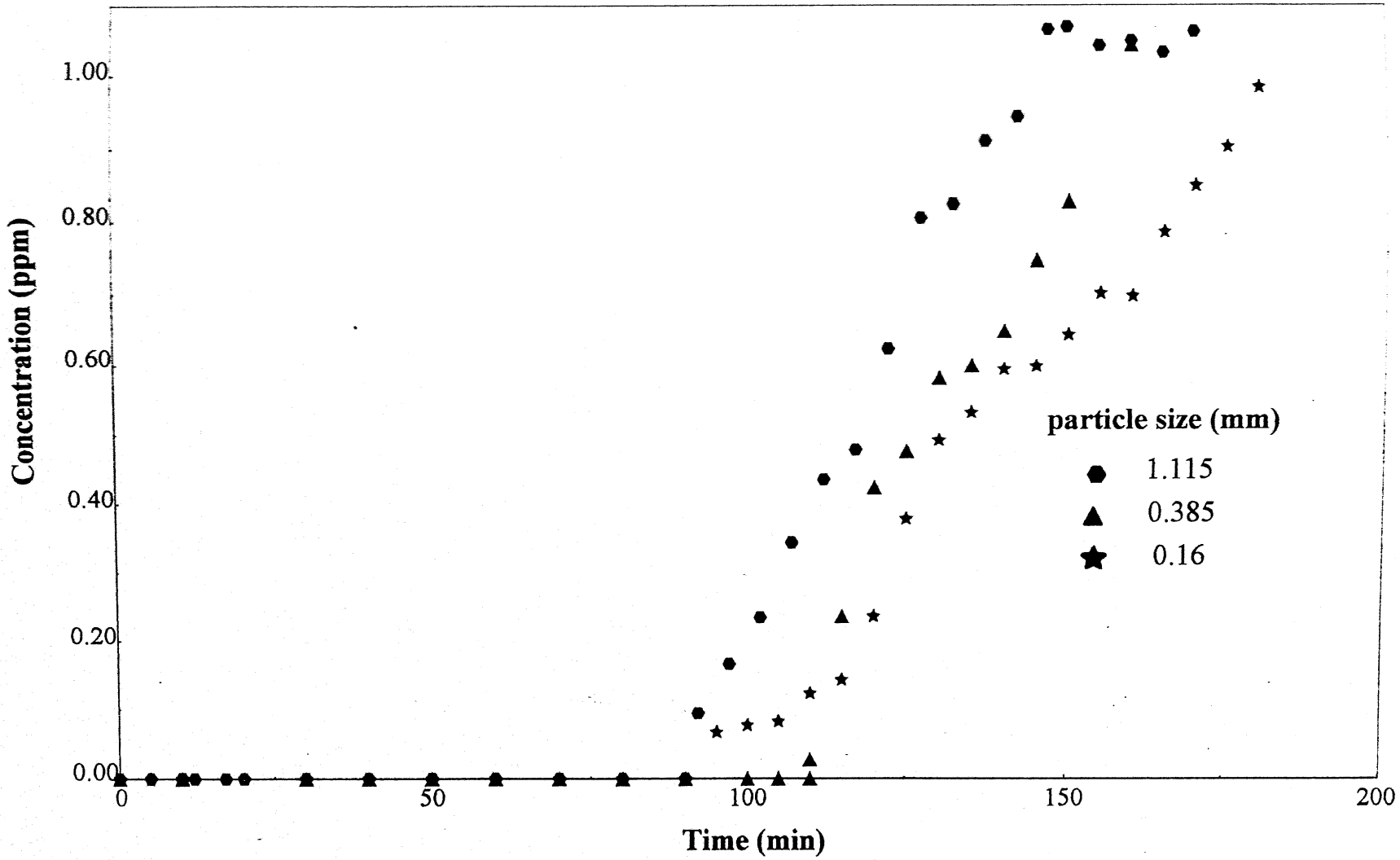

Figure 5.17: Effect of pellet size on SO_2 adsorption by zeolite

(Q = 300 cc/min, W = 5 g, T = 75^{0}C, Cg_{inlet} = 5000 ppm, De = 2.54e-6 m^2/s, Dc = 1e-12 m^2s)

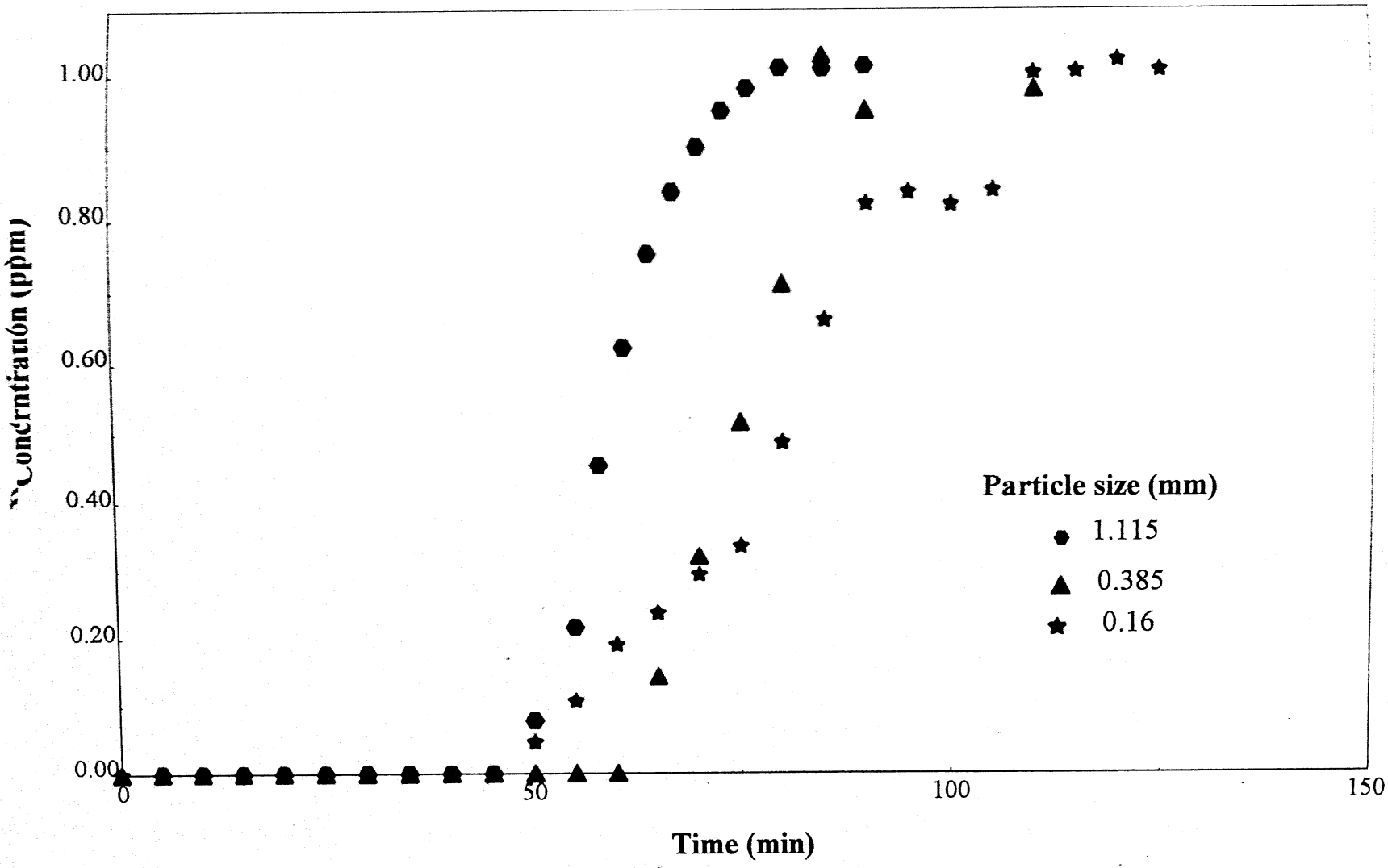

Figure 5.18: Effect of pellet size on SO_2 adsorption by zeolite

(Q = 300 cc/min, W = 5 g, T = 75^{o}C, Cg_{inlet} = 10000 ppm, De = 2.54e-6 m^2/s, Dc = 1e-12 m^2s)

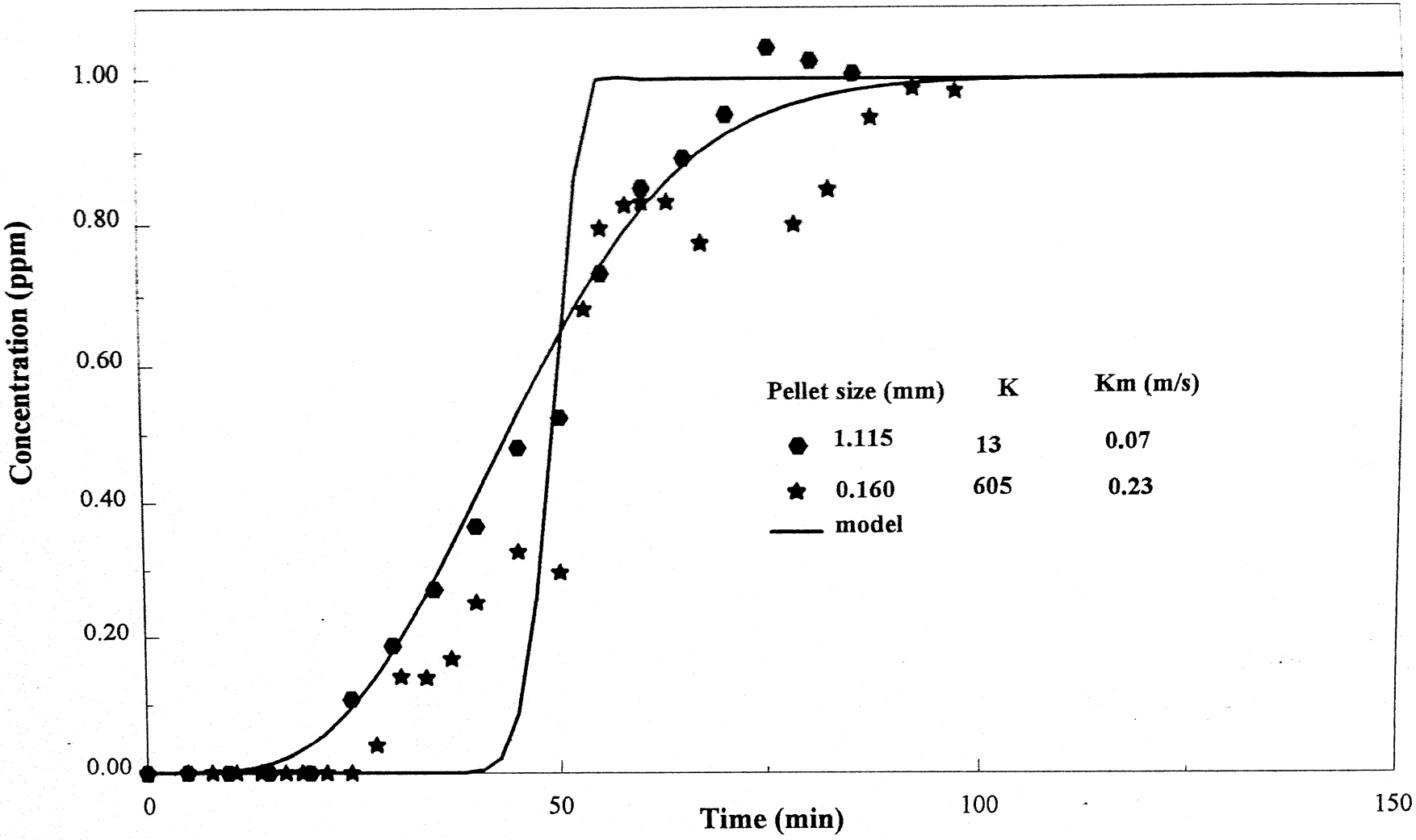

Figure 5.19: Effect of pellet size on SO_2 adsorption by zeolite

(Q = 600 cc/min, W = 5 g, T = 75^{0}C, Cg_{inlet} = 5000 ppm, De = 2.54e-6 m^2/s, Dc = 1e-12 m^{2}s)

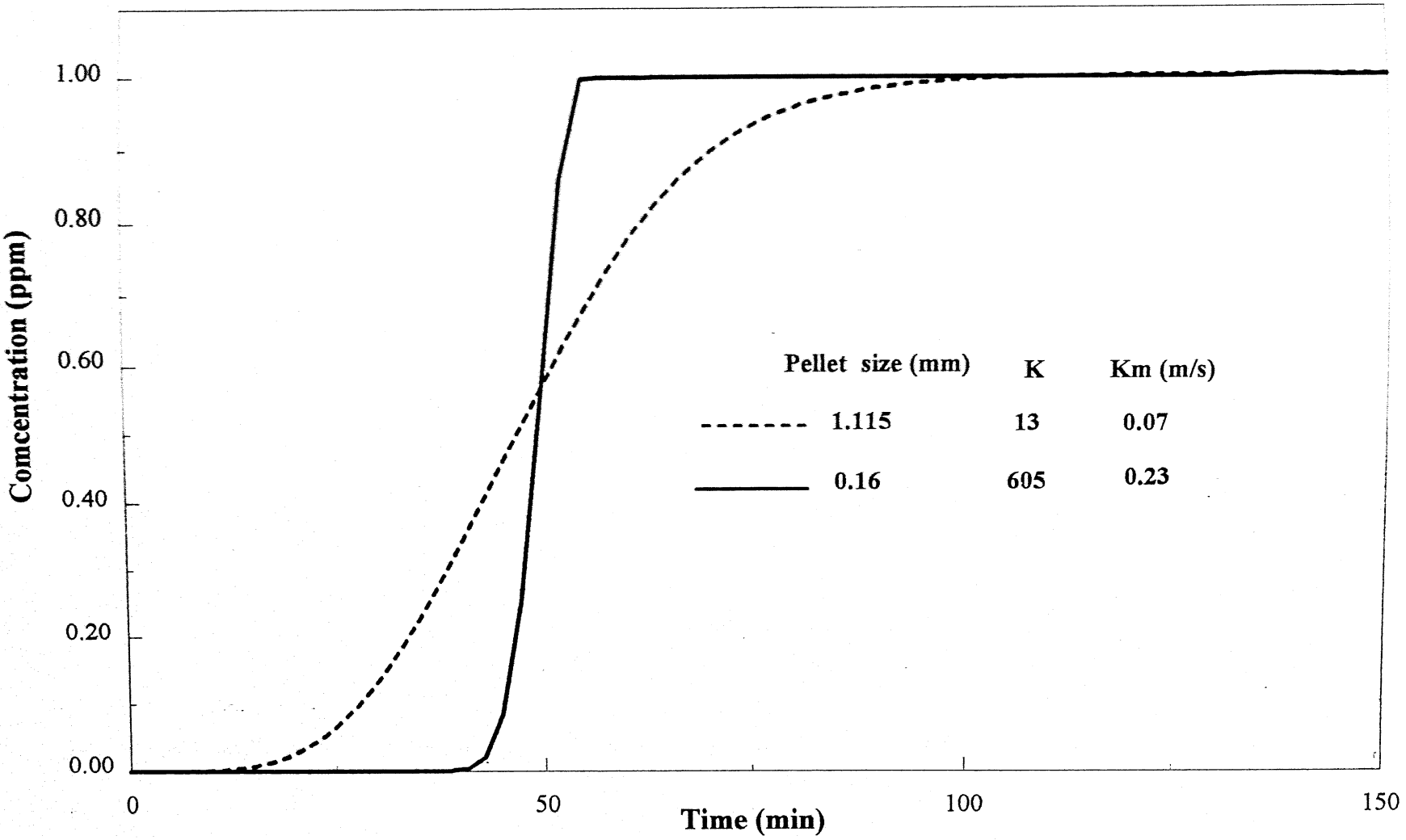

Figure 5.20: Average concentration in the macro-pore during SO_2 adsorption

(Cg_{inlet} = 5000 ppm, Q = 600 cc/min, T = 75 ^{0}C, W = 5 g, De = 2.54e-6 m^2/s, Dc = 1e-12 m^2/s)

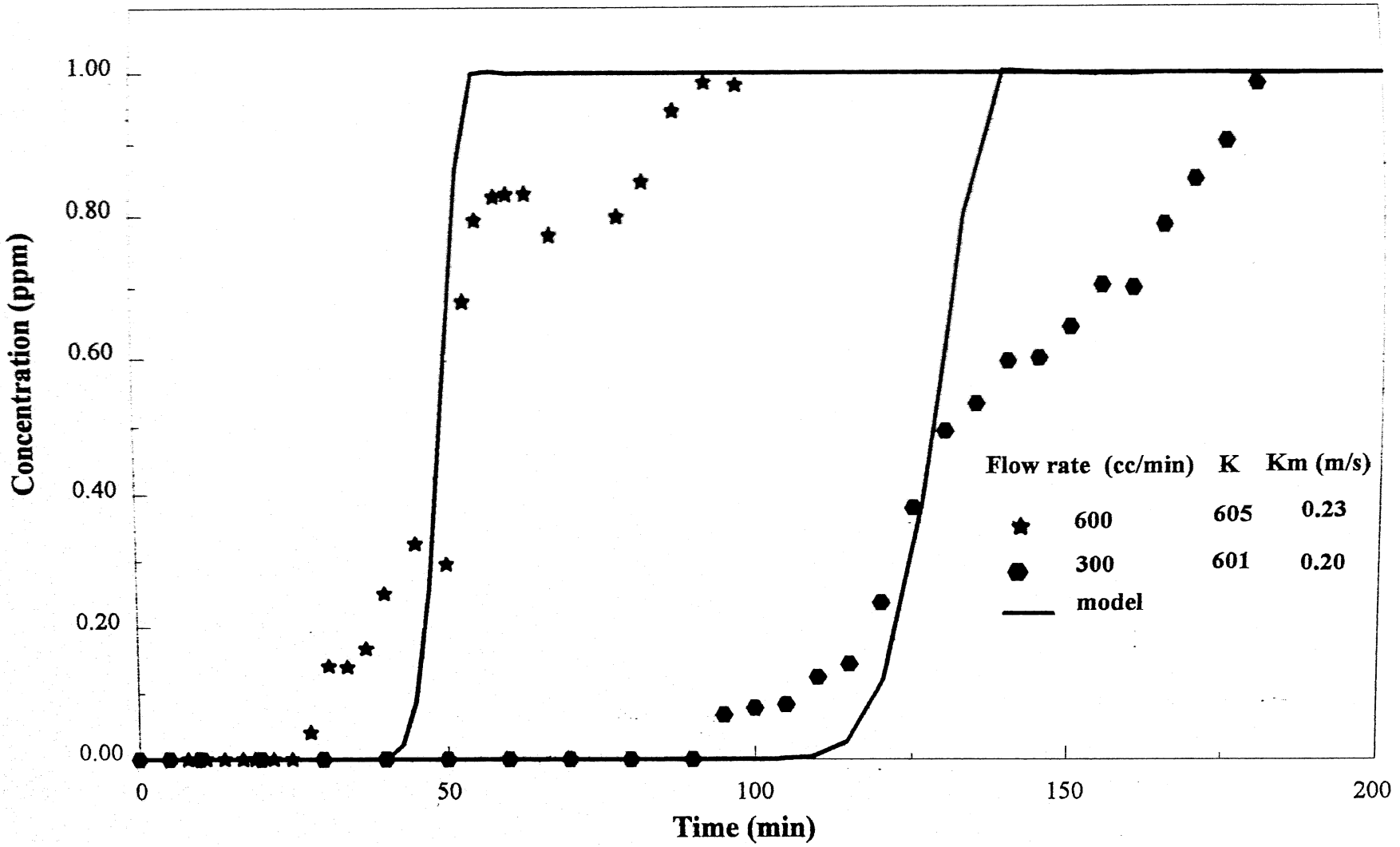

Figure 5.21: Effect of flow rate on SO_2 adsorption by zeolite

(Rp = 0.16 mm, Cg_{inlet} = 5000 ppm, T = 75 ^{o}C, W = 5 g, De = 2.54e-6 m^2/s, Dc = 1e-12 m^2/s)

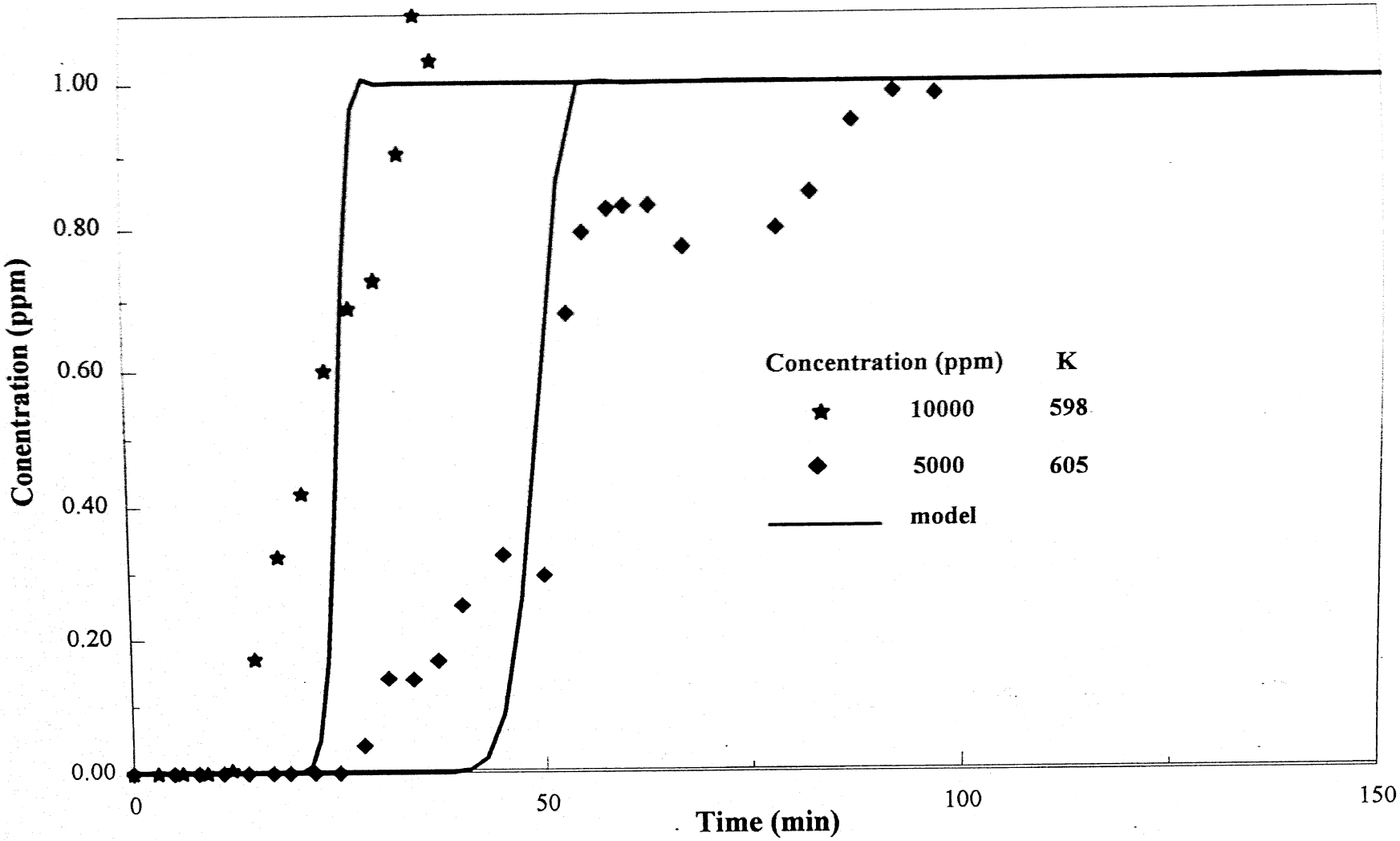

Figure 5.22: Effect of concentration on SO_2 adsorption by zeolite

(Rp = 0.16 mm, T = 75 ^{0}C, Q = 600 cc/min, W = 5 g, De = 2.54e-6 m^2/s, Dc = 1e-12 m^2/s)

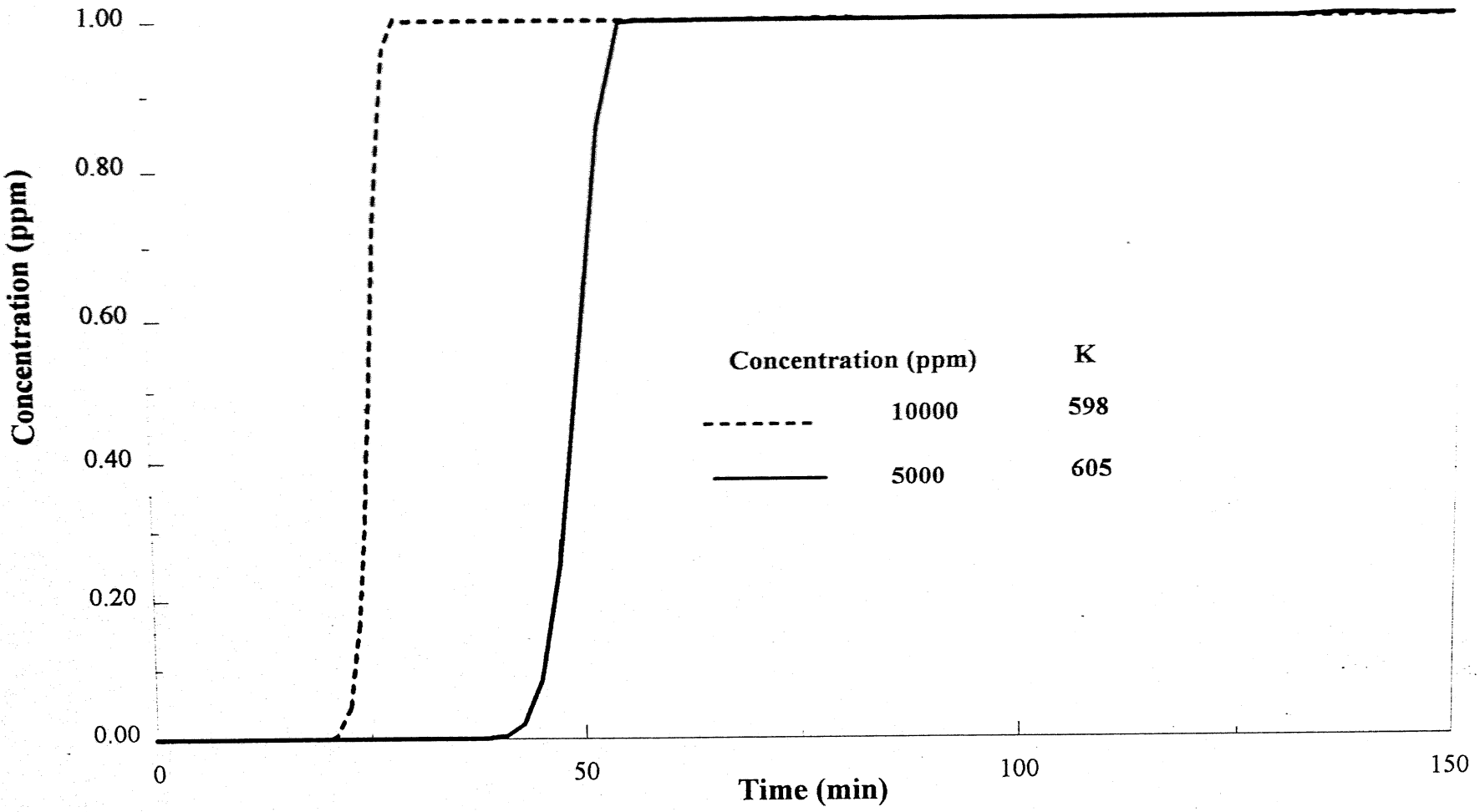

Figure 5.23: Average concentration in the macro-pore during SO_2 adsorption

(Rp = 0.16 mm, T = 75 ^{o}C, W = 5 g, Q = 600 cc/min, De = 2.54e-6 m^2/s, Dc = 1e-12 m^2/s)

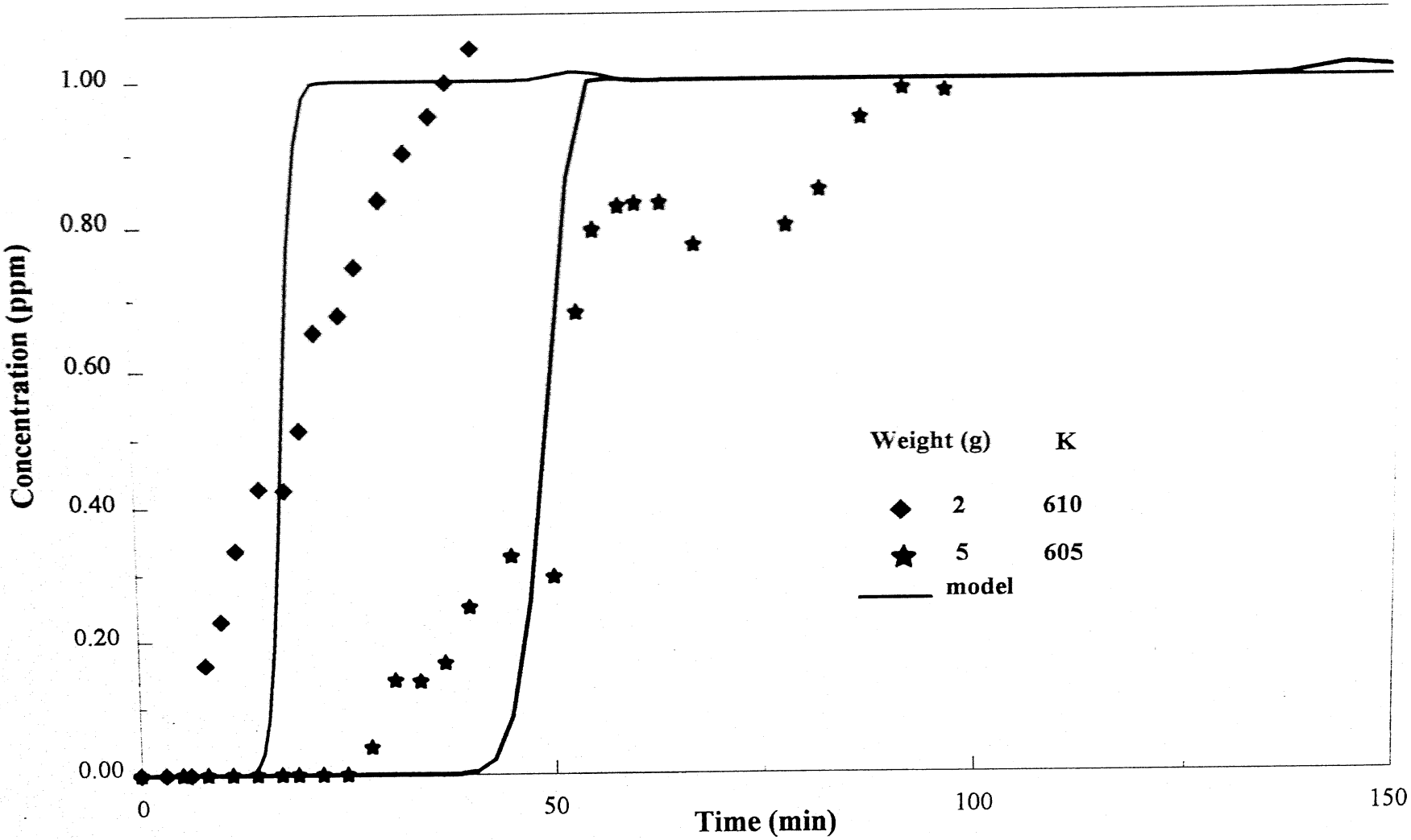

Figure 5.24: Adsorption of SO_2 by zeolite for various amount

(Rp = 0.16 mm, Q = 600 cc/min, T = 75^{0}C, Cg_{inlet} = 5000 ppm, De = 2.54e-6 m^2/s, Dc = 1e-12 m^2s)

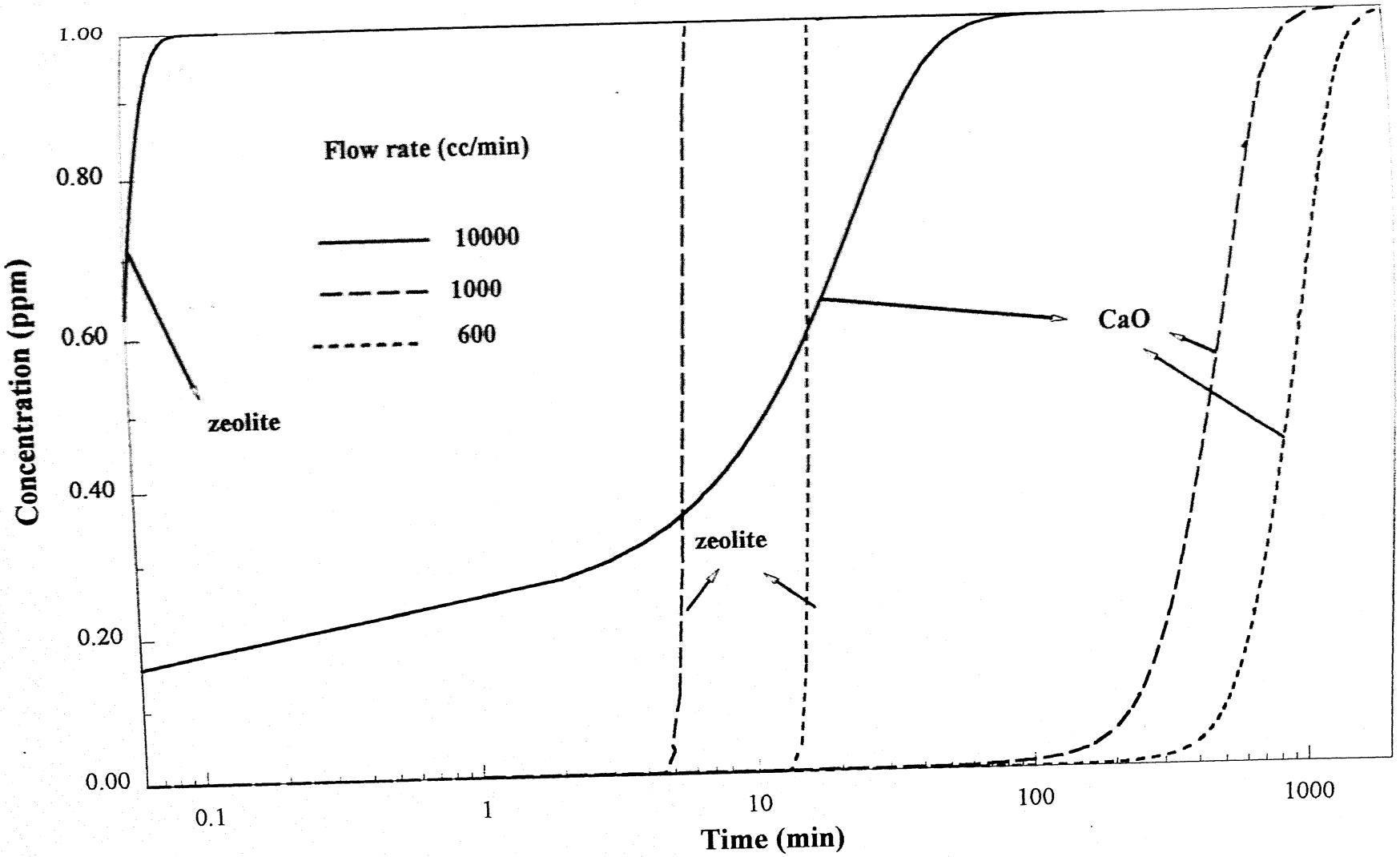

Figure 5.25: Comprasion of SO_2 sorption by zeolite and CaO

(zeolite: T = 75^{0}C, CaO: T = 850^{0}C, W = 5 g, Cg_{inlet} = 10000 ppm)

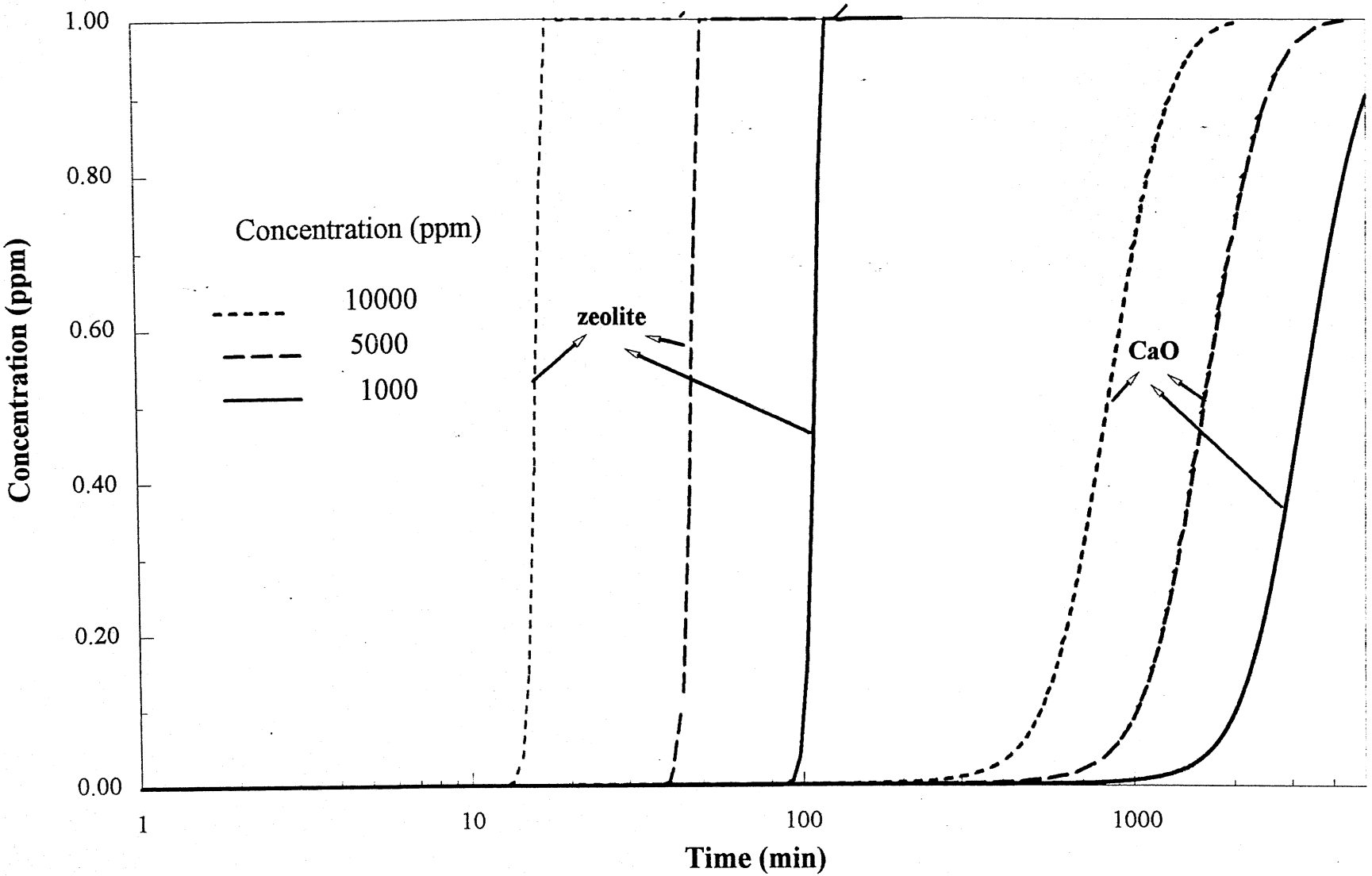

Figure26: Comprasion of SO_2 sorption by zeolite and CaO

(zeolite: T = 75^{o}C, CaO: T = 850^{o}C, W = 5 g)

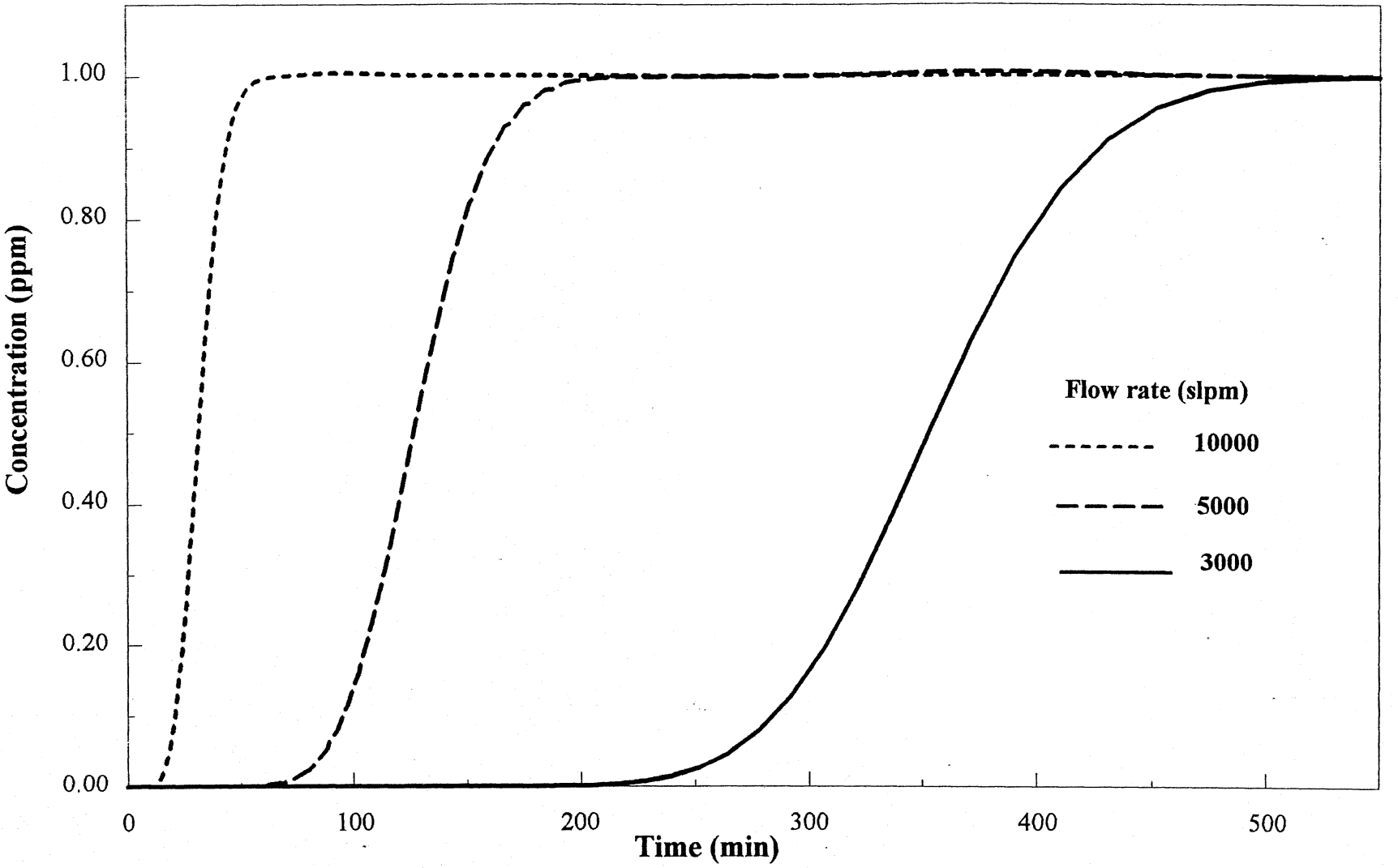

Figure 27: Model predictions for SO_2 adsorption by Zeolite on an industrial scale

(Rp= 1.115 mm, L = 3.15 m, I.D = 0.3 m, T = 75^0C, W = 120 kg, Cg_{inlet} = 10000 ppm)

S.No.	Sample	Temperature (°C)	Break-through Time (min)	Reaction Time (min)	Sulphate conversion (%)
1	$CaCO_3$	750	25	150	24.63
2	$CaCO_3$	950	25	380	52.98
3	$Ca(OH)_2$	950	90	400	48.60
4	Calcium acetate	750	60	235	54.77
5	Calcium acetate	850	100	480	56.08
6	Calcium acetate	950	65	395	49.02

Table5.1: Breakthrough time, reaction time and sulphate conversion of different commercial sorbents at different temperatures

S.No.	CaO + MgO (g)	Temperature (°C)	Break-through time (min)	Reaction Time (min)	Sulphate Conversion (%)
1	0.25 + 1.75	850	20	140	18.55
2	1.25 + 0.75	850	60	410	70.23
3	1.5 + 0.5	850	40	240	40.13
4	1.75 + 0.25	850	65	370	64.69

Table5.2: Breakthrough time, reaction time and sulphate conversion of different mixer (CaO + MgO) ratios of sorbents

S.No.	Types of sorbents	Break through Time (min)	Reaction time (min)	Final wt. (g)	Sulphate conversion (%)
1	c-$CaCO_3$	25	150	2.618	24.63
2	Ppt-$CaCO_3$	35	165	3.42	28.79
3	Ppt-$CaCO_3$ + $CaCl_2$ (0.05/1.0)	40	220	3.314	41.07
4	ppt-$CaCO_3$ + $CaCl_2$ (0.1/1.0)	40	260	3.735	54.68
5	ppt-$CaCO_3$ + $CaCl_2$ (0.2/1.0)	40	65	2.847	26.65

Table 5.3: Breakthrough time, reaction time and sulphate conversion of different sorbents at temperature 750°C

S.No.	Types of sorbents	Break through Time (min)	Reaction time (min)	Final wt. (g)	Sulphate conversion (%)
1	c-$CaCO_3$	25	380	4.332	52.97
2	ppt-$CaCO_3$	30	440	4.557	56.19
3	Ppt-$CaCO_3$ + $CaCl_2$ (0.01/1.0)	55	290	3.812	45.69
4	ppt-$CaCO_3$ + $CaCl_2$ (0.02/1.0)	105	400	3.913	44.61
5	ppt-$CaCO_3$ + $CaCl_2$ (0.05/1.0)	120	410	3.992	62.18
6	ppt-$CaCO_3$ + $CaCl_2$ (0.1/1.0)	50	370	3.914	50.49
7	ppt-$CaCO_3$ + $CaCl_2$ (0.15/1.0)	50	360	3.991	38.01

Table 5.4: Breakthrough time, reaction time and sulphate conversion of different sorbents at temperature 950°C

S.No.	Types of sorbents	Temperature (°C)	Break-through Time (min)	Reaction Time (min)	Sulphate Conversion (%)
1	Calcium carbonate	950	25	380	52.98
2	Calcium hydroxide	950	90	400	48.6
3	Calcium acetate	850	100	480	56.08
4	CaO + MgO (1.25+0.75)	850	60	410	70.23
5	ppt-$CaCO_3$	950	30	440	56.19
6	ppt-$CaCO_3$ + $CaCl_2$ (0.05/1.0)	950	120	410	62.18

Table 5.5: Comparative performance of various non-regenerative sorbents

S.No.	Temperature (°C)	Break-through Time (min)	Adsorption Time (min)
1	50	10	40
2	75	50	90
3	100	35	80

Table 5.6: Breakthrough and adsorption time at different temperature

S.No.	Particle size (mm)	Conc. (ppm)	Flow rate (cc/min)	Break-through time (min)	Adsorption time (min)
1	1.115	10000	300	50	90
2	1.115	5000	300	92	170
3	0.385	10000	300	55	105
4	0.385	5000	300	100	170
5	0.160	10000	300	50	125
6	0.160	5000	300	95	180

Table 5.7 Breakthrough time and adsorption time at different flow rate and concentration for various particle size

S.No	Pellet radius (mm)	Wt (g)	Temp (°C)	Flow rate (cc/min)	Conc. (ppm)	Molecular diffusivity (Dm) (m^2/s)	Effective diffusivity (De) (m^2/s)	Crystal diffusivity (Dc) (m^2/s)	Mass transfer coefficient (Km) (m/s)	Partitioning coefficient K
1	1.115	5	75	600	5000	2.07e-5	2.54e-6	1e-12	0.07	13
2	1.115	5	50	300	10000	1.85e-5	2.3e-6	2.57e-13	0.05	45
3	1.115	5	75	300	10000	2.07e-5	2.54e-6	1e-12	0.05	13
4	1.115	5	100	300	10000	2.3e-5	2.77e-6	3.24e-12	0.05	4
5	0.16	2	75	600	5000	2.07e-5	2.54e-6	1e-12	0.23	610
6	0.16	5	75	600	5000	2.07e-5	2.54e-6	1e-12	0.23	605
7	0.16	5	75	300	5000	2.07e-5	2.54e-6	1e-12	0.20	601
8	0.16	5	75	600	10000	2.07e-5	2.54e-6	1e-12	0.23	598

Table 5.8: Various Input parameters for model predictions
($R_c = 2x10^{-6}$ m, P = 1 atm, $\alpha = 0.64$)

S.No.	Wt. (g)	Height (cm)	Flow rate (cc/min)	Mano-meter Height (CCl_4) (cm)	$\frac{V_{bed}-V_{zeo}}{V_{bed}}$ (ε_b)	Data pressure P=ρgh (N/m^2)	Pressure (Ergun eq) at (ε_b) (N/m^2)	Error $\frac{(P_{exp}-P_{the})*100}{P_{exp}}$ (%)
1	2	3	300	4.0	0.354	624.1	7.04	98.87
2	2	3	600	10.0	0.354	1560.2	14.09	99.09
3	5	6	300	8.7	0.192	1357.2	138.22	89.82
4	5	6	600	19.5	0.192	3042.0	276.44	90.91
5	7	8	300	9.5	0.152	1482.5	409.13	72.40
6	7	8	600	20.0	0.152	3120.1	818.25	73.77

Table 5.9: The experimentally and theoretically calculated pressure drop across the reactor for 1.115mm particle

S.No.	Wt. (g)	Height (h) (cm)	Flow rate (cc/min)	Mano-meter Height (CCl_4) (cm)	Data for Pressure P=ρgh	$\frac{V_{bed}-V_{zeo}}{V_{bed}}$ (ε_b)	Pressure (Ergun eq) (N/m^2)	Error $\frac{(P_{exp}-P_{the})*100}{P_{exp}}$ (%)
1	2	4	300	27.0	4212.4	0.5149	83.63	98.01
2	2	4	400	65.0	10141.0	0.5149	111.51	98.90
3	2	4	450	88.0	13729.4	0.5149	112.45	99.17
4	5	8	150	75.0	11701.2	0.3938	291.93	97.50
5	5	8	200	83.5	13105.3	0.3938	389.25	97.03

Table 5.10: The experimentally and theoretically calculated pressure drop across the reactor for 0.16mm particle

CHAPTER 6
CONCLUSIONS

In the present work, a combined experimental and theoretical study was done to understand the kinetics and mechanism of SO_2 removal by 5A zeolite materials. The emphasis was on determining the suitability of the commercially available zeolites in the adsorption of SO_2 under varying operating conditions. Experimental screening of various non-regenerative types of Ca-based sorbents was also carried out to determine their comparative sorption performances measured in the breakthrough time and total sulphate conversion. Most of the sorbents, such as $CaCO_3$, $Ca(OH)_2$, $Ca(CH_3COOH)_2$ were commercially obtained. Some of the sorbents were prepared or modified in the laboratory.

The main findings of this work can be summarized as follows. CaO obtained on calcination of calcium acetate was found to be superior amongst all sorbents used in this work, with relatively lower reaction temperature (850°C), longer breakthrough time (100 min), longer reaction times (480 min) and also, higher sulphate conversion (~70%). CaO obtained on calcination of CO_2 precipitated carbonate in the laboratory exhibited marginally superior performance relative to that obtained commercially. However, the addition of small quantity of $CaCl_2$ in ppt-$CaCO_3$ (0.05:1) significantly improved the performance, as the breakthrough time increased from 25 min to 120 min and the corresponding sulphate conversion from 50% to 60%. $CaCl_2$ being hygroscopic in nature, the incorporation of trace amount of moisture in the sorbents resulted in decrease of the volume of the sulphate layers. The pore closure phenomenon was thus delayed. Magnesium based sorbents were found to be the least suitable for SO_2 sorption.

In the case of adsorption by zeolites, the various experimental conditions included the reaction temperature, inlet gas concentration, flow rate, particle size and the amount of zeolites. The optimum adsorption temperature was determined to be 75°C. The adsorbents of smaller size exhibited relatively longer breakthrough and reaction times. A mathematical model for zeolites (bi-porous) was developed to predict the SO_2 breakthrough characteristics in a packed bed under a wide range of operating conditions. The theoretical analysis incorporated the effects of gas diffusion in the adsorbent bed, in

the macro-pore and within the crystal. A simplified approach based on linear driving approximation and average radial concentrations significantly reduced the computation time. The model had only one adjustable parameter, the equilibrium or partitioning constant or coefficient. The model predictions were found to be in good agreement with the experimental data.

6.1 Scope of future study:

Further search on or development of novel sorbents is required. As the sorption process suffers from premature termination due to pore closure mechanism, an optimum gas solid contacting pattern is required, as in a fluidized bed. Additionally, simulated moving bed, high gravity contactor can also be tried to improve upon the mass transfer rate from bulk of the gas to the surface of the particle.

In this work, the adsorption of SO_2 by 5A type zeolite was carried out. A study on novel adsorbents, such as different types of zeolites such as13X molecular sieve, molecular sieve carbon (MSC), and activated carbon fibers (ACF) is required. The regenerative characteristic of the adsorbents should be investigated so as to reuse the adsorbent and make the process continuous. A surface analysis of the sorbent materials before and after the reaction, using SEM, XPS should be carried out to determine the change in the morphology/structure of the particles during the course of the reaction. Similarly, pore size distribution and BET area measurements should also be done to determine change in the pore structure of the particles.

Bibliography

[1] Agnihotri, R., S.K.Mahuli, R. Jadhav, S. Chauk and L.S. Fan "Combined calcination, sintering and sulfation model for $CaCO_3$ – SO_2 reaction", *AIChE J.*, **45**, pp 366-80 (1999)

[2] Bird, R.B., W.E. Stewart, and E.N. Lightfoot, "Transport Phenomena", Wiley, New York, NY (1960).

[3] Borgwardt, R. H. "Calcination kinetics and surface area of dispersed limestone particles", *AIChE J.*, **31**, pp103-09 (1985)

[4] Bruce, K.R., B.K.Gullet, and L.O. Beach, "Comparative SO_2 reactivity of CaO derived from $CaCO_3$ and $Ca(OH)_2$", *AIChE J*, **35**, pp 37-41 (1989)

[5] Cutler, A.J.B., T. Flatley, and K.A. Hay, "Fire-side corrosion in power-station boilers", *Combustion*, pp 17-25 (1980)

[6] Claus, J., J.C.S.Chang, T.G.Brna, " Evaluation of sorbents and additives for dry SO_2 removal" Environmental progress vol. **6** no.2, pp26-32,(1987).

[7] Duong, D.Do, " Adsorption analysis Equilibria and Kinetics", Imperial College Press (1998)

[8] Dasgupta, K., "Breakthrough and sulphate conversion analysis during removal of sulphur-dioxide by calcium oxide sorbents", M.Tech Thesis, Department of Chemical Engineering, Indian Institute of Technology Kanpur, February (2001)

[9] Dogu, T., "The importance of pore structure and diffusion in the kinetics of gas-solid non-catalytic reactions: reaction of calcined limestone with SO_2", *Chemical Engineering J*, **21**, p 213-222 (1981)

[10] Dogu,T., D. Gulsen, A. Pekediz, "Dynamic analysis of viscous flow and diffusion in porous solids" *AIChE J. Vol.* **32**, pp 1370-75 (1989)

[11] Flood, H.W., "Sulfur & SO_2 developments", CEP, New York, NY (1971)

[12] Hartman, M., and R.W. Coughlin, "Reaction of sulfur dioxide with limestone and the grain model", *AIChE J, Vol* **22**, pp 490-98 (1976)

[13] Haynes, H. W. "The Determination of effective diffusivity by gas chromatography", *AIChE J. Vol. 27* No.1, pp 81-91 (1981)

[14] Kopac, Turkan, "Non-isobaric adsorption analysis of SO_2 on molecular sieve 13X and activated carbon by dynamic technique", *Chemical Engineering and processing* **38** 45-53 (1999).

[15] Kopac, Turkan, Erdogan Kaymakci and Mehmet Kopac Departyment of chemistry, Zongudak, Turkey (1997).

[16] Liu, H.F. and B.G.Liptak, "Air Pollution", Lewis Publishers, New York, NY(2000)

[17] Mahuli, S.K., R. Agnihotri, C. Shriniwas, A. Ghosh-Dastidar, S. H. Wei and Liang-Shih Fan "Pore-structure optimization of calcium carbonate for enhanced sulfation", *AIChE J*, **43**, pp 2323-2333 (1997)

[18] Manahan, S.E, "Environmental Chemistry", Lewis Publishers, New York, NY (2000)

[19] McCabe, W.L., J.C. Smith, P. Harriott, "Unit Operations of Chemical Engineering", 5th edition, McGraw Hill, New York, NY (1956).

[20] Octave Levenspiel, "Chemical Reaction Engineering", Wiley, New York, NY (1972)

[21] Orbey, N., G. Dogu and T. Dogu, "Breakthrough analysis of non catalytic solid-gas reactions, reaction of SO_2 with calcined limestone", *Can. J. Chem. Eng.* **60** pp 314-20 (1982)

[22] Perry, R.H. and D. Green, "Perry's Chemical Engineers' Handbook", 6th Ed., McGraw-Hill, New York, NY (1984)

[23] Ramachandran, P.A and L.K. Doraiswamy "Modeling of non-catalytic gas – solid reactions" *AIChE J.* **28 (6)** pp 881-898 (1982)

[24] Rice, W.R, G.A.Bond, Flue gas desulfrization by In-duct dru scrubbing using calcium hydroxide" *AIChE. J*, **36**, pp 473-81 (1990)

[25] Seinfeld, and Pandis " Atmospheric Chemistry and Physics", Wiley, New York, NY (1998).

[26] Simons, G.A, A.R. Garman, "Small pore closure and the deactivation of the lime stone sulfation reaction", *AIChE. J*, **32**, pp 1491-99 (1986)

[27] Smith, J.M., "Chemical Engineering Kinetics", Mc Graw-Hill, New-York, NY (1956).

[28] Tsibranska,I, A.Assenov, "Experimental verification of the model of adsorption in biporous particles *Chemical Engineering and processing* **39**, pp 149-159(2000).

[29] Yiannis, A., W.Zhu, D.L.Wise, G.A.Simons, "Effectiveness of calcium magnesium acetate as an SO_x sorbent in coal combustion" *AIChE. J*, **39**, pp 761-733 (1993)

[30] Yang, R.T., "Gas Separation by Adsorption Processes", Imperial College Press (1997)

APPENDIX

The following calculations are used in the model based on the experimental conditions:

gas flow rate = 600 cc/min

$$superficial\ gas\ velocity = \frac{(Flowrate)(R)(Temp)}{(22.4)(60)(\Pr essure)(\pi d^2_t / 4)} \quad \text{(A1)}$$

where,

flow rate is in lit/min

R = universal gas constant in J/kg K

Temp = temperature in K

Pressure in N/m^2

Cross sectional area in m^2

$$\text{superficial velocity} = \frac{(0.6)(8.314)(348)(4)}{(22.4)(60)(101325)(\pi(0.014)^2)} = 0.0828 \text{ m/s}$$

$$\text{Residence time of gas in the reactor} = \frac{length}{vel} \quad \text{(A2)}$$

$$Residence\ time = \frac{0.08}{0.0828} = 0.9661 \text{ s}$$

$$Concentration = \frac{(pressure)(molfraction)(mol.wt)10^{-3}}{(R)(Temperature)} \quad \text{(A3)}$$

$$= \frac{(101325)(0.01)(64)\times 10^{-3}}{(8.314)(348)} = 0.0224\ kg/m^3$$

Bed porosity

Amount of sorbent = 5 gm

density of sorbent = 670 kg/m^3

$$\text{Volume of CaO} = \frac{5\times 10^{-3}}{670} = 7.4626\times 10^{-6}\ m^3$$

$$\text{Volume of the packed bed} = \frac{\pi}{4}(0.014)^2(0.08) = 12.308\times 10^{-6} m^3$$

$$\text{Bed porosity } \epsilon_b = \frac{(12.308 - 7.4626)\times 10^{-6}}{12.308\times 10^{-6}} = 0.3936 \quad \text{(A4)}$$

Bed porosity $\epsilon_b = \frac{(12.308 - 7.4626)\times 10^{-6}}{12.308\times 10^{-6}} = 0.3936$ (A4)

Intra-particle porosity $(\frac{1}{d_a} - \frac{1}{d_s})/\frac{1}{d_a}$ (A5)

$$(\frac{1}{0.71} - \frac{1}{1.97})/\frac{1}{0.71}$$

$$= 0.64$$

Density of gas

$$\rho = \frac{(pressure)(mol.wt)}{(Temperature)(R)} \quad (A6)$$

$$= \frac{(101325)(64\times 10^{-3})}{(8.314)(348)} = 2.2413 \ kg/m^3$$

Reynolds number based on particle diameter

$$\mathrm{Re} = \frac{(density)(\sup vel)(particlediameter)}{(vis\cos ity)} \quad (A7)$$

$$= \frac{2.2413\times 0.0828\times 1.6\times 10^{-4}\times 2}{2\times 10^{-5}} = 2.96$$

Schmidt number

$$\mathrm{Sc} = \frac{(vis\cos ity)}{(density)(moleculardiffusivity)} \quad (A8)$$

$$= \frac{2\times 10^{-5}}{2.2413\times 2.073\times 10^{-5}} = 0.43$$

Dispersion co-efficient

The dispersion co-efficient (*Dz*)is expressed as

$$dispersion - coefficient = \frac{(particle.dia)(vis\cos ity)}{(density)(Pe)} \quad (A9)$$

where Pe is Peclet Number.

The Peclet number are correlated with Reynold's number and Schmidt number by the correlation

$$\frac{1}{Pe} = \frac{0.3}{\mathrm{Re}\times Sc} + \frac{0.5}{1+3.8/(\mathrm{Re}\times Sc)} \quad (A10)$$

$$\frac{1}{Pe} = \frac{0.3}{(2.96)(0.43)} + \frac{0.5}{(1+3.8/(2.96\times 0.43))}$$

$$\text{Pe} = 2.77$$

$$Dz = \frac{(2\times 1.115\times 10^{-3})\times 2\times 10^{-5}}{2.2413\times 2.77} = 7.2\times 10^{-9} m^2/s$$

For $0.008 < \text{Re} < 400$

$0.28 < \text{Sc} < 2.2$

The *mass transfer co-efficient* is calculated using the following correlations:

$$Sh = 2.0 + 1.1(Sc)^{0.33}(\text{Re})^{0.6} \qquad \text{(A11)}$$

$$K_m = \frac{(2+1.1(Sc)^{0.33}(\text{Re})^{0.6})(mol.diffusivity)}{(part.diameter)}$$

$$K_m = \frac{(2+1.1(0.43)^{0.33}(2.96)^{0.6})(2.073\times 10^{-5})}{(2\times 1.6\times 10^{-4})}$$

$$K_m = 0.233 \text{ m/s}$$

Calculation of diffusivity:

The effective diffusivity inside the pores is given by a combination of both Knudsen and molecular diffusion.

The *Knudsen diffusivity* is given by

$$D_K = \frac{2\times r_p}{3}\left(\frac{8RT}{\pi M}\right)^{\frac{1}{2}} = 97\times R_{pore}\left(\frac{T}{M}\right)^{\frac{1}{2}} \qquad \text{(A12)}$$

where

R_{pore}= pore radius in m

M = Molecular weight

T = Temperature in K

D_k = Knudsen diffusion

The *Molecular diffusivity* for a binary gas mixture is given by the Chapman – Enskog equation given by

$$D_m = \frac{10^{-4}[1.084 - 0.249(\frac{1}{M_A}+\frac{1}{M_B})^{\frac{1}{2}}]T^{\frac{3}{2}}(\frac{1}{M_A}+\frac{1}{M_B})^{\frac{1}{2}}}{(P)(r_{AB})(f(\frac{KT}{\in}))} \qquad \text{(A13)}$$

Here

D_m = Molecular diffusivity m^2/s

T = Temperature in K

M_A, M_B = Molecular weight of the two interacting species

P = Total Pressure N/m^2

$f(\frac{KT}{\in})$ = Collision integral, a function of $k\,T/\varepsilon$ where k is Boltzaman constant.

$$\frac{\in_A}{K} = 335.4K$$

$$\frac{\in_B}{K} = 71.4K$$

$$\frac{\in_{AB}}{K} = \sqrt{335.4 \times 71.4}$$

$$= 2.248 \text{ K}$$

$$f(\frac{KT}{\in}) = 0.46$$

$$r_{AB} = \frac{r_A + r_B}{2}$$

$$r_{SO_2-N_2} = \frac{0.4112 + 0.3798}{2} \quad \text{nm}$$

$$= 0.3955 \quad \text{nm}$$

Substitute all the values in A(12)

$$D_m = \frac{10^{-4}[1.084 - 0.249(\frac{1}{64} + \frac{1}{28})^{\frac{1}{2}}]T^{\frac{3}{2}}(\frac{1}{64} + \frac{1}{28})^{\frac{1}{2}}}{(101325)(0.3955)^2(0.46)}$$

$$=2.073\text{x}10^{-5} \text{ m}^2/\text{s}$$

The *combined diffusivity* contributed by both molecular and Knudsen diffusion is given by

$$\frac{1}{D} = \frac{1}{D_K} + \frac{1}{D_m} \qquad \text{(A14)}$$

D = Diffusion co-efficient

The actual diffusion path in the pores will not be equal to the distance in the radial direction, but will be quite tortuous. The actual path depends on the pore structure and the tortuosity factor is defined as the ratio between the actual diffusion path length and the net distance in the direction of flux or radial distance.

The effective diffusivity inside the pores is found by using the formula

$$D_e = \frac{\alpha D}{\tau} \qquad \text{(A15)}$$

where

α = intraparticle porosity

D = diffusivity co-efficient

τ = tortuosity factor

Calculation of diffusivities

For macro-pore radius 0.3 μm

$$\text{The Knudsen diffusivity} = (97)(0.3\times10^{-6})\sqrt{\frac{348}{64}}$$

$$= 6.78\text{x}10^{-5}\ \text{m}^2/\text{s}$$

The Molecular diffusivity $= 2.073\text{x}10^{-5}\ \text{m}^2/\text{s}$

The Diffusion co-efficient is given by

$$\frac{1}{D} = \frac{1}{6.78\times10^{-5}} + \frac{1}{2.07\times10^{-5}}$$

$$D = 1.58\times10^{-5} m^2/\text{sec}$$

The effective diffusivity is calculated as follows

$$D_e = \frac{D\alpha}{\tau}$$

where $\tau = 4$, $\alpha = 0.64$

$$= \frac{1.58\times10^{-5}\times0.64}{4} = 2.54\times10^{-6} m^2/\text{s}$$

Calculation for activation energy:

$$K = K_o e^{-\frac{E}{RT}} \qquad \text{A(16)}$$

$$\ln\frac{K_1}{K_2} = -\frac{E}{R}[\frac{1}{T_1} - \frac{1}{T_2}]$$ for $K_1 = 45$ at 323 K

and $K_2 = 13$ at 348 K

E (activation energy) was calculated

$$\ln\frac{45}{13} = \frac{E}{8.314}[\frac{1}{323} - \frac{1}{348}]$$

E = 46.4 KJ/mol

The temperature dependence of Crystal diffusivity is Arrhenius-type expression

$$D_c = D_o e^{-\frac{H_D}{RT}} \qquad \text{A(17)}$$

at temperature 348 K the crystal diffusivity is assumed to be $1x10^{-12}$ m^2/s

H_D = 12.09 Kcal/mol Ref: [C.Wu et al., 1984]

$$(D_c)_{323K} = 10^{-12} e^{\frac{12.09\times4.18\times10^3}{8.314}[\frac{1}{348} - \frac{1}{323}]}$$

$$(D_c)_{323K} = 2.57\times10^{-13} m^2/s$$

Sample calculation for the conversion analysis:

After the reaction is over, the sample was analysed for the amount of sulphate present in %. The sorbent after reaction has un-reacted CaO as well as $CaSO_4$ formed after the reaction. Suppose the analysis revealed a 30.8 % SO_4^{2-} after the reaction.

100 gm of sample gives 53.41 gm SO_4^{--}

3.992 gm (final wt.) will give = $\frac{3.992\times53.41}{100} = 2.132$

Now 96 gm of sulphate gives 136 gm of $CaSO_4$

2.132 gm will give gm of $CaSO_4$ = $\frac{136\times2.132}{96} = 3.0205$

Reaction CaO $\longrightarrow$ $CaSO_4$

56 gm CaO gives 136gm CaSO4

2 gm $\longrightarrow$ $\frac{136 \text{ x } 2}{56}$ = 4.857

4.857 gm $CaSO_4$ will obtain at 100% conversion

3.0205 gm $CaSO_4$ will obtain at $\frac{100 \times 3.0205}{4.857} = 62.188$

Pressure Drop Calculations:

Experimental Pressure drop across the reactor 150 mm long and 14mm ID

$$\Delta P = \rho g \Delta h \qquad \text{(A18)}$$

where

ρ = density of manometric liquid

g = acceleration due to gravity

Δh = difference in the level of manometric liquid

The reading in the manometer is 4 mm of CCl_4

$\Delta P = (4.0e\text{-}2)(9.81)(1.592x10^3)$

$= 624.06\ N/m^2$

Pressure drop across sorbent bed as per Ergun equation (McCabe et al, 1960)

$$\Delta P = \frac{150 \mu V_z (1 - \epsilon_b)^2 L}{\phi^2_s D^2_p \epsilon_b^3} \qquad \text{(A19)}$$

where

μ = viscosity of the gas

V_z = superficial velocity

ϵ_b = bed porosity

L = length of the packed bed

ϕ_s = sphericity (assumed = 1)

D_p = diameter of particle

$$\Delta P = \frac{(150)(2e-5)(0.0414)(1-0.354)^2(3e-2)}{(2 \times 1.15e-3)^2 (0.354)^3} = 7.04\ N/m^2$$

Reynold's Number based on tube diameter

$$Re = \frac{(1.4 \times 10^{-2})(0.0414)(2.2413)}{(2e-5)} = 64.95 < 2100$$

The pressure drop across the tube

$$\Delta P = \frac{32\mu V_z^{'} l}{D_t^{2}} \qquad \text{(A20)}$$

where

μ = viscosity

V_z = superficial velocity

l = length of the reactor

D_t = diameter of the tube

$$\Delta P = \frac{(32)(2e-5)(0.0414)(146e-3)}{(14e-3)^2} = 0.0197 N/m^2$$

$$\Delta P_{experimental} = \Delta P_{bed} + \Delta P_{reactor} + \Delta P_{mesh}$$

```
C     Last change:  I   13 Feb 2002    7:25 pm
C     Last change:  SA  27 Feb 2001    8:48 pm

      IMPLICIT DOUBLE PRECISION (A-H,O-Z)
      IMPLICIT INTEGER (I-N)
C*******************************************************

C     Parameter statements for principal dimensions

      PARAMETER ( NPAR = 10 , NSPAR = 1, NSTEQ = 2)
      PARAMETER ( LRW  = 5000000 , LIW = 70000 )
      PARAMETER ( NPTMAX = 100001 )

C     Dimension statements and Externals

      DIMENSION Y(NSTEQ,NPTMAX),YPRIME(NSTEQ,NPTMAX)
      DIMENSION INFO(18),RWORK(LRW),IWORK(LIW)
      DIMENSION RPAR(NPAR),IPAR(NSPAR)
      DIMENSION ZGRID(NPTMAX)
      EXTERNAL DIFF,FUNC,BNRY,ESUB
      COMMON/prop/poros,dl,vel,dlen,rp,dka,pden,bdkm,dporos1,pdiff1,
     1 rc,cdiff,beta


      OPEN(UNIT=1,FILE="c:\agupta1\code\i.txt",STATUS="UNKNOWN")
      OPEN(UNIT=2,FILE="c:\agupta1\code\2a.txt",STATUS="UNKNOWN")
      OPEN(UNIT=3,FILE="c:\agupta1\code\3a.txt",STATUS="UNKNOWN")
      OPEN(UNIT=4,FILE="c:\agupta1\code\4a.txt",STATUS="UNKNOWN")
      READ(1,*) Gflow,gvis,tdia,dlen,Pmolin,gmw,Temp,Pres,bdm,rp,
     1  pden,dka,wt,pdiff1,cdiff,rc,Tactual,npts,tgrad,dporos1

      wRITE(4,*) Gflow,gvis,tdia,dlen,Pmolin,gmw,Temp,Pres,bdm,rp,
     1  pden,dka,wt,pdiff1,cdiff,rc,Tactual,npts,tgrad,dporos1
      CLOSE(1)

      PI=4.0D0*ATAN(1.0D0)
      Rcons=8.314          !universal Gas constant  (J/gmol-K)
      Temp=Temp+273.0   !K
      Vel=4.0*Gflow*Rcons*Temp/(22.4*60.0*Pres*PI*tdia**2.0)  !superficial gas Velocity,m/s
      Gden=Pres*Gmw*1.0e-3/(rcons*Temp) !kg/m3
      Re=gden*vel*rp*2.0/gvis
      sc=Gvis/(gden*bdm)
      pe=1/(0.3/(re*sc)+0.5/(1+3.8/(re*sc)))!peclet no from Yang
      Dl=(2.0*rp*gvis)/(Gden*pe)  ! m2/s
      bdkm=(2.0+(1.1*(sc)**0.33*(re)**0.6))*bdm/(2.0*rp)
      Cgin=pres*Pmolin*gmw*1.0e-3/(rcons*temp) ! kg/m3
      WRITE(4,*)"Gden,re,sc,pe,Dl,bdkm"
      WRITE(4,*)Gden,re,sc,pe,Dl,bdkm
      Time=dlen/Vel                    !sec
      WRITE(4,*)"time,vel,cgin"
      WRITE(4,*)time,vel,cgin
```

```
      poros=(dlen*pi*tdia**2/4.0-wt*1e-3/pden)*4.0/(dlen*pi*tdia**2)
      WRITE(4,*)"poros=",poros
      c1= (1.0-dporos1)*27*cdiff*dka/(rc**2)
      d1= 15*pdiff1/rp**2
       beta=bdkm*rp**2/((bdkm+(5*pdiff1/rp))*pdiff1*dporos1)*(c1-d1)

      WRITE(4,*)" beta=", beta
      WRITE(4,*)"c1=",c1
      WRITE(4,*)"d1=",d1

      IF(beta.Ge.0)WRITE(6,*)"beta is POSITIVE"
      RTOL = 1.0D-5
      ATOL = 1.0D-5

C     NPTS = number of points for axial grid (= 1 + #intervals)
C     RTOL = relative tolerance for PDESAC; an absolute tolerance is
C                    calculated later

C     Preliminaries are done; now set things up for PDESAC

      ICORD = 0.0
C     Integration times and initial values for states
C     at the discretization points ZGRID(I)

      T=0
      ntout=100000


C     Initial values for state variables
C     Impurity concn: use an exponential function in z
C     Pressure: use a linear profile for p(z)


      DO 30 I=1,NPTS
       ZGRID(I) = DBLE(I-1)/DBLE(NPTS-1)
       Y(1,I)=0.0
       y(2,I)=0.0

30    CONTINUE

      ZGRID(NPTS)=  1.0D0
      Y(1,NPTS)  =  0.0
      y(2,npts)  =  0.0

C     Prepare for nag001: Insert the INFO(j) values.
C                    Indicate that we have a banded Jacobian: info(6).
C                    Ask PDESAC to evaluate the initial yprime: info(11).
C                    All others are "default" settings

      DO 40 J = 1,18
       INFO(J) = 0
```

```
40   CONTINUE
     INFO(6)  = 1


C    Supply the bandwidths of the iteration matrix.

     IWORK(1) = 2*NSTEQ - 1
     IWORK(2) = 2*NSTEQ - 1

C    Integration loop. Call the implicit integrator PDESAC.

      WRITE(2,102)tOUT*time/60.0,y(1,1),y(1,npts/2),y(1,npts)
      WRITE(3,102)tout*time/60.0,y(2,1),y(2,npts/2),y(2,npts)

     tout=tgrad
     DO 110 IOUT = 1,NTOUT
c     WRITE(2,*)iout,"1"
      IF(tout*time.ge.tactual)GO to 11

       Tout=1.05*tout

50     CALL nag001(T,ZGRID,Y,YPRIME,TOUT,INFO,RTOL,ATOL,
    1            IDID,RWORK,LRW,IWORK,LIW,RPAR,IPAR,
    2            NSTEQ,NPTS,ICORD,DIFF,FUNC,
    3            BNRY,ESUB)


C      Write results regardless of the integration status.
c      Stop if IDID is negative.
c     write(2,*)iout
       IF (IDID .Lt. 0) THEN
        WRITE(1,160) IDID
        GO TO 140
       ENDIF

             WRITE(2,102)tOUT*time/60.0,y(1,1),y(1,npts/2),y(1,npts)
       WRITE(3,102)tout*time/60.0,y(2,1),y(2,npts/2),y(2,npts)
110     CONTINUE

11     continue
101   FORMAT(f15.5,(F15.9))
102   FORMAT(f15.5,3(F15.9))
140   WRITE(1,150)IWORK(11),IWORK(12),IWORK(13),IWORK(14)
150   FORMAT(/1X,'Number of steps taken so far :=',I5/
    1       1X,'Number of function calls    :=',I5/
    2       1X,'Number of Jacobian calls    :=',I5/
    3       1X,'Number of error test fails  :=',I5/)
160   FORMAT(/1X,'Integration Failed with IDID =',I5)

C    End of main program
```

```
c     STOP
      END

      SUBROUTINE FUNC(T,X,U,UX,DUXX,FVAL,NSTEQ,RPAR,IPAR,IRES)
      IMPLICIT DOUBLE PRECISION (A-H,O-Z)
      IMPLICIT INTEGER (I-N)
      DIMENSION U(1),UX(1),DUXX(NSTEQ,1),FVAL(1),RPAR(1),IPAR(1)
      COMMON/prop/poros,dl,vel,dlen,rp,dka,pden,bdkm,dporos1,pdiff1,
     1 rc,cdiff,beta

      alpha=-1.0/poros
      theta=dl/(vel*dlen*poros)

      eta =15*(1.0-poros)*bdkm*pdiff1*dlen/(poros*rp**2*vel*
     +   (bdkm+(5*pdiff1/rp)))

      Fval(1)=alpha*ux(1)+theta*duxx(1,1)-eta*(U(1)-U(2))


       Fval(2)=-beta*(u(1)-u(2))

      RETURN
      END


      SUBROUTINE DIFF(T,X,U,DVAL,NSTEQ,RPAR,IPAR,IRES)
      IMPLICIT DOUBLE PRECISION (A-H,O-Z)
      IMPLICIT INTEGER (I-N)
      DIMENSION U(1),DVAL(NSTEQ,1),RPAR(1),IPAR(1)

C     Supply the multiplier of second derivative.

      DVAL(1,1) = 1.0
      Dval(2,1) = 0.0

      RETURN
      END


      SUBROUTINE BNRY(T,X,U,UX,DELTA,NSTEQ,RPAR,IPAR,IRES,IBNRY)
      IMPLICIT DOUBLE PRECISION (A-H,O-Z)
      IMPLICIT INTEGER (I-N)
      DIMENSION U(1),UX(1),DELTA(1),RPAR(1),IPAR(1)

      IF (IBNRY .EQ. 1) THEN        !!! Left boundary (Z=0)
        DELTA(1)=U(1)- 1.0
        delta(2)=u(2)-1.0

      ENDIF

      IF (IBNRY .EQ. 2) THEN        !!! Right boundary (Z=1)
```

```
DELTA(1) = UX(1)-
0.0
      delta(2) = ux(2)-
0.0

    ENDIF

    RETURN
    END

    SUBROUTINE
ESUB
    RETURN

    END
```

****

Input file for the bi-porous model:

0.3 2.0e-5 0.014 0.08 0.005 64.0 75 101325 2.073e-5 0.16e-3
670 601 5.0 2.54e-6 1e-12 2e-6 12000 100 0.01 0.64

Gflow, gvis, tdia, dlen, pmolin, gmw, Temp, Pres, bdm, rp,
pden, dka, wt, pdiff1, cdiff, rc, Tactual, npts, tgrad, dporos1

Determination of various parameters in so2vipp.txt

1. flow in std litre per minute
2. viscosity(kg/m-sec)
3. tube dia in m
4. tube lenghth in metre
5. mol fraction
6. molecular weight (g/gmol)
7. temperature in °C
8. pressure in N/m^2
9. molecular diffusivity (m^2/sec)
10. radius of partical (m)
11. bulk density of zeolite (kg/m^3)
12. adsorption equilbirium constant
13. porosity of bed
14. diffusion of SO_2 in pores (m^2/sec)
15. diffusion of SO_2 in crystal (m^2/sec)
16. crystal radius (m)
17. actual time (sec)
18. number of axial grids
19. time gradint
20. intraparticle porosity